MANGANESE(II) INDENYL COMPOUNDS: SYNTHESIS, CHARACTERIZATION AND

REACTIVITIES WITH OXYGEN DONOR LIGANDS

By

Ryan M. Meier

Dissertation

Submitted to the Faculty of the

Graduate School at Vanderbilt University

in partial fulfillment of the requirements

the degree of

Doctor of Philosophy

in

Chemistry

August, 2012

Nashville, Tennessee

Approved:

Timothy P. Hanusa

C.M. Lukeheart

David Wright

James Wittig

To my friends and family, especially my parents, for all of their patience, support, and

sacrifices over my decades of schooling.

ACKNOWLEDGEMENTS

There are a number of influential people who greatly impacted my education over the years that I would also like to thank, starting with all of my general chemistry teacher Professor David Cedeno, who was the first teacher to get me truly interested in chemistry. Next are all of my undergraduate chemistry professors at Knox: Diana Cermak, Linda Bush, Thomas Clayton, Lawerence Welch, Andrew Mehl, and Mary Crawford. On top of being fantastic teachers whom not only gave me an education that prepared me well for graduate school, they also gave me a great appreciation of the teacher-student interactions at a liberal college. This appreciation is something that I still hold on to today and is one of the biggest reasons I will now be a professor at a liberal arts college myself.

TABLE OF CONTENTS

LIST OF TABLES

LIST OF FIGURES

BHT	butylated hydroxytoluene
bipy	bypyridine
Cp	cyclopentadienyl
Cp*	pentamethylcyclopentadienyl
HOMO	highest occupied molecular orbital
i-Pr	isopropyl
Im	imidizole
Ind	indenyl
Ind^{Me-1}	1-methylindenyl
Ind^{Me-2}	2-methylindenyl
$Ind^{2Me-4,7}$	4,7-dimethylindenyl
$Ind^{3Me-1,2,3}$	1,2,3-trimethylindenyl
$Ind^{3Me-2,4,7}$	2,4,7-trimethylindenyl
Ind^{7Me} or Ind*	1,2,3,4,5,6,7-heptamethylindenyl
Ind^{Si-1}	1-trimethylsilylindenyl
Ind^{Si-2}	2-trimethylsilylindenyl
$Ind^{2Si-1,3}$	1,3-bis(trimethylsilyl)indenyl
$Ind^{2i-1,3}$	1,3-diisopropylindenyl
KODipp	potassium diisopropylphenoxide
LIESST	light-induced excited spin state trapping
LUMO	lowest unoccupied molecular orbital
Me	methyl
MLCT	metal to ligand charge transfer

NIESST	nuclear decay induced excited spin state trapping
PVA	polyvinyl alcohol
por	porphyrin
pz	pyrazolyl
SCO	spin crossover
t-Bu	tertiary-butyl
TCNE	tetracyanoethylene
TCNQ	tetracyanonapthoquinone
terpy	terpyridine
Tp	tris(pyrazolyl)borates
Tpp	tetraphenylporphinato

CHAPTER I

SYMMETRY AND STERIC EFFECTS ON SPIN STATES
IN TRANSITION METAL COMPLEXES

Introduction

Control over the magnetic characteristics of transition metal complexes is a major

research area in inorganic and organometallic chemistry, and is important to the fields of

information storage, imaging science, and molecular switching.[1] Such control is typically

achieved by varying the electron donor/acceptor properties of coordinated ligands, but

alterations of temperature, light, magnetic fields, and lattice characteristics (for solids)

can influence the spin state behavior of compounds as well.[2] These changes modify the

energies of metal d-electron levels, which affect the overlap of metal-ligand orbitals, and

ultimately alter metal-ligand (M-L) distances. Conversely, manipulation of metal-ligand

distances through pressure or steric effects can affect the strength of the ligand field.

Divalent iron complexes of 1,10-phenanthroline were among the first systems

known in which interligand steric crowding and the associated bond length changes

affected the relative stability of the metals' spin states. These discoveries of the 1960's

have been extended to a variety of complexes containing other *N*-donor ligands such as

substituted pyridines and poly(pyrazoyl)borates, and in more recent years to

metallocenes; they will be described in additional detail below.

Another method of influencing spin states depends on changes in the rotational

conformation of ligands, which through orbital symmetry interactions alter the HOMO-

LUMO gap in a complex. Among the most extensively studied examples of these

systems are substituted bis(indenyl)metal complexes, [MInd$_2$], which are related to the

[MCp$_2$] metallocenes. In the latter, the exact rotational conformation of the

cyclopentadienyl (Cp) ligands does not appreciably affect their interactions with d

orbitals. In contrast, the nodal properties of the indenyl ligand are sufficiently different

from those of cyclopentadienyl that in susceptible compounds of Cr^{II}, the relative

orientation of the ligands around the metal influences its spin state, giving rise to low-

spin, high-spin, and spin-crossover species. Such "magnetism with a twist" provides an

additional means for designing and manipulating the magnetic behavior of related

substituted species.

A comprehensive review of the magnetochemistry of spin-crossover species is

available;[2] but the initial motivation for much of the work in this dissertation was with

regards to the steric and symmetry effects on magnetic spin states. The remainder of this

chapter serves as a literature survey focusing on the manipulation of the magnetic spin

states of molecules through symmetry and steric effects.

Steric Effects on Magnetism in Inorganic Complexes

In many classes of transition metal compounds, metal–ligand distances are

relatively insensitive to steric effects, even though ligand field strengths and the

associated splitting of metal d-electron levels are in fact sensitive functions of M–L

separation. A ligand field analysis of metal complexes with neutral ligands concluded

that Δ_o varies as μ/a^6, where μ is the dipole moment of the ligand and a = M–L distance.[3]

Given this order of dependence, Δ_o would be reduced by half from a change in metal-

ligand bond length from 2.00 Å to 2.25 Å. Such a bond length change, although

substantial, is not unusual for metal ions in different spin states, and there are several

classes of compounds in which steric effects explicitly affect metal-ligand distances

enough to alter the metal's spin multiplicity. Often these involve spin-crossover (SCO)

species (sometimes called spin transition, spin equilibrium, or spin isomer systems),[2] and

the low-spin to high-spin transition in such complexes is entropically favored. The

entropy change (ΔS) for the process varies as the log of the ratio of the spin multiplicities

($\ln[(2S+1)_{HS}/(2S+1)_{LS}]$);[3] consequently, among first-row transition metal complexes,

those containing Fe^{II} ($\Delta S = \ln(5/1)$) and Mn^{II} ($\Delta S = \ln(6/2)$) are the most likely to display

SCO behavior.

In most of the cases described in this chapter, a ligand substituent with somewhat

greater steric demand than a hydrogen atom (often a methyl group suffices) provides

enough steric congestion that metal-ligand bonding is distorted and lengthened, leading to

weaker ligand field strength and higher spin species. Typically the bulkier substituent is

relatively close to the metal center so that the interference in the M–L bonding is directly

apparent, and several categories of these systems will be described in the following

sections.

There are, however, cases where a substituent is remote from a metal and yet the

resulting complex displays high-spin or SCO behavior, even though the compound with

unsubstituted ligands does not. An example of this involves iron complexes of 2,2′-

bipyridine; the unsubstituted $[Fe(bipy)_3]^{2+}$ cation (Figure 1; **1**) is low spin at all

temperatures, but the $[Fe(3,3′-Me_2-2,2′-bipyridine)_3](PF_6)_2$ complex (Figure 1; **2**)

transitions from low spin at 90 K ($\mu_{eff} = 1.1\ \mu_B$) to an intermediate spin at 363 K ($\mu_{eff} = 4.0\ \mu_B$).[4] The methyl groups in the 3,3′-Me₂-2,2′-bipyridine ligand are not near the metal,

and would be expected to increase the donor strength of the ligand through inductive effects. However, the methyl groups sterically interact with each other, causing a twist distortion of the ligand, and causing interference with both σ- and π-donation. As a consequence, the methylated bipyridine is an intrinsically weaker donor than the unsubstituted ligand. A similar steric influence is found in complexes of the 1,1′-biisoquinoline ligand (Figure 1; **3**).
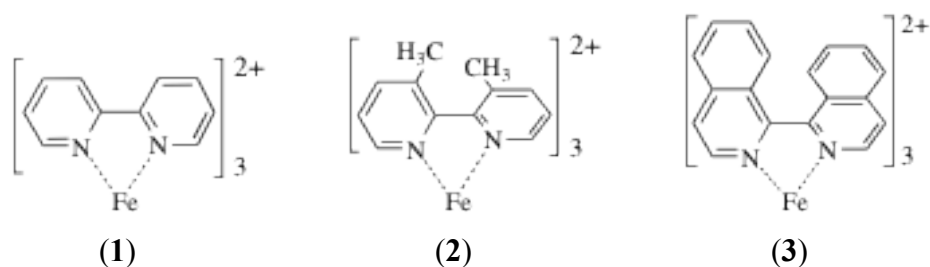
Figure 1. (**1**) [Fe(bipy)$_3$]$^{2+}$ cation. (**2**) [Fe(3,3′-Me$_2$-2,2′-bipyridine)$_3$](PF$_6$)$_2$. (**3**) [Fe(1,1′-biisoquinoline)$_3$]$^{2+}$.

Another issue that arises in this context is the electronic donor effect of a ligand substituent, as distinct from the effect of its steric bulk. For example, alkyl groups are frequently considered as net electron donors, regardless of the ligand type to which they are attached. Such behavior should not be expected in all molecular contexts, however. Alkyls are donors through induction to conjugated π systems such as aromatic rings, for example. However, when methyl groups are attached to an amine, they can function as electron-withdrawing groups, owing to hyperconjugative effects.[5] Thus the presence of an alkyl group on a non-conjugated ligand can weaken the ligand field strength through both steric and electronic effects, and it may not always be possible to determine which, if either, has the stronger influence.

Diimines and Terimines.

The first example of a synthetic Fe^{II} SCO species was reported in the 1960's, when the thermally induced $^5T_{2g} \rightarrow {}^1A_{1g}$ spin transition in [Fe(1,10-phenanthroline)$_2$(NCS)$_2$] was described.[6] This discovery prompted much interest in the SCO behavior of divalent iron complexes, in part from to the ability to analyze such species with Mössbauer spectroscopy. Divalent iron complexes of 1,10-phenanthroline were also among the first systems known in which interligand steric crowding and the associated bond length changes were identified as affecting the relative stability of the metal spin states.

For example, the complex [Fe(phen)$_3$]$^{2+}$ (phen = 1,10-phenanthroline) (Figure 2; **4**) is diamagnetic at all temperatures, but the related methyl-substituted complex [Fe(2-Me-phen)$_3$]$^{2+}$ (Figure 2; **5**) is a SCO species, and strongly paramagnetic at room temperature ($S = 2$). These results would be counterintuitive if the stronger σ-donor ability of the methyl group relative to hydrogen in aromatic rings was considered by itself. The methyl groups of [Fe(2-Me-phen)$_3$]$^{2+}$ plainly interfere with the metal–ligand bonding, however. This is evident in the asymmetry in the Fe–N$_{Me}$ and Fe–N$_H$ distances in the crystal structure of the compound (2.25 Å and 2.17 Å, respectively, at 298 K), a difference that would be exacerbated in a low-spin Fe^{II} environment. The resulting weaker ligand field strength is also reflected in the longer avg. Fe–N distances in **5** (2.21 Å) compared to those in **4** (1.98 Å), typical for high-spin and low-spin Fe–N distances, respectively. The congestion around the metal center is such that attempts to form the [Fe(2,9-Me$_2$-phen)$_3$]$^{2+}$ ion have been unsuccessful.[7]
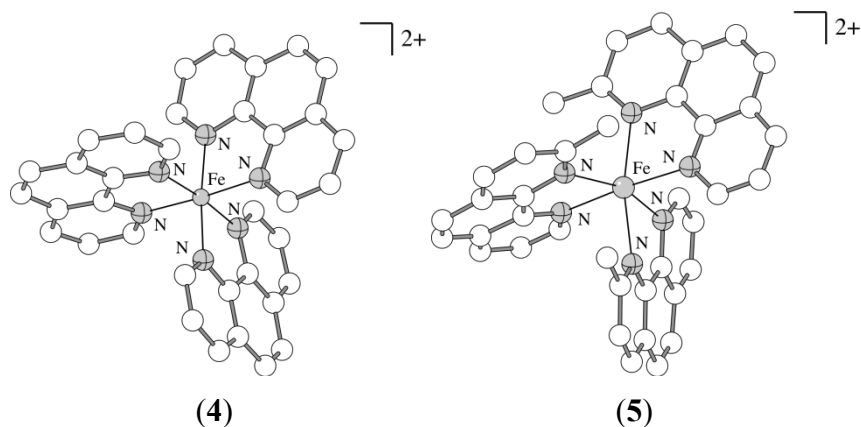
Figure 2. (4) $[Fe(phen)_3]^{2+}$. **(5)** $[Fe(2\text{-}Me\text{-}phen)_3]^{2+}$.

In nuclear decay induced excited spin state trapping (NIESST) experiments, Fe^{II} complexes can be generated from the radioactive decay of precursor $^{57}Co^{II}$ complexes, and their Mössbauer spectra collected. Such experiments have demonstrated that $[^{57}Fe(2\text{-}Me\text{-}phen)_3]^{2+}$ is initially generated in a long-lived high-spin ($^5T_2$) excited state even at 4.2 K, a temperature at which the ground state would be low-spin.[8] Light alone can induce a high-spin state in **5** embedded in a PVA film; LIESST (light-induced excited spin state trapping) experiments have demonstrated that irradiation of **5** with 514.5 nm light at 12 K will bleach the MLCT band characteristic of the low-spin state. If the temperature is held below 40 K, the high-spin excited state can persist for hours.[9]

Balancing the donor/acceptor properties and steric bulk of a ligand can also be used to tune the ligand field strength. Owing to the stronger donor properties of a methoxy group compared to methyl, the 2-CH_3O-substituted analogue $[Fe(2\text{-}(CH_3O)\text{-}phen)_3]^{2+}$ requires higher temperatures for the SCO to occur than in **5**. Conversely, the 2-Cl-substituted variant is persistently high-spin, aided by the electron-withdrawing properties of the chloride ligand.

The same effects of methylation on spin states is observed in other 1,10-phenanthroline derivatives such as [Fe(2-Me-phen)$_2$X$_2$] (X = Cl, Br, NCS, N$_3$), and [Fe(2,9-Me$_2$-phen)$_2$(NCS)$_2$]. These are high-spin species between 78 K and room temperature; the corresponding unsubstituted (or 4-Me-, 5-Me-substituted) analogues are low spin or exhibit SCO behavior. The X-ray crystal structure of [Fe(2,9-Me$_2$-phen)$_2$(NCS)$_2$] (Figure 3; **6**) reveals the distortions induced by the methyl groups; in particular, the Fe–NCS bond distances are extremely long (2.316(3) Å avg.) owing to multiple close contacts (< 4 Å) with the phenanthroline ligand (the avg. of all four Fe–N$_{phen}$ distances is 2.27(5) Å). The iron atoms lie an avg. of 1.04 Å out of the place of the phenanthroline ligands in **6**, compared to a displacement of only 0.077 Å for [Fe(phen)$_2$(NCS)$_2$]. These distortions serve to weaken the π-back donation to the iron, and help support the high-spin state in the complex.[10]
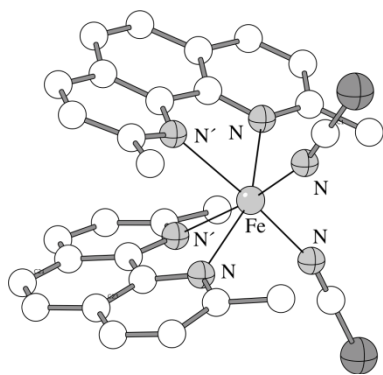
(6)

Figure 3. [Fe(2,9-Me$_2$-phen)$_2$(NCS)$_2$].

As noted at the beginning of Section 2, derivatives of 2,2′-bipyridine also display sterically induced SCO. The use of methyl substitution at the 6-position in bipyridine (Figure 4; **7**) leads to an SCO Fe^{II} species, whereas the unsubstituted [Fe(bipy)$_3$]$^{2+}$ cation is low spin. As is the case with 1,10-phenanthroline, steric congestion prevents formation of the [Fe(6,6′-Me$_2$-bipy)$_3$]$^{2+}$ derivative. Terpyridines are similar to the bipyridines in

that the unsubstituted iron complexes are low spin, but when R^1 is phenyl, the resulting complex displays SCO behavior. Terpyridines containing methyl or phenyl groups at both the R^1 and R^3 positions (Figure 4; **8**) are isolable, and are high spin in both the solid state and in solution.[11]
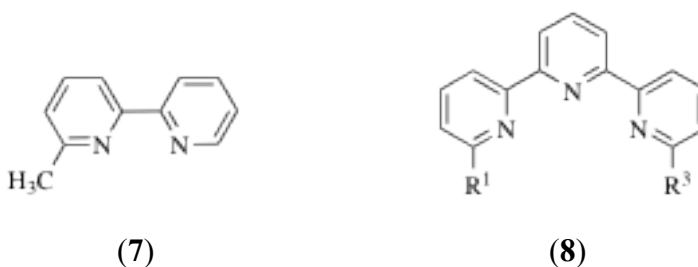
Figure 4. (**7**) 6-Me-bipy. (**8**) 6,6´-R$_2$-terpy.

It should be noted that, all else being equal, SCO behavior is more difficult to induce in complexes containing five-membered heterocyclic ligands than in their six-membered counterparts. Geometric considerations place substituents farther away from the metal center in the former, where they are less able to cause steric crowding. Thus not only can a tris Fe^{II} complex of 4,4´-dimethyl-bi-2-thiazoline (Figure 5; **9**) be generated (which as noted above, is not possible for 2,9-Me$_2$-phen), but the complex is low spin even at room temperature.[12] However, when both 5- and 6-membered rings are involved, as in some analogues of terpyridine (Figure 5; **10**) or imidazoline (Figure 5; **11**), SCO transitions can be observed in the resulting iron complexes. If the bulk of **11** is augmented with a methyl group to produce the (6´-methyl-2´-pyridyl)imidazoline ligand (Figure 5; **12**), its yellow Fe^{II} complex displays a magnetic moment between 77–298 K that is consistent with a high-spin ground state; its magnetic susceptibility follows Curie-Weiss behavior.[13]

8

| **(9)** | **(10)** | **(11)** | **(12)** |
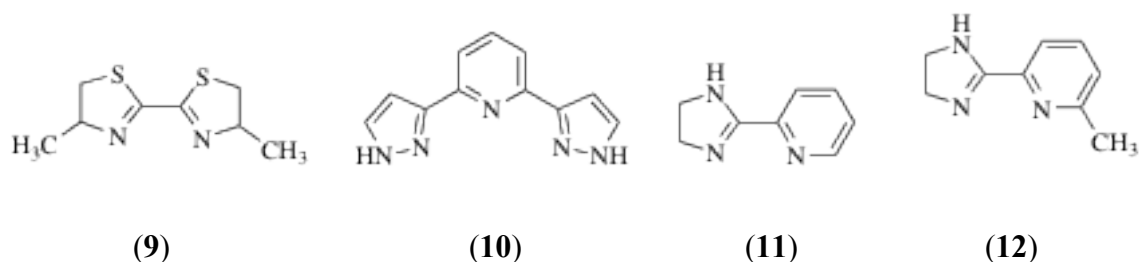
Figure 5. (**9**) 4,4′-dimethyl-bi-2-thiazoline. (**10**) 2,6-di(1H-pyrazol-3-yl)pyridine. (**11**) (2′-pyridyl)imidazoline (**12**) (6′-methyl-2′-pyridyl)imidazoline.

Pyrazolylborates

Tris(pyrazolyl)borates and the related pyrazolylmethane derivatives are well-studied systems that can display SCO behavior. [Fe(Tp)$_2$] (Tp = HB(pz)$_3$) is weakly paramagnetic from 78 K to room temperature, but transitions at ca. 380 K to the $^5T_{2g}$ ground state, assisted by a crystallographic phase change. The 3,5 derivative is high spin at room temperature but converts to the low-spin state at 150 K, and the 3,4,5 analogue is essentially high-spin at all temperatures between 40 and 295 K. The methyl group in the 4-position was originally thought to interfere with the normal contraction of the lattice on cooling, hence blocking the spin state change.[14] Recent investigations on the trimethyl substituted compound (Figure 6; **13**) and related complexes containing cyclopropyl substituents have shown that intramolecular interactions lead to twisting of the pyrazolyl rings, and interfere with the bite angle of the ligands. If the FeN–NB torsion angle is greater than about 11°, complexes that are high spin at room temperature will not display SCO behavior on cooling.[15]
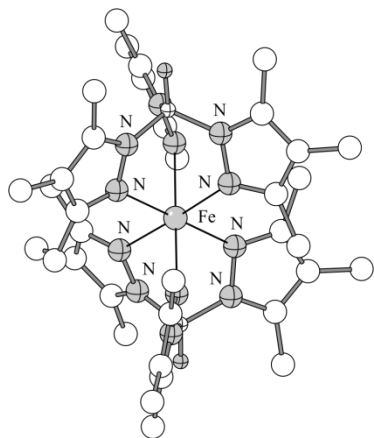
(13)

Figure 6. (**13**) [Fe(HB(3,4,5-(Me)$_3$(pz)$_3$)$_2$].

Much of the complex magnetic behavior of poly(pyrazolyl)borate complexes is observed only in the solid state; in solution, both [Fe(HB(3,5-(Me)$_2$(pz)$_3$)$_2$] and **13** are high-spin between 200 and 295 K, and even the unsubstituted [FeTp$_2$] displays a magnetic moment of 2.71 μ_B in CH$_2$Cl$_2$ at room temperature, consistent with a mixture of high- and low-spin species.

An indirect steric effect that supports the low-spin state occurs when the hydrogen on the central boron is substituted with an additional pyrazolyl ring or a phenyl group; e.g., [Fe(B(pz)$_4$)$_2$] and [Fe(PhB(pz)$_3$)$_2$] are low spin in solution. Intraligand steric crowding is thought to compress the other ligands, generating a smaller bite angle that favors low-spin Fe^{II}.[16]

Macrocyclic systems

The strong field ligand 1,4,7-triazacyclononane is the basis for a hexadentate ligand system that supports the low-spin state of Fe^{II}.[17] When a single methyl group is added to the 6-position in one ring (Figure 7; **14**; R = Me), the steric influence causes the

complex to display SCO behavior. It has been argued that the activation process for the

spin state change in solution involves a trigonal twist motion, and the relatively high

value of the activation parameter for the quintet-singlet transition in the Fe^{II} complex of

14 with R = Me (9.4($\pm$0.6) kJ mol^{-1}) has been ascribed to its stiff ligand system. In

contrast, the Fe^{II} complex based on the ligand bis(2-pyridylmethyl)amine (Figure 7; **15**),

for example, can more easily accommodate such twisting, and its activation parameter is

correspondingly lower (2 kJ mol^{-1}).[18]

(**14**)   (**15**)
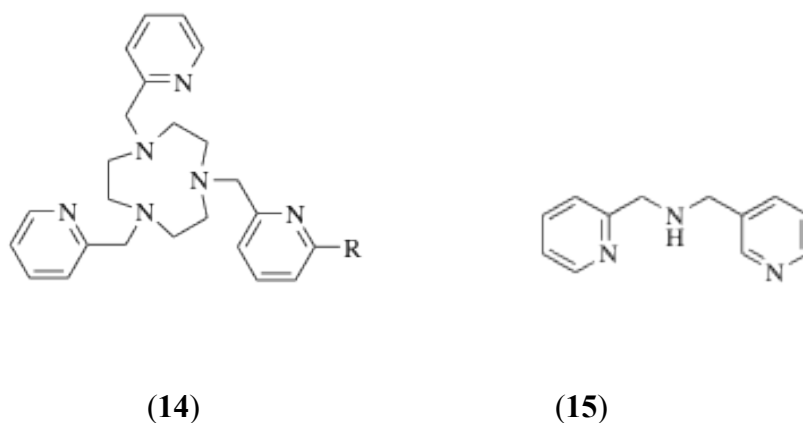
Figure 7. (**14**) [1,4,-(2´-pyridyl)$_2$-7-(6´-R-2´-pyridyl)]-triazacyclononane. (**15**) bis(2-pyridylmethyl)amine.

The relevance of iron porphyrinate systems to the allosteric mechanism of

hemoglobin oxygenation has made their SCO species the subjects of repeated

investigation. In some cases, the relative stability of spin states of porphyrinate

complexes has been attributed to steric effects of the axial ligands. In the bis(2-

methylimidazole)(octaethylporphinato)iron(III) complex ([Fe(OEP)(2-MeIm)$_2$]ClO$_4$)

(Figure 8; **16**), for example, the 2-MeIm ligand plane comes to within 22° of eclipsing the

nearby Fe–N$_{por}$ bond, and the resulting congestion is thought to prevent the imidazole

from approaching the metal center closely enough to stabilize a low-spin state. The

11

orientation and corresponding high-spin state (μ_{eff} = 5.52 μ_B at room temperature) is strictly a solid-state effect; in solution, where the axial ligands are free to rotate, SCO behavior is exhibited. Interestingly, its solution behavior is similar to that of the related [Fe(TPP)(2-MeIm)$_2$]ClO$_4$, but the latter complex is low spin in the solid state. The crystal structure of the TPP complex reveals that the imidazole ligand is rotated farther from the nearest Fe–N$_{por}$ bond; the imidazole can then approach the metal more closely and support its low-spin state.[19] Related examples have been described elsewhere.[20]
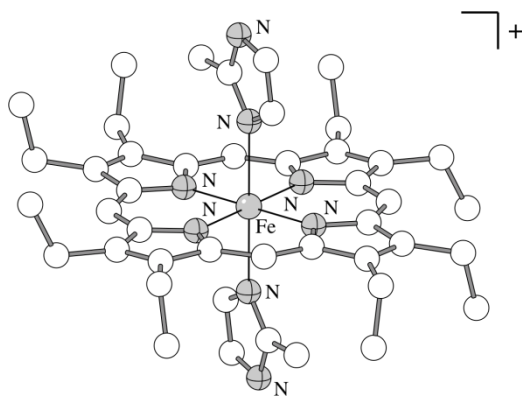
(16)

Figure 8. (**16**) Bis(2-methylimidazole)(octaethylporphinato)iron(III).

The sometimes confounding effects of steric crowding and electron donation are exemplified in a series of Fe[III] cyclamacetate complexes in which the axial ligands are acetate and either fluoride or OFeCl$_3$, and in which the cyclamate ring is either unsubstituted or trimethyl substituted. Based on crystal structure data, DFT calculations were conducted on a model compound (Figure 9; **17**). When R = H, the complex is low spin ($S = {}^1/_2$); if R = Me, the complex is high spin ($S = {}^5/_2$), in agreement with

experimental measurements. The reason for the difference was assigned to steric

crowding from the methyl groups (e.g., the crystal structure of the high-spin complex

reveals non-bonded hydrogen contacts as short as 2.23 Å), and to the electron-

withdrawing effects of the methyl groups on the amine nitrogens. Although the net result

is that the Fe–N bonds lengthen with methyl substitution (by 0.13 Å in the calculations),

thus weakening the ligand field, it was not possible to determine whether steric crowding

or electron withdrawal contributes more to the high-spin state.[5] Solvation effects,

however, appear to be comparatively unimportant.
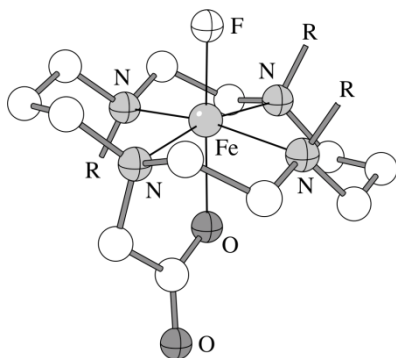
(**17**)

Figure 9. (**17**) Fe^{III} cyclamacetate model complex.

Other multidentate ligands

The pyridine-containing branched chelating ligands tetrakis(2-pyridylmethyl)-1,2-

ethanediamine (tpen) (Figure 10; **18**; R = H) and the closely related 6-methylpyridyl

substituted derivative (mtpen) (Figure 10; **18**; R = Me) differ by only a single methyl

group on one arm. The Fe^{II} tpen derivative displays SCO behavior, in both solution and

the solid state, yet the mtpen analogue (**19**) is strictly high spin. Evidence from the X-ray

crystal structure was used to show that steric influence of the methyl group was enough to prevent the approach of the pyridyl group to the distance (ca. 2.0 Å) required for a low-spin complex; at 2.17 Å, the Fe–N$_{py}$ distance will only support the high-spin state.[21]
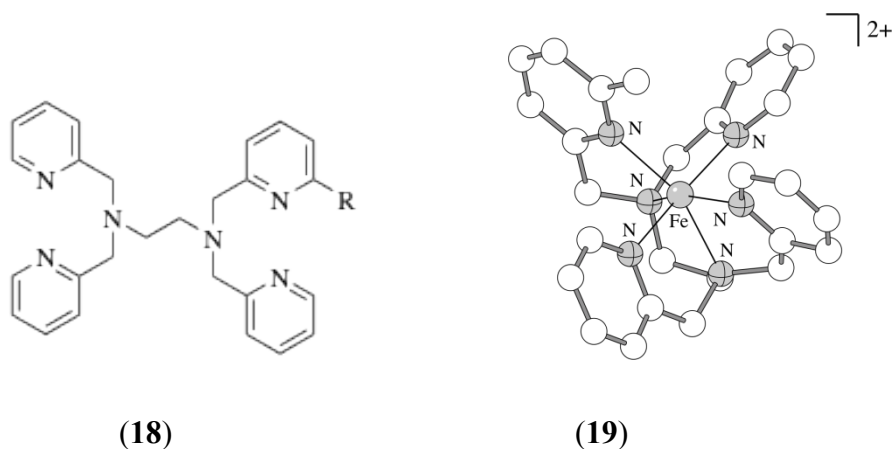
Figure 10. (18) R = H, tpen; R = Me, mtpen. **(19)** Fe[mtpen]$^{2+}$.

A smoothly varying example of variation in SCO temperature as a response to steric pressure is provided by the series of Fe^{II} compounds based on the hexadentate ligand tris[4-[(6-*R*)-2-pyridyl]-3-aza-3-butenyl]amine (Figure 11; **20**), where *R* is either H or CH$_3$ (Figure 11; **21**).[22] The complex with all *R* = H is low spin up to 400 K. When one of the three *R* groups is methyl, the complex undergoes a low-spin to high-spin transition at 380 K. With two and three methyl groups, the transition temperature drops to 290 K and then 215 K, respectively. The increasing steric pressure from the methyl groups lengthens and weakens the Fe–N interactions, which in turn disfavor the low-spin state.
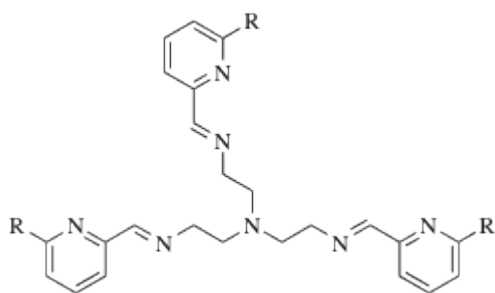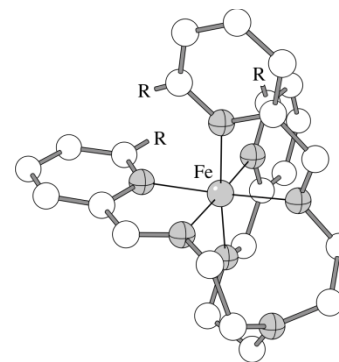
(20)   **(21)**

Figure 11. (20) Tris[4-[(6-*R*)-2-pyridyl]-3-aza-3-butenyl]amine. **(21)** Fe[tris[4-[(6-*R*)-2-pyridyl]-3-aza-3-butenyl]amine]$^{2+}$

The competition that can exist between the donor and steric properties of a ligand and their effect on magnetic properties is nicely illustrated in complexes of 2-pyridinalpheylimine (Figure 12; **22**), which can be tuned for the proportion of their high- or low-spin states depending on the presence of methyl substituents. [FeL$_2$(NCS)$_2$] (R^1, R^2, R^3 = H) displays SCO behavior, but at 4.2 K, 60% of the complex is still in the high-spin form. Addition of a methyl group to the ligand (R^1 = Me) causes the resulting complex to convert entirely to the low-spin state by 78 K; evidently the donor effect of the methyl group overrides any extra congestion that may be generated around the metal center. If the methyl group is added at R^2 or at R^1 and R^2, however, the crowding around the metal center overrides the inductive effects of the methyl group(s). Interestingly, when methyl groups are present at R^1 and R^3, the complex is also high spin at all temperatures, and Mössbauer spectra display a single quadrupole doublet, typical for high-spin species. It is believed that the R^3 methyl group sterically interacts with the hydrogen on the imine carbon, causing twisting of the ligand and reducing its donor ability.[23]
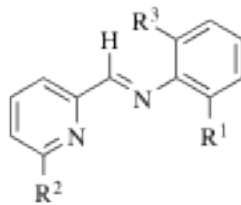
(22)

Figure 12. (**22**) 2-pyridinalpheylimine model compound

Although certainly established, SCO in Co^{II} systems has far fewer documented examples than the corresponding Fe^{II} species. Steric crowding appears to be the reason that the tris Co^{II} complex dication with the 6-methyl pyridine-substituted ligand (Figure 13; **23)** (R = Me) displays a magnetic moment of 3.50–4.31 μ_B over the temperature range from 80–383 K, whereas the same complex with R = H cannot reach the high-spin state under similar conditions (μ_{eff} = 2.41 μ_B at 385 K).[24] Steric effects have also been implicated in derivatives containing the ligands (Figure 13; **24)** (R = *t*-Bu, *i*-Pr) and the facially coordinating tripyridylamine (Figure 13; **25)** (R = Me). In the latter, a spin transition from μ_{eff} = 2.15 μ_B at 95 K to 3.82 μ_B at 373 K is observed when R = H; when R = Me, however, the complex is strictly high spin.
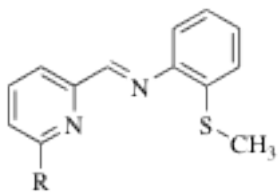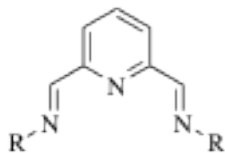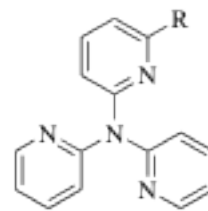
(23)   **(24)**   **(25)**

Figure 13. Structures of the substituted pyridine ligands (**23**), (**24**), and (**25**).

Metallocenes

With relatively few exceptions, metallocenes are low-spin compounds, a consequence of the strong field nature of the cyclopentadienyl (Cp) ligand. They are characterized by a large HOMO–LUMO gap between the frontier nonbonding and antibonding molecular orbitals. This is particularly true for 4th and 5th row transition metals, with the result that 4d and 5d cyclopentadienyl compounds are exclusively low spin. Even among first-row metallocenes, the ability to display variable spin states is confined to those of manganese and to a much smaller extent, chromium.

Manganocenes

Manganocene ([MnCp$_2$]) is an anomaly when compared to its neighboring metallocenes; owing to its half-filled d electron shell, there is no ligand field stabilization energy (LSFE), and a high-spin ground state ($^6A_{1g}$) is found at room temperature. The high-spin preference is only 2.1 kJ mol^{-1},[25] and although its solution magnetic moment is 5.5 μ_B at room temperature, it undergoes SCO at reduced temperatures (μ_{eff} = 1.99 μ_B at 193 K).[26] These moments are relatively close to the spin-only values for 5 and 1 unpaired electrons (5.92 μ_B and 1.73 μ_B, respectively).

Changing the substituents on the Cp ligands can modify the relative preference for spin states in manganocenes. Addition of a single methyl group to each Cp ligand results in a compound that exhibits a spin state equilibrium between two states at room temperature.[25] Further methylation of the Cp ligand can produce a completely low-spin compound (μ_{eff} = 2.18 μ_B), as observed with decamethylmanganocene ([MnCp*$_2$], Cp* = $_{C5Me5}$).[27] An important structural difference between the high and low-spin manganocenes

is exhibited in their Mn–C distances. In the case of the high-spin [MnCp$_2$], the avg. Mn–C distance is 2.41 Å, which is considerably longer than that in [MnCp*$_2$] (avg. of 2.11 Å). The short distance exists despite the increased steric bulk of the Cp* ligand, which in the absence of a spin state change might be expected to lengthen the metal-cyclopentadienyl separation.[27]

However, sufficient steric interactions can in certain cases override electronic donor effects in manganocenes. For example, the isopropyl metallocene [M(Cp^{3i})$_2$] (Cp^{ni} = C$_5$(^{i}Pr)$_n$H$_{5-n}$) displays SCO behavior; it is low spin at low temperature (1.89 μ_B at 5 K), with Mn–C distances typical of the low-spin state (2.130(6) Å), but reaches a moment of 3.25 μ_B at 348 K, indicative of an incomplete spin state change.[28] In contrast, [Mn(Cp^{4i})$_2$] (Figure 14; **26**) is entirely high-spin (5.5 ± 0.1 μ_B) from room temperature down to 10 K.[28] This is despite the presence of an additional electron donating i-Pr group on each ring, which should help stabilize a low-spin compound. The increased steric bulk of the Cp ligand instead generates considerable intramolecular strain, as demonstrated from the displacements of the isopropyl methine carbons by up to 0.26 Å from the Cp ring plane. This leads to a bent structure in the solid state (Cp$_{centroid}$–Mn–Cp$_{centroid}$ = 167°) and elongated Mn-C bonds (avg. = 2.42(2) Å), which are characteristic of high-spin manganocenes.
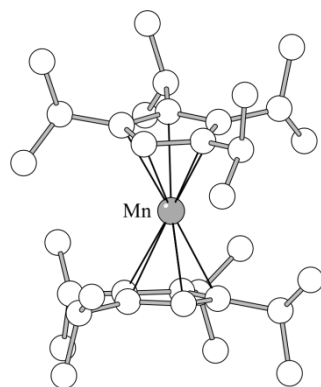
(26)

Figure 14. (**26**) Octaisopropylmanganocene

The difference in spin state leads to a notable difference in the reactivity of the two manganocenes. The SCO compound [Mn(Cp^{3i})$_2$] reduces tetracyanoethylene (TCNE) in acetonitrile at room temperature to form the [TCNE]$^{\bullet-}$ radical anion. In contrast, the high-spin [Mn(Cp^{4i})$_2$] undergoes a tricyanovinylation reaction with TCNE to form C$_5$(*i*-Pr)$_4$HC(CN)=C(CN)$_2$.[28]

Trimethylsilyl and *t*-butyl substituted manganocenes show trends in magnetic behavior that to some extent parallel those observed with the hexa- and octaisopropyl manganocenes, although not always for the same reason.[29] In the case of the trimethylsilyl substituted manganocenes, the presence of single trimethylsilyl group on each Cp ring produces a compound that is high spin from 150–300 K (μ_{eff} = 5.9 μ_B), although the effective magnetic moment drops to ~5.3 μ_B at 100 K. Addition of a second and third trimethylsilyl group to each Cp ring produces compounds that are completely high spin at from 5–300 K (μ_{eff} ~5.9 μ_B). There is clearly intramolecular crowding in some of the molecules; in [Mn{1,2,4-(Me$_3$Si)$_3$C$_5$H$_2$}$_2$], the silicon atoms of the

trimethylsilyl groups are displaced from the ring plane by an avg. of 0.27 Å.

Trimethylsilyl groups on Cp rings are net electron-withdrawing substituents, however, and this is undoubtedly the fundamental source of the high-spin states.

In contrast, both electronic and steric effects on magnetic behavior are clearly observed with t-butyl substituted manganocenes. The singly substituted [Mn{(Me$_3$C)C$_5$H$_4$}$_2$] is high spin at room temperature (μ_{eff} ~5.8 μ_B) but displays SCO behavior, with an effective magnetic moment of ~2.2 μ_B near 175 K. The additional electron donation from a second t-butyl group causes [Mn{1,3-(Me$_3$C)$_2$C$_5$H$_3$}$_2$] to be low spin at room temperature (μ_{eff} = 2.2–2.3 μ_B). Addition of a third t-butyl group to each Cp ring, however, leaves [Mn{1,3,4-(Me$_3$C)$_3$C$_5$H$_2$}$_2$] (Figure 15; **27**) entirely high spin at all temperatures, with a moment of 5.8-5.9 μ_B from 5–300 K. The steric strain provided by the rings in **27** is apparent from the bent solid state structure (Cp$_{centroid}$–Mn–Cp$_{centroid}$ = 169°), in which the quaternary carbon is displaced from the ring plane by 0.21 Å and the Mn–C bond lengths range from 2.350(4) Å to 2.470(4) Å, typical for a high-spin manganocene.
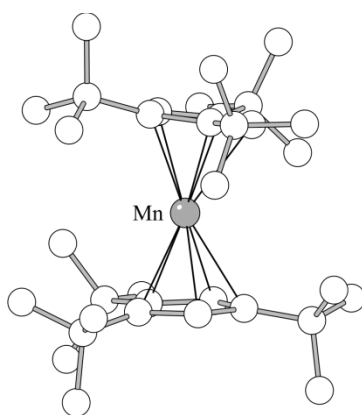
(**27**)

Figure 15. (27) [Mn{1,3,4-(Me$_3$C)$_3$C$_5$H$_2$}$_2$].

Chromocenes

Using the value of the $(\ln[(2S+1)_{HS}/(2S+1)_{LS}])$ ratio as a guide (see beginning of

Section 2), complexes containing Cr^{II} ($\Delta S = \ln(5/3)$) should be among the least likely to

display SCO behavior, and barring orbital symmetry effects (see Section 3),

organometallic compounds of Cr^{II} with π-bound ligands are almost always low-spin

species. For example, whereas $[Mn(Cp^{3i})_2]$ displays SCO behavior, the chromium

analogue $[Cr(Cp^{3i})_2]$ is low spin at all temperatures. $[Cr(Cp^{4i})_2]$ is a rare exception to this

rule and exhibits SCO behavior in the solid state (Figure 1), becoming high spin ($\mu_{eff} =$

4.90 μ_B) at room temperature.[30] In toluene solution at room temperature, however

$[Cr(Cp^{4i})_2]$ is low spin, reflecting the lack of cooperative effects from a solid state lattice.
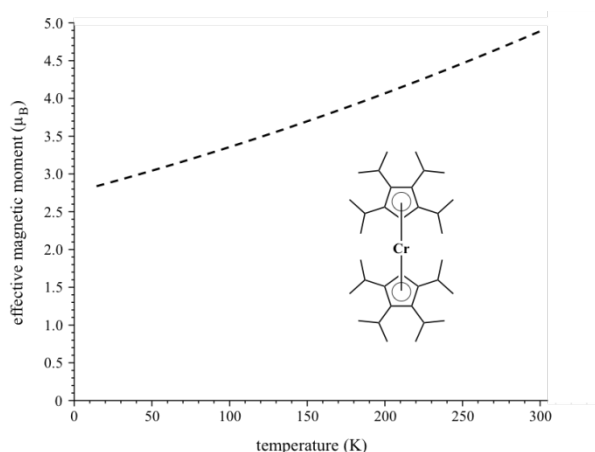
Figure 16. SQUID magnetometry data for $[Cr(Cp^{4i})_2]$ showing its SCO behavior from S
= 1 to S = 2.

Symmetry Effects on Magnetism in Coordination and Organometallic Complexes

Apart from their donor/acceptor differences and steric effects, the relative

orientation of ligands around a metal center can affect the spin state of a complex. The

situations in which this occurs vary, but most commonly it involves changes in the

21

overlap of ligand π orbitals and the metal d orbitals.

The orientation of ligands in coordination compounds such as six-coordinate Fe^{III} Schiff base and porphyrinate complexes is thought to affect the spin states of the metal centers. An instructive example is provided by the imidazole ring alignments in Fe^{III} complexes of several quadridentate Schiff bases.[31] The complex $[Fe(L^1)(HIm)_2]ClO_4$ (Figure 17; **28**) is high spin at room temperature ($\mu_{eff} = 5.89\ \mu_B$); in the solid state, the imidazole ligands are roughly parallel to each other (dihedral angle of 10.2°) and bisect the O–Fe–N angles. In contrast, the two imidazole ligands in $[NaFe(L^2)(HIm)_2(ClO_4)_2]$ (Figure 17; **29**) are twisted by 79° relative to each other, and are oriented along the N–Fe–O diagonals of the equatorial ligand plane. This places them in a near optimum arrangement for competent d_π-p_π Fe–L bonding, and arguably helps stabilize the low-spin state that **29** displays from 4.2–300 K ($\mu_{eff} = 2.10\ \mu_B$). Other examples in which axial ligand orientation is associated with spin state differences are described elsewhere.[20]

(**28**)   (**29**)
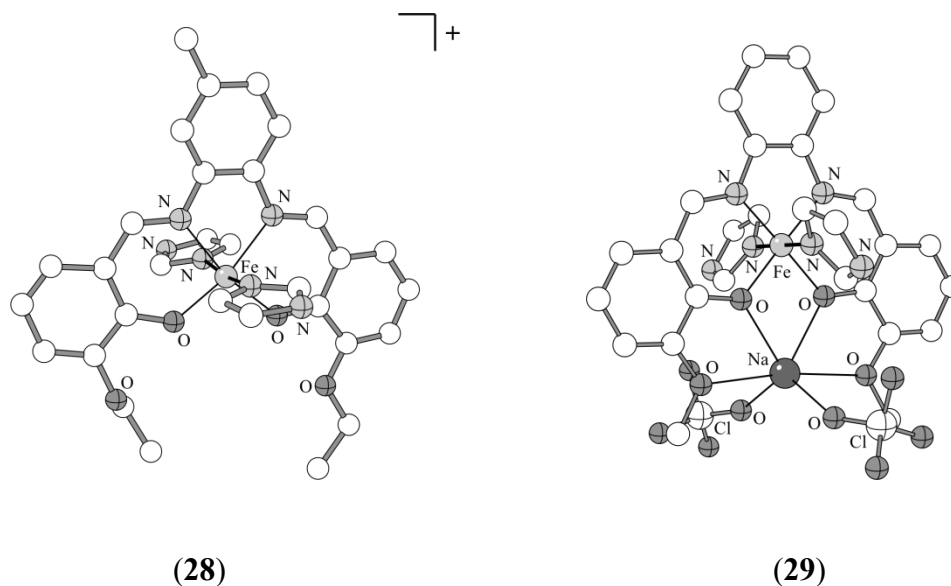
Figure 17. (**28**) $[Fe(L^1)(HIm)_2]ClO_4$. (**29**) $[NaFe(L^2)(HIm)_2(ClO_4)_2]$.

An extensive set of organometallic compounds that displays magnetic behavior controlled by the orientation of the ligands is found among the bis(indenyl) complexes of Cr^{II}. Despite the parallels that are sometimes drawn between the indenyl and Cp ligands, such conformationally controlled magnetochemistry is not shared with metallocenes. The rotational conformation of Cp ligands need not be considered when rationalizing their interactions with d orbitals, nor when analyzing their effect on d-orbital energy levels and splitting.[32]

By replacing the Cp ligand in sandwich complexes with the less symmetrical indenyl anion (Figure 18), symmetry-induced effects can play a role in determining their magnetic properties. Qualitative molecular orbital diagrams[33] illustrate the difference in the interactions between the π orbitals of the indenyl anion and the metal d orbitals in staggered (Figure 19) and gauche (twisted) (Figure 20) forms of [CrInd$_2$].
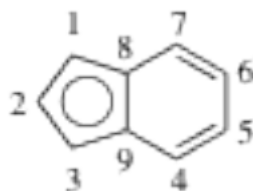
Figure 18. Indenyl ligand with numbering scheme
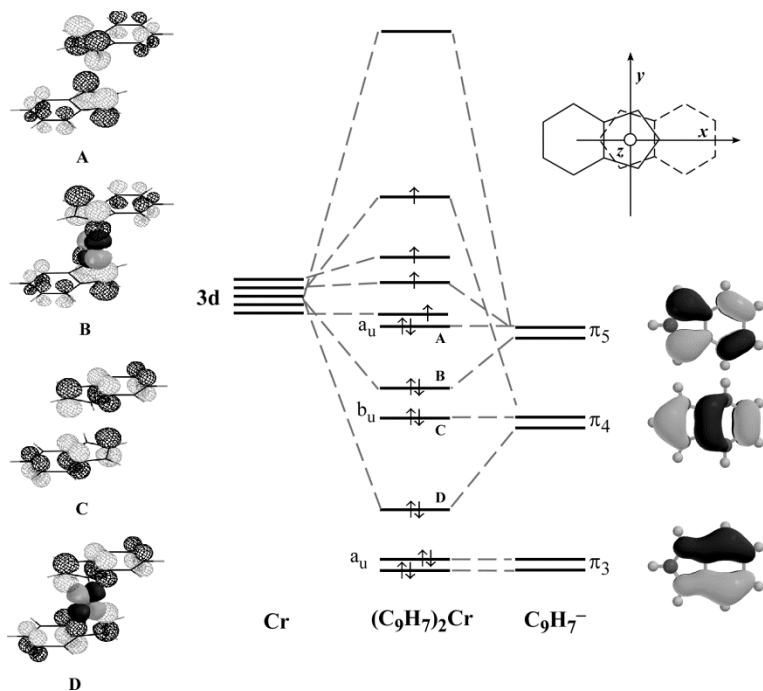
Figure 19. Qualitative molecular orbital diagram for bis(indenyl)chromium(II) with a staggered conformation.
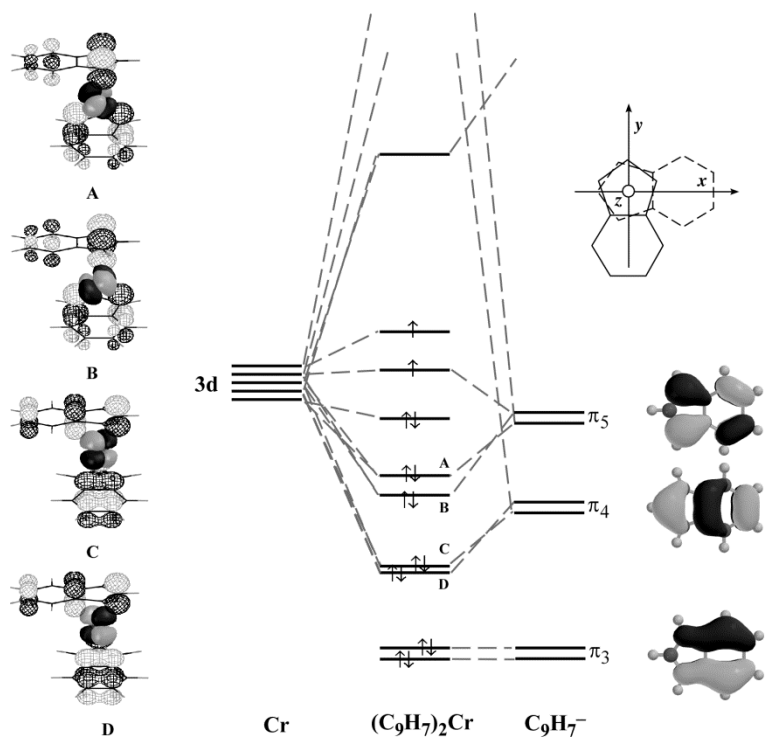
Figure 20. Qualitative molecular orbital diagram for bis(indenyl)chromium(II) with a gauche conformation.

As can be seen in Figure 19, a centrosymmetric (staggered) geometry stabilizes a high-spin state due to the inability of *ungerade* combinations of the indenyl π orbitals to interact with the d orbitals of chromium. The HOMO of the complex is an antibonding combination of a metal d orbital and π_4, with the next three filled orbitals being primarily metal-centered. The a_u and b_u combinations of the π_4 and π_5 orbitals are nonbonding, and the electrons in the ligand π_3 orbitals display limited interaction with the metal 3d orbitals owing to their relative energy differences.

When the indenyl ligands in an [MInd$_2$] complex are rotated to a gauche conformation (Figure 20), the molecular point group is lowered to C_2. Greater mixing of the d orbitals can now occur with the π-orbitals of the indenyl anion. The symmetric and antisymmetric combinations of both the indenyl HOMO (π_5-π_5) and HOMO-1 (π_4-π_4) orbitals are of the proper symmetry to mix with the metal $d_{x^2-y^2}$, d_{z^2}, and d_{xy} (A symmetry) and d_{yz}, d_{xz} (B symmetry) orbitals. This is most clearly seen in the case of the π_4 orbitals, which combine with the d orbitals to form bonding orbitals C and D. The corresponding antibonding combinations are raised far above the energy of a largely non-bonding orbital, which has now become the HOMO. A similar effect occurs with the π_5 orbitals.

Bis(indenyl)chromium(II) complexes with methylated ligands

Bis(indenyl)chromium(II) compounds have been prepared that display a variety of spin state behaviors depending on the substitution of the indenyl ligand. The parent unsubstituted bis(indenyl)chromium(II) is a diamagnetic dimer,[34] but the addition of a single methyl group to the 5-membered ring of the indenyl ligand leads to the isolation of

monomeric species that can have from 2 to 4 unpaired electrons depending on the location of the methyl groups and the overall geometry of the molecule. Evidence for the ability of a staggered bis(indenyl) geometry to stabilize a high-spin state is found in $[Cr(2-MeC_9H_6)_2]$ (Figure 21; **31**), in which the addition of the methyl group in the 2-position leads to the isolation of a purple monomeric complex with a staggered geometry.[35] Magnetic data on **31** shows it to be high spin over all temperatures both in solution ($\mu_{eff} > 4.5\ \mu_B$) and in the solid state (4.3-4.4 μ_B above 25 K). The avg. Cr–C bond for **31** is 2.308(7) Å, typical for high-spin bis(indenyl)Cr^{II} compounds.

Substitution in the 1-position of the indenyl ligand leads to a green monomeric species, $[Cr(1-MeC_9H_6)_2]$, with an eclipsed structure in the solid state (Figure 21; **32**).[35] Magnetic susceptibility measurements indicate that **32** undergoes a slightly incomplete spin transition from 2 to 4 unpaired electrons, starting with a magnetic moment of 2.87 μ_B at 20 K, close to the spin-only value for 2 unpaired electrons (2.83 μ_B). The moment then increases to a value of 4.1 μ_B at 275 K. Solid **32** dissolves in toluene to yield a purple solution, and is found to be high spin ($\mu_B > 4.6\ \mu_B$) over the range from 185–275 K, likely due to the adoption of a staggered geometry in solution, as there are no crystal packing effects to enforce an eclipsed structure. Further evidence of the spin transition can be observed from crystal data, as the avg. Cr–C bond increases from 2.179(9) Å at 105 K (typical for low-spin bis(indenyl)Cr(II) complexes, which generally range from 2.18–2.22 Å) to 2.262(10) Å at 298 K.

(31) (32)
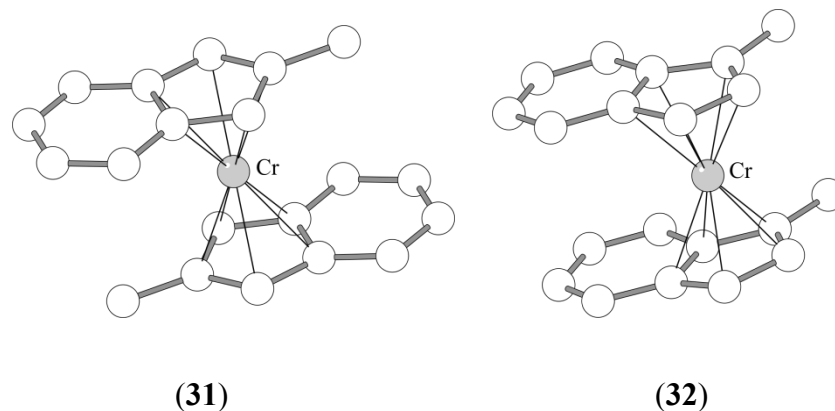
Figure 21. (31) Bis(2-methylindenyl)chromium(II) (staggered). **(32)** Bis(1-methylindenyl)chromium(II) (eclipsed).

Additional methylation of the front side of the indenyl ligand, as in [Cr(1,2,3-Me$_3$C$_9$H$_4$)$_2$], leads to a compound that displays SCO in the solid state despite having a staggered structure.[36] The complex is low spin below 115 K (μ_{eff} = 2.7-3.0 μ_B), but the effective magnetic moment continuously rises to 4.4 μ_B at 225 K, effectively reaching a high-spin state. This SCO behavior is likely due to competition between the electron donating groups on the indenyl ligand that help to stabilize a low-spin state and the symmetry preference for a high-spin configuration. A crystal structure obtained for the compound at 173 K, in the middle of the spin state transition, revealed an avg. Cr–C bond distance of 2.239(11) Å, which is appropriately between the values characteristic of low-spin and high-spin complexes for Cr^{II}.

The presence of methyl substitution on the benzo portion of the indenyl ligand has been examined in the case of [Cr(4,7-Me$_2$C$_9$H$_5$)$_2$]. The monomeric compound has an eclipsed conformation and displays SCO behavior, undergoing an incomplete transition from 2 to 4 unpaired electrons over the temperature range from 110 K (3.1 μ_B) to 300 K (4.0 μ_B).[35] The avg. Cr–C distance in the compound is 2.18(1) Å at 173 K, which is

consistent with a low-spin Cr[II] compound. In solution, the compound has a magnetic moment of 3.4 μ_B at room temperature, reflecting a mostly low-spin compound at room temperature. This suggests that regardless of its exact conformation in solution, the two methyl groups on the benzo ring are enough to keep the compound low spin. Methyl substitution on the 4,7 positions should strongly affect the energy of the HOMO (π_5) and HOMO-2 (π_3) orbitals, and calculations indicate that the energy of the π_3 orbital is raised by roughly 0.3 eV relative to the unsubstituted anion.[36] In such a condition, interaction with the π_4 orbital of the ligand is destabilizing if the molecule remains in the high-spin state. The energy of the entire molecule can be lowered if it transitions to the low-spin state.

The addition of a methyl group to the front side of the ring in addition to the two benzo methyl groups leads to the formation of [Cr(2,4,7-Me$_3$C$_9$H$_4$)$_2$], which displays SCO behavior in both the solid state and in solution but undergoes an incomplete transition in both cases. This is likely caused by the presence of the two structural conformers in the same unit cell with different magnetic properties (a partial unit cell is given in Figure 22). Crystal structure determinations of the complex were obtained at 173 K and 293 K; at 173 K, the avg. Cr–C bond in the eclipsed conformer is 2.168(5) Å, and is statistically indistinguishable from that in the staggered structure (2.172(4) Å). Both of these values are consistent with low-spin Cr[II]. At 273 K, the avg. Cr–C bond in the eclipsed conformer is 2.187(9) Å (Δ_{Cr-C} = 0.019 Å) while that of the staggered structure has lengthened to 2.227(3) Å (Δ_{Cr-C} = 0.055 Å). This asymmetrical lengthening in co-crystallized, otherwise identical molecules provides unambiguous evidence for the operation of relative ligand orientation on the metal spin state.
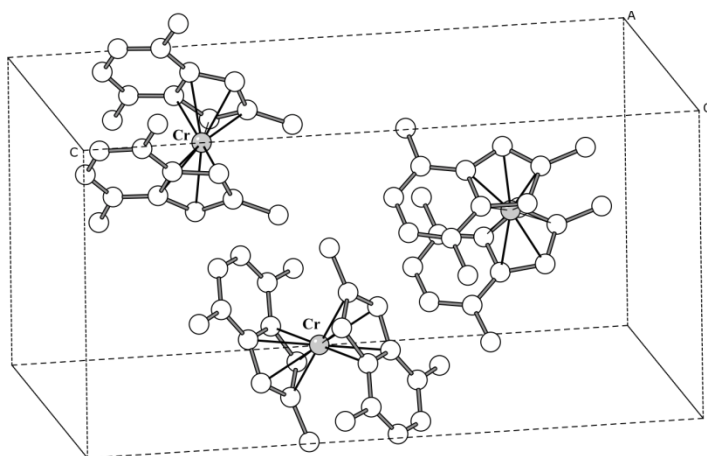
Figure 22. Partial unit cell of bis(2,4,7-trimethylindenyl)chromium(II) showing both staggered and eclipsed conformers.

Complete methylation of the benzo portion of the ligand in the cases of [Cr(2,4,5,6,7-Me$_5$C$_9$H$_2$)$_2$] and [Cr(1,2,3,4,5,6,7-Me$_7$C$_9$)$_2$] leads to monomeric compounds that are nearly entirely low spin in the solid state despite their staggered geometries.[33,37] The pentamethyl indenyl complex remains low spin up until 175 K (2.83-2.86 μ_B), and then appears to begin a spin transition as the moment rises slightly to 3.1 μ_B by 275 K (Figure 23). In solution, the pentamethyl complex shows no signs of SCO behavior from 242–293 K, maintaining a magnetic moment of 3.5 μ_B throughout. Its solid-state structure reveals an avg. Cr–C bond length of 2.17(1) Å at 173 K, indicative of a low-spin Cr^{II} center. The heptamethyl complex remains low spin at all measured temperatures. The fact that these compounds exhibit a low-spin moment despite their staggered geometries demonstrates that the effects of symmetry on spin state are not absolute in the presence of sufficient electronic donation.
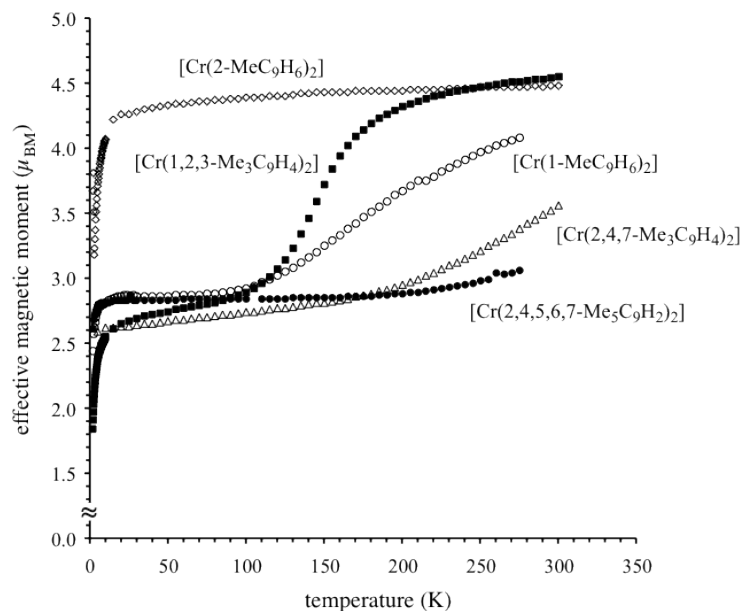
Figure 23. SQUID magnetometry data for methylated bis(indenyl)chromium compounds.

Bis(indenyl)chromium(II) complexes with bulkier substituents

By increasing the steric bulk of the substitution in the 1-position on the indenyl ligand from a methyl group to a *t*-butyl, a staggered geometry will be preferred for steric reasons. The monosubstituted alkyl $[Cr(1-(t-Bu)C_9H_6)_2]$ displays a high-spin state in solution (μ_{eff} = 4.8 μ_B from room temperature down to 183 K).[33] The avg. Cr–C bond distance in the solid state is 2.32(2) Å, also consistent with a high-spin metal center.

The substitution of a trimethylsilyl group in the 1-position of each indenyl ligand produces $[Cr(1-(SiMe_3)C_9H_6)_2]$, whose magnetic properties mirror that of the monosubstituted *t*-butyl complex. It is high spin at all temperatures, with an effective magnetic moment of 4.9 μ_B in solution from room temperature down to 183 K, and a moment of 4.1 μ_B in the solid state from room temperature down to 30 K (Figure 24).
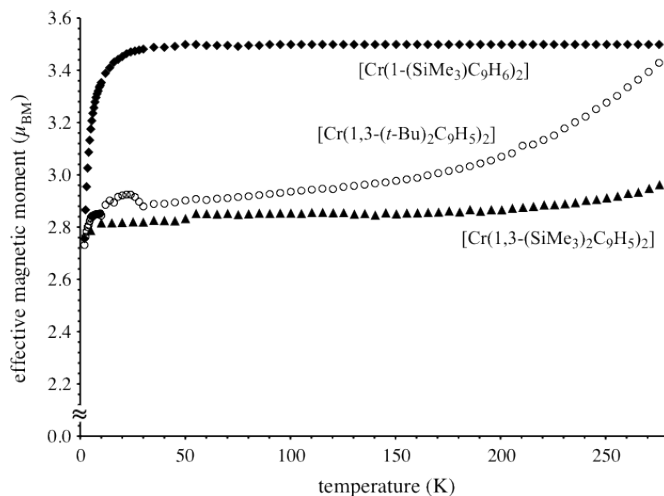
Figure 24. SQUID magnetometry data for bis(indenyl)chromium(II) compounds with *t*-Bu and SiMe$_3$ substitutions.

Addition of a second trimethylsilyl group in the 3-position of the ligand leads to formation of [Cr(1,3-(SiMe$_3$)$_2$C$_9$H$_5$)$_2$]; it has a gauche conformation that reduces intramolecular crowding. With its lowered symmetry (ideally C_2), the gauche conformation favors a low-spin state, both in the solid state (μ_{eff} = 2.8–3.3 μ_B over the range from 10-350 K) and in solution (μ_{eff} = 3.0–3.2 μ_B from 183-300 K). The solid-state structure is also consistent with a low-spin Cr^{II} center (avg. Cr–C bond distance of 2.20(2) Å), despite the large amount of steric bulk on the indenyl ligand that causes the trimethylsilyl groups to be displaced from the ring plane by 0.31 Å.

The analogous *t*-butyl complex [Cr(1,3-(*t*-Bu)$_2$C$_9$H$_5$)$_2$] (Figure 25; **33**) is also monomeric with a gauche conformation,[33] and is low spin in the solid state with an effective magnetic moment of 2.8 μ_B up to 120 K; it rises slightly to 3.4 μ_B by 275 K. In solution **33** displays an incomplete SCO between 213 K (μ_{eff} = 2.9 μ_B) and 300 K (μ_{eff} = 3.6 μ_B), and changes color from green at 213 K to brick red at room temperature. The solid state structure shows an avg. Cr–C bond distance of 2.22(2) Å, which is at the high

31

end of the range observed for low-spin Cr^{II} centers; it is nevertheless considerably shorter than the 2.32(2) Å found in $[Cr(1-(t-Bu)C_9H_6)_2]$.

(33)   **(34)**
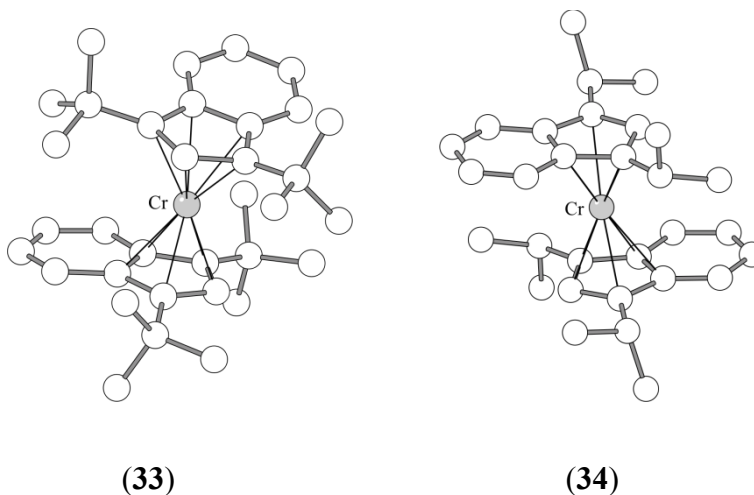
Figure 25. (33) $[Cr(1,3-(t-Bu)_2C_9H_5)_2]$. **(34)** $[Cr(1,3-(i-Pr)_2C_9H_5)_2]$.

The ability of symmetry constraints to influence spin states is also evident when comparing the properties of **33** to its isopropyl analogue $[Cr(1,3-(i-Pr)_2C_9H_5)_2]$ (Figure 25; **34**). The reduced steric strain from the replacement of the *t*-butyl groups with isopropyl groups leads to a molecule with a staggered geometry and approximate C_i symmetry. Appropriately, **34** is high spin at all temperatures, with an effective magnetic moment of 4.4-4.6 μ_B from 20-350 K in the solid state and 4.9 μ_B in solution at room temperature.[38]

32

CHAPTER II

STRUCTURAL FEATURES OF ORGANOMANGANESE COMPOUNDS

Introduction

Compounds of manganese containing M–C bonds present challenges in synthesis and characterization that slowed the development of their chemistry relative to that of neighboring first row transition metals. There are many historical examples of this; for example, the binary carbonyls $Fe(CO)_5$ and $Cr(CO)_6$ were reported in 1891 and 1926,[39,40] respectively, whereas the parent carbonyl of manganese, $Mn_2(CO)_{10}$, was not characterized until 1954 (from a reaction with a yield of 1%).[41] Gilman reported without details the synthesis of phenylmanganese iodide and diphenylmanganese in 1937,[42,43] but even this was almost two decades after Hein described the first of his 'polyphenylchromium' compounds (1919).[44] Structural authentication of organomanganese compounds was also slow in appearing; the polymeric solid state structure of manganocene, $\{Cp_2Mn\}_\infty$, for example, was not described until 1978,[45] 26 years after the sandwich structure of the monomeric ferrocene was confirmed crystallographically.[46] And although a route to pure diphenylmanganese was described in 1959,[47] its structure determination by X-ray crystallography was first reported 50 years later.[48]

There are several reasons for the experimental difficulties encountered in organomanganese chemistry, including such basic issues as differences in the reactivity of manganese halides prepared by various methods,[41] the disparate outcomes of reactions

using different hydrocarbyl transfer agents (e.g., LiPh vs. MgPh$_2$),[47,49] and the changes in reaction products from the presence of even trace amounts of polar solvents.[48] In addition, the high-spin d^5 valence electron configuration found in many complexes of Mn^{II} provides no ligand field stabilization energy, and these compounds display appreciable 'ionic' character; i.e., higher kinetic lability and a broader variety of stereochemistries than compounds of adjacent divalent metal ions. Useful comparisons can in fact be made between complexes of Mn^{II} and those of Mg^{II}, stemming from the similarities of their charge/size ratios ($r_{Mn^{II}}$ = 0.81 Å; $r_{Mg^{II}}$ = 0.86 Å).[50,51] For compounds of Mn^{II}, there is a correspondingly weaker correlation between solution and solid state structures than is true for manganese species in other oxidation states. The discontinuity of the properties of organomanganese(II) complexes relative to other first row counterparts is such that they have been dubbed the 'black sheep' of the organometallic world.[52]

Structural characterization of organomanganese complexes relies on the same battery of techniques (e.g., optical, IR, microwave, NMR and ESR spectroscopy, kinetic and electrochemical methods, mass spectrometric studies, and X-ray crystallography) that are used for compounds of other metals. There are some considerations associated specifically with manganese complexes that are outlined here.

Spectroscopic and Crystallographic Characterization

Nuclear Magnetic Resonance Spectroscopy

As with other organometallic compounds, both ^{1}H and ^{13}C NMR spectroscopy are extensively used in the characterization of organomanganese compounds. The ^{55}Mn nucleus is quadrupolar (100% nat. abund., $I = {}^5/_2$), however, meaning that even in

diamagnetic compounds the signal of atoms directly bound to the metal will typically be broad and not well-resolved. This of course principally affects ^{13}C NMR spectra, and can interfere with the observation of intermolecular exchange processes. One way this has been circumvented in the case of metal carbonyls is with the use of ^{17}O NMR spectroscopy, as ^{55}Mn–^{17}O coupling is not observed in Mn–CO linkages. In the case of $CH_3Mn(CO)_5$, for example, only one broad resonance is observed for the carbonyl groups in its ^{13}C NMR spectrum;[53] in the room temperature ^{17}O NMR spectrum, however, two resonances corresponding to 4 equatorial and 1 axial carbonyls are observed, demonstrating that exchange is not occurring.[54] Other uses of ^{17}O NMR spectroscopy have been found in the study of demetalation reactions and polymetallic complexes.[55-58]

Paramagnetic NMR (principally ^{1}H and ^{13}C) has been used in the study of various organomanganese complexes,[59,60] and in the case of manganocenes, it is possible to observe mixtures of low- and high-spin species in solution.[61,62] In many reports of paramagnetic organomanganese complexes, however, NMR spectra are not reported, and often it is not clear whether attempts were made to observe a signal. Studies with ^{55}Mn NMR spectroscopy are less common, and owing to the large quadrupole moment of ^{55}Mn, resonances with line widths of several kHz can be encountered.[63] A substantial body of data has been accumulated, however,[63-66] and DFT calculations have been used with some success in correlating ^{55}Mn NMR chemical shifts.[67] Solid state ^{55}Mn NMR has only rarely been used in the study of organometallic complexes,[68,69] but the technique has been shown to be highly sensitive to the local environment of the manganese center, and it may be a promising characterization tool when other methods such as X-ray crystallography are not applicable.

X-ray Crystallography

By far the premier method for the determination of organomanganese structures has been single crystal X-ray crystallography; powder diffraction has been used to a much smaller extent.[70] As with other areas of manganese chemistry with M–C bonds, crystal structures were slow to appear; the first was for $Mn_2(CO)_{10}$ in 1957,[71] and the second not until 1963 (that of $CpMn(CO)_3$,[72] although preliminary details were released in 1960).[73] Since those early days, the number of crystallographically characterized compounds has increased steadily, and the total now exceeds 3000. Such studies have been critical to clarifying the nature of M–C bonding, and serve as the major focus of this review. Despite its value in locating the positions of hydrogen atoms bound to metals, the necessity for large crystals and the scarcity of appropriate radiation sources has meant that neutron diffraction studies have rarely been reported for organomanganese compounds.[74-76]

General Considerations for Manganese–Carbon Bonds

A summary of crystallographically established Mn–C and Mn–Mn bond lengths is given in Table 1; the distributions are discussed in more detail below.

Mn–C Bonds. The distribution of manganese-carbon single bonds is centered at 1.84 Å, with an esd of 0.10 Å (Figure 26); there is substantial tailing on the long end, out beyond 2.5 Å. It should be noted that metal-carbonyl bonds are by far the most common Mn–C bond types, representing over 94% of the total. The length of terminal manganese–carbonyl bonds is fairly tightly clustered around 1.81 Å (esd of 0.04 Å) and dominates the distribution. Excluding terminal or bridging M–CO bonds, and terminal cyano

ligands, the average Mn–C bond length increases to 2.11 Å, although the resulting spread

is clearly multimodal (Figure 26). Many complexes containing isonitrile ligands are

found in the peak centered around 1.9 Å; many alkyls and aryls are found in the 2.1–2.2

Å range.

Table 1. Distribution of Mn–C and Mn–Mn Bonds in Organometallic Compounds

Bond Type	Mean Length (Å)	Range (Å)
Mn–C	1.84	1.6–2.6
Mn–C (without M–CO bonds)	2.11	1.7–2.5
Mn=C	1.87	1.7–2.1
Mn≡C	1.67	1.6–1.7
Mn–Mn	2.85	2.3–3.2
Mn=Mn[a]	2.39	
Mn≡Mn[b]	2.17	

[a]Only two compounds known. [b]Only one compound known.
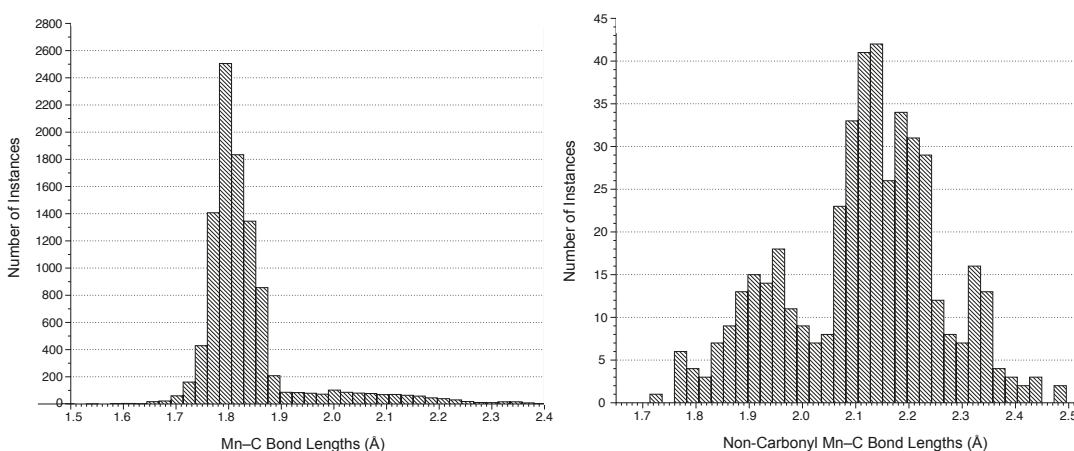
Figure 26. Spread in manganese-carbon single bond lengths; on the left, including M–CO bonds; on the right, with M–CO and M-cyano bonds omitted.

37

Although there are crystal structure determinations that report Mn–C bonds

shorter than 1.70 Å, including some less than 1.50 Å,[77,78] many such structures are

afflicted with disorder, or are room temperature studies in which the bond distances are

artificially shortened because of high thermal motion. This is especially true of those that

list Mn–C bonds of 1.60 Å or less, and such studies should be viewed with caution. At

the long end of the range (up to ~2.65 Å) are weak contacts that involve bridging ligands

and special electronic situations; examples are found in the semibridging carbonyl

Mn···C contact at 2.648 Å in the heterobimetallic complex $CpMoMn(CO)_3(\mu\text{-}CO)(\mu\text{-}\eta^2\text{-}$

$pyS)(\mu\text{-}\eta^1\text{-}pyS)$ (Figure 27; **35**)[79] and the Mn···C3 distance in $Mn_2(CO)_8[\mu\text{-}\eta^2\text{-}C_3H_3NEt_2]$

(Figure 27; **36**) at 2.56 Å.[80] Constrained geometries can also lead to long metal-carbon

bonds; the hemiporphyrazine (Figure 27; **37**)[81] displays average Mn–C distances of 2.481

Å and agostic C-H interactions with the metal. The η^1-coordinated cyclopentadienyl

ligand in $Cp_2Mn\{HN=C(NMe_2)_2\}_2$ (Figure 27; **38**) is at 2.356 Å,[82] and among the longest

carbonyl alkyl bonds is that of $(CO)_5Mn\text{--}CH_2CH=CHCOOPh$ (Figure 27; **39**) at 2.214

Å.[83]
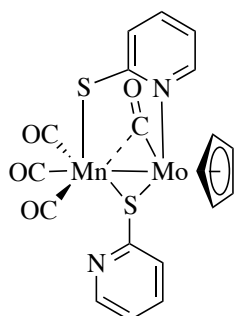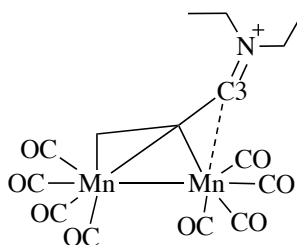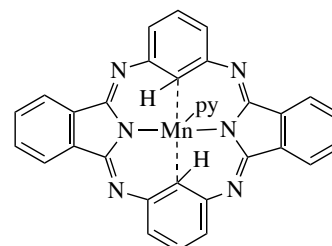
(**35**)   (**36**)   (**37**)
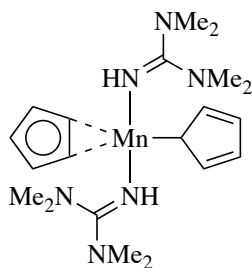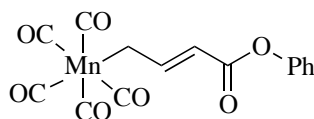
(38)   **(39)**

Figure 27. Structures of selected organomanganese compounds exhibiting noteworthy Mn-C bond lengths.

Mn=C Bonds. The length of manganese-carbon double bonds averages to 1.87 Å, but this number is of limited significance because the distribution of bond distances is at least bimodal (Figure 29). The most clearly defined maximum, centered at 1.77 Å and extending from 1.68 Å (found in (**40**); Figure 28) to about 1.81 Å, consists exclusively of conjugated Mn=C=C units (e.g., vinylidenes, diylidenes). Only a few such species are found at longer lengths (e.g., in (**41**; Figure 28), at 1.872 Å). The longer bonds have apparent maxima at ca. 1.89 Å and 1.96 Å, although the compounds are not cleanly separated into defined structural fragments. In general, however, the longest bonds are found in complexes that contain multiple ligands with strong *trans* influence; especially common are those with 4 CO ligands (e.g., 2.038 Å in **42**; Figure 28)[84] or $(CO)_3/(PR_3)_2$ ligands (e.g., 2.004 Å in **43**; Figure 28).[85] The middle range of distances is dominated by complexes containing the more weakly donating $CpMn(CO)_2$ or $CpMn(CO)PR_3$ fragments. It is clear that the M=C bond length is highly context-specific.
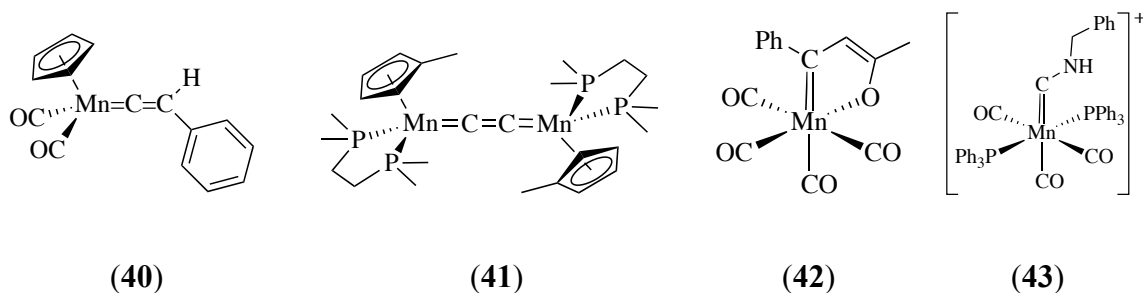
Figure 28. Structures of selected organomanganese compounds exhibiting noteworthy Mn=C bond lengths.
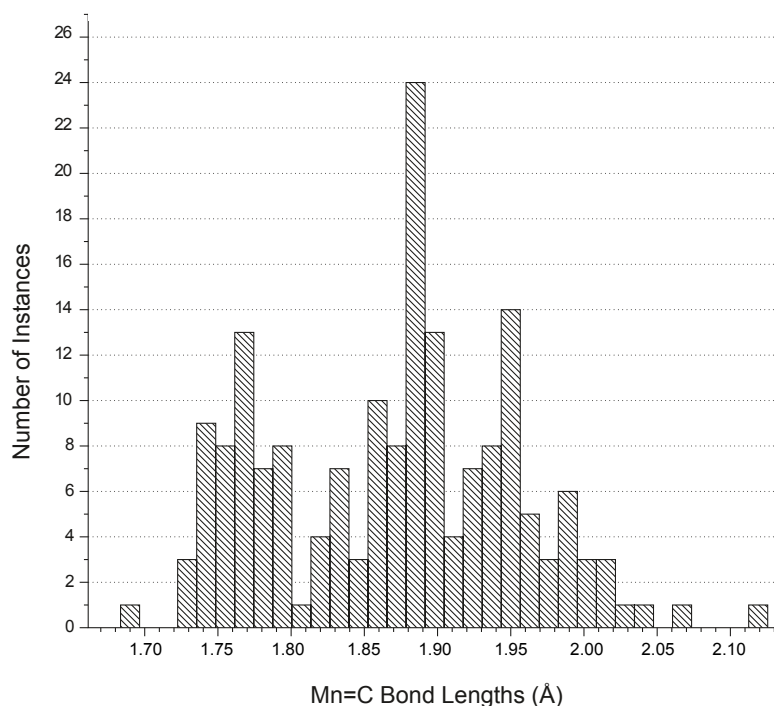
Figure 29. Spread in manganese-carbon double bond lengths.

Mn≡C Bonds. The distribution of manganese-carbon triple bond lengths is grouped around 1.67 Å; both the shortest known example, [(MeCp)(dmpe)Mn≡CCH₂CH₂C≡Mn(dmpe)(MeCp)][PF₆]₂, (Figure 30; **44**)[86] and the longest ([[(MeCp)(dmpe)Mn≡C–C≡Mn(dmpe)(MeCp)][PF₆]₂) (1.734 Å) (Figure 30; **45**)[87] are dicationic, dinuclear complexes with Mn^{III} centers. Two independent molecules are

found in the unit cell of (**44**), with Mn≡C bonds of 1.638 Å and 1.653 Å, which indicates the amount of variation that can ascribed to packing forces alone.
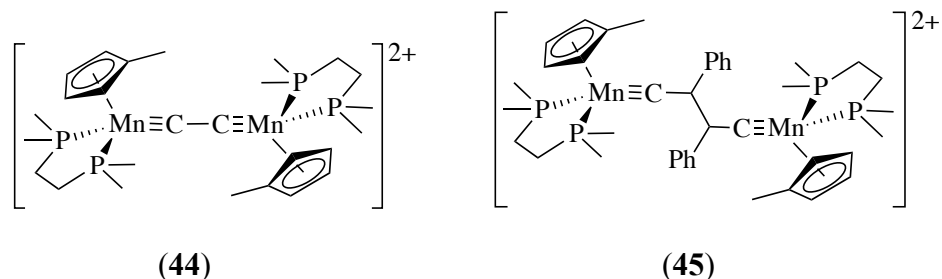
Figure 30. Structures of selected organomanganese compounds exhibiting noteworthy Mn≡C bond lengths.

Mono(cyclopentadienyl) compounds

The largest class of cyclopentadienyl manganese compounds is the cymantrenes (Cp′Mn(CO)$_3$) and their derivatives. These Mn^I compounds are 18e$^-$ species that are extraordinarily stable and have classic three-legged piano stool geometry. The Cp′Mn(CO)$_3$ unit can also serve as an organometallic substituent on an otherwise inorganic complex (Figure 31; **46**); there are more than 230 crystallographically characterized molecules for which such units (or closely related species such as (indenyl)Mn(CO)$_3$) are the only organometallic fragment. A related and even larger class of structurally authenticated molecules (approximately 320 examples) consists of those in which the cyclopentadienyl manganese dicarbonyl fragment, –MnCp(CO)$_2$, is a substituent on a complex (Figure 31; **47**); the 16e$^-$ fragment (Cym′) is isolobal with singlet methylene (:CH$_2$) and the methyl cation (CH$_3^+$). In both classes of compounds, the structural features involving the metal do not vary greatly.

41

(46)   **(47)**
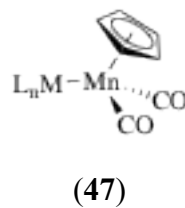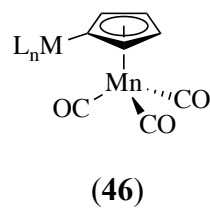
Figure 31. Cymantrene as an organometallic substituent (**46**) and as $16e^-$ fragment bound to a metal (**47**).

As mentioned above, $(CpMn(CO)_2)$ is a $16e^-$ unit capable of accepting $2e^-$ ligands. Likewise, the CpMn subfragment itself is a $12e^-$ moiety capable of coordinating three $2e^-$ donor ligands. In addition to carbonyls, various other donor ligands such as phosphines, nitrosyls, isonitriles, and carbenes can coordinate to the Mn center to yield cymantrene-like compounds $CpMn(CO)_{3-x}L_x$ ($x = 0$–3). Of these carbonyl replacements, phosphines are by far the most common, but are usually only structurally interesting as sources of steric bulk.

In nearly all cymantrene-like compounds $(CpMnL_3)$, the Mn-Cp interaction and overall geometry is relatively unchanged from the basic three-legged piano stool configuration. Examples of this include $(MeCp)Mn(CO)(PPh_3)_2$ (Figure 32; **48**)[88] and $(MeCp)Mn(CNBPh_3)(P(OPh)_3)(NO)$ (Figure 32; **49**).[89] In **48**, the average Mn–C(Cp) bond length is 2.150 Å, and the Mn–C(O) bond is 1.749 Å, both very near the averages observed in cymantrenes. In **49**, the non-Cp ligands display interligand angles closer to 90° rather than the 109.5° expected for an ideal tetrahedral arrangement. Such angular compression is typical for $CpMnL_3$ complexes. The average Mn–C(Cp) distance is unexceptional at 2.147 Å; the Mn-P bond of 2.213 Å, the Mn–C≡N bond length of 1.929 Å, and the C-N distance of 1.142 Å compare favorably to the distances in other $CpMnL_3$ complexes, where the averages are 2.222, 1.920 and 1.155 Å, respectively.

42

(48)   (49)
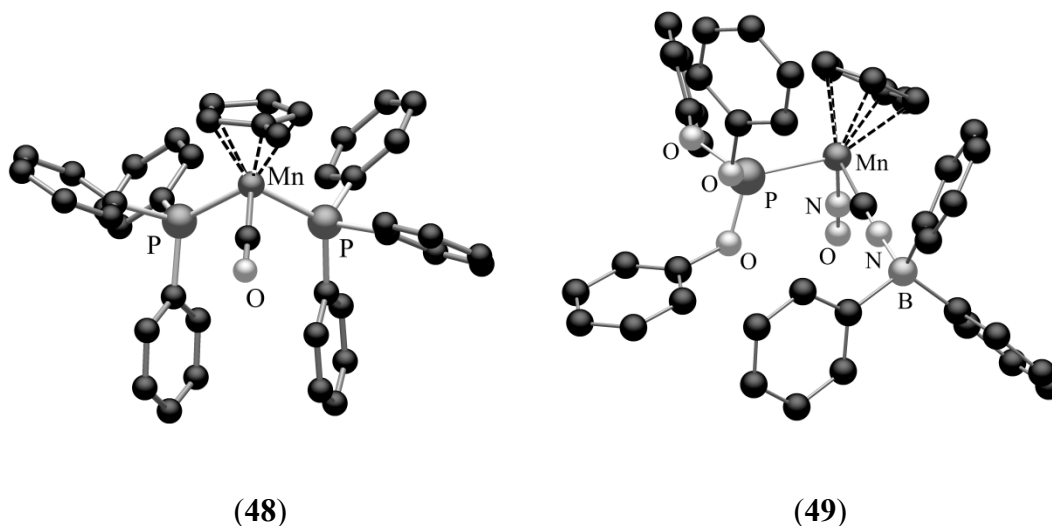
Figure 32. Solid state structures of (**48**) and (**49**).

The average Mn-C(Cp) distance for derivatives of cymantrene that contain either one or no carbonyls is 2.156 Å, which is nearly identical to that found in with the Cym′ fragment itself (2.145 Å). There exist complexes that display deviations from these averages, but regardless of the donor ligands that replace CO, none stray more than 0.1 Å from the mean. Large deviations in the Mn-Cp interaction are only observed when the compound is actually no longer that of the classic $(\eta^5\text{-Cp})Mn^IL_3$ type, such as when the cyclopentadienyl ligand is protonated to generate 5-*exo*-$(MeCp)Mn^0(CO)(NO)(PPh_3)$ (Figure 33; **50**),[90,91] or when a Mn^{II} center is present, such as in $(MeCp)(tmeda)Mn^{II}(C{\equiv}CPh)$ (Figure 33; **51**).[92]

(50)   **(51)**
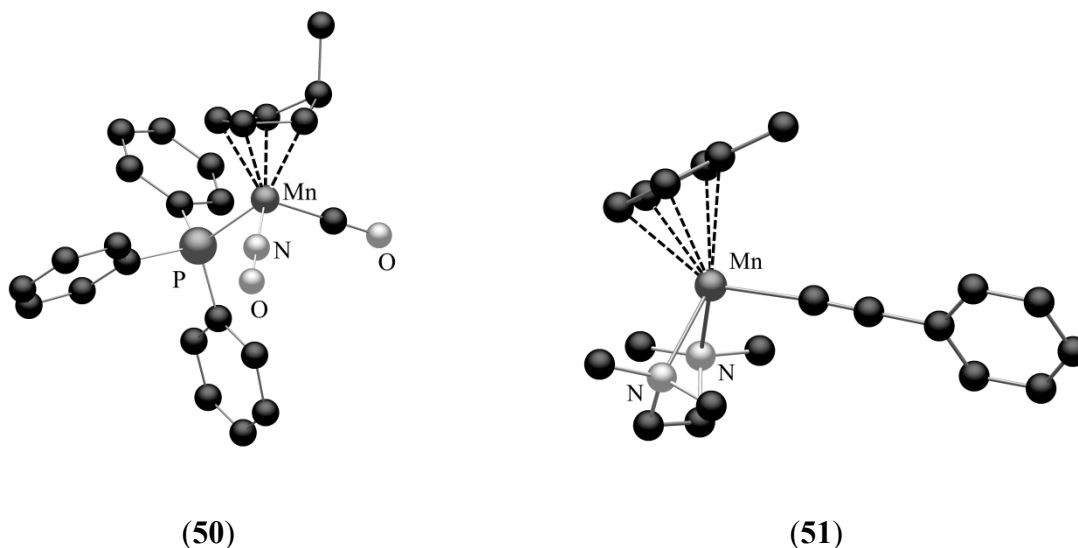
Figure 33. Solid state structures of (**50**) and (**51**).

Compound **50** is one of two products isolated from the reaction of

[CpMn(CO)(NO)(PPh$_3$)]PF$_6$ with LiCH$_3$ and NaBH$_4$; the Cp ligand is methylated by the

alkyl lithium reagent. The geometry around the Mn is roughly tetrahedral with slightly

distorted L-M-L bond angles (L $\neq$ Cp) that range from 93.9° to 102.8°. This is similar to

ranges observed in most cymantrene-like compounds that display the classic piano stool

structure; however, the protonation of the Cp ligand causes the carbon on the ring bound

to the methyl group (C1) to shift upward from the C$_5$ ring plane by 0.53 Å, and the plane

created by C2, C3, C4 and C5 forms an angle of 147° with the plane created by C1, C2,

and C5. The result is a complex with an η^4-coordinated cyclopentadiene ligand (Mn–C =

2.126 (avg.)); the Mn-C1(Cp) distance of 2.692 Å is non-bonding. Besides being a

unique derivative of cymantrene, (**50**) also represents a rare example of a formally Mn^0

organometallic complex (other than those for which M–C interactions involve only

carbonyl ligands) that has been structurally authenticated.

Compound (**51**) was prepared by the reaction of (MeCp)$_2$Mn(tmeda) with PhC≡CH or PhC≡CSnMe$_3$ in THF at room temperature, resulting in the displacement of a MeCp ligand by the acetylene. The geometry of the ligands around Mn in (**51**) is similar to that of many cymantrene-type compounds with a near tetrahedral arrangement of the ligands, but the bond lengths are considerably different. The average Mn-C(Cp) bond length of 2.514 Å is considerably longer than those for cymantrene derivatives; this is a consequence of the high spin Mn^{II} metal center, which typically supports bonds that are elongated in comparison to those in Mn^{I} compounds. The bond length differences are similar to those observed in high- and low-spin manganocenes.

The gap in bond lengths due to oxidation and spin state in mono(cyclopentadienyl)manganese complexes is evident in Figure 67 below, where all compounds with a Mn-C(Cp) distance of less than 2.24 Å are either Mn^{I} species or low spin ($S = 1/2$) Mn^{II}. There are also a much larger number of CpMn^{I} complexes known owing to the fact that Mn^{I} offers ligand field stabilization to form stronger metal–ligand bonds.
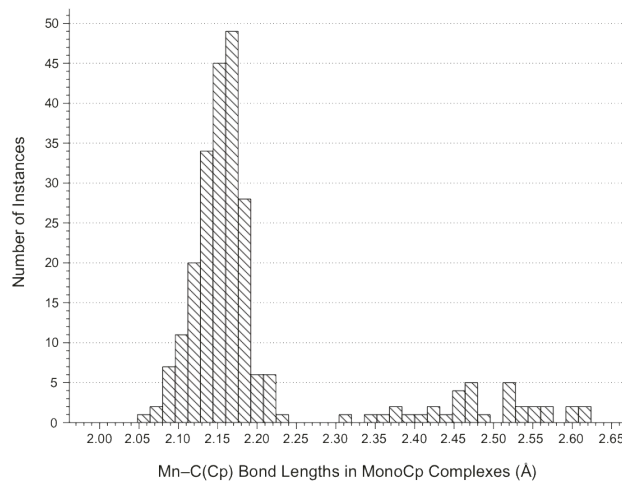
Figure 34. Spread in Mn-C(Cp) distances in mono(Cp) manganese complexes.

Pi-bound systems

Other than the CpMn(CO)$_2$ fragment, the first example of a CpMn complex bound to a multihapto hydrocarbyl complex was (η^5-MeCp)Mn(η^6-7-exo-phenylcyclohepta-1,3,5-triene) (Figure 35; **52**)[93]. The compound was synthesized by irradiating a mixture of (MeCp)Mn(CO)$_3$ and 7-phenylcyclohepta-1,3,5-triene with UV light to produce both the *endo* and *exo* isomers; a crystal structure was obtained for the *exo* species. The two rings are parallel (Figure 35), and the average Mn-C bond lengths of 2.123 Å for the cyclopentadienyl and 2.101 for the cycloheptatriene ligand are in the range expected for Mn^I complexes.
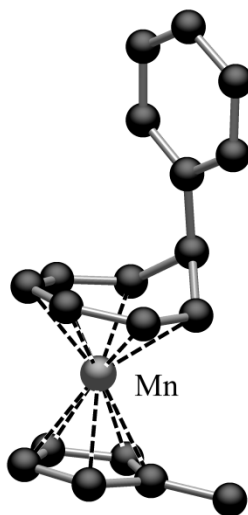
Figure 35. Solid state structure of (**52**).

A set of similar sandwich complexes **53**, **54**, **55** was synthesized by the same method of irradiating a cymantrene in the presence of cyclooctatetraenes (COT) to produce Mn(η^5-C$_5$R$_4$)(η^6-C$_8$X$_8$) (R = H in (Figure 36; **54**), and Me in (Figure 36; **53**) and (Figure 36; **55**); X = F in **54** and **55**, and H in **53**). The complexes are structurally

analogous, which is somewhat surprising given the enhanced stability of the perfluorinated species both thermally and in air. Metallotropic shifts can be observed with NMR spectroscopy for the nonfluorinated compound, but neither perfluorinated species displays fluxional behavior in their ^{19}F NMR spectra.

(53)   **(54)**   **(55)**
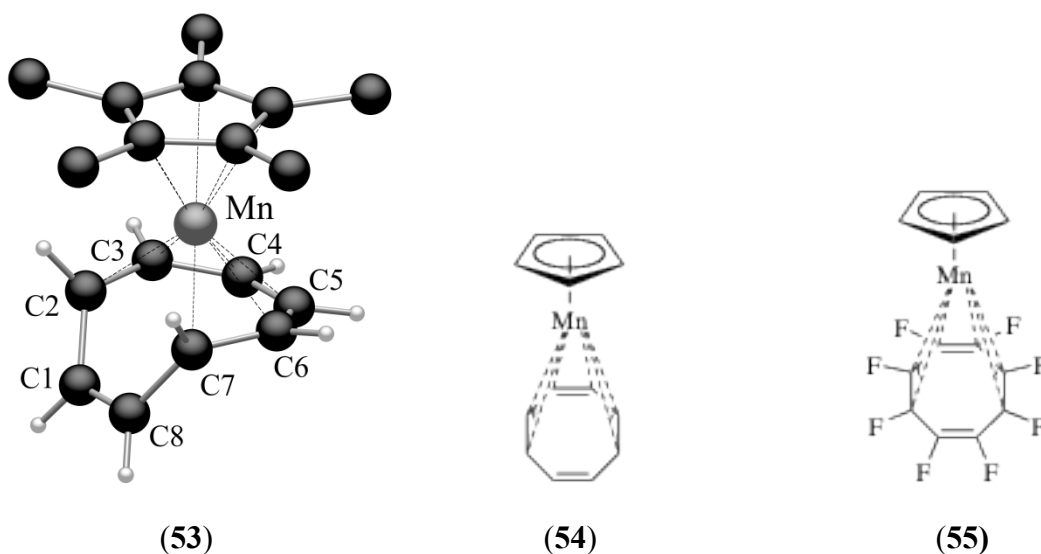
Figure 36. Solid state structure of (**53**) and analogous structures for (**54**) and (**55**).

CpMn(C$_6$H$_5$R) compounds can be prepared by the reaction of MnCl$_2$ and one equivalent of NaCp to produce the mono(cyclopentadienyl) manganese chloride that can then be further treated with phenylmagnesium bromide in THF to produce a mixture of CpMn(C$_6$H$_6$) (**56**), CpMn(C$_6$H$_5$-Ph) (Figure 37; **57**), and biphenyl.[94] The structures of (**56**) and (**57**) were both determined with X-ray crystallography, which revealed a large amount of disorder in (**56**) due to the interchangeability of Cp and benzene in the complex. The structure of (**57**) demonstrates that the average Mn-C distance to the benzene is shorter than that to the cyclopentadienyl ligand (2.106 Å and 2.124 Å, respectively).
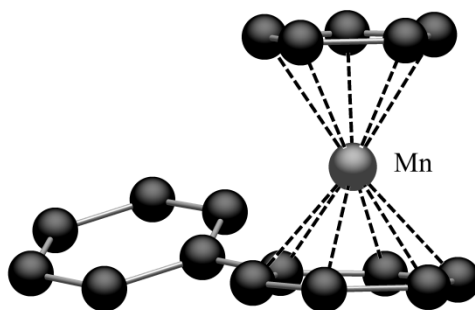
(**57**)

Figure 37. Solid state structure of (**57**).

Other mono(cyclopentadienyl) complexes

Photolysis of $CpMnL_{3-x}L'_x$ ($x = 0-3$; L = CO; L′ = PR$_3$) complexes in the presence of silanes can result in the coordination of Mn to the silane or to a Si-H bond on the silane in the form of a three-center two-electron bond.[75,95,96] Stronger electron donating groups on coordinated phosphines, or the presence of two coordinated phosphines and no carbonyls, helps to facilitate Si-H bond cleavage and the formation of Mn^{III} silyl hydride complexes, as in CpMn(dmpe)(H)(SiHPh$_2$) (Figure 38; **58**).[96] Although the hydrogen atoms could not be located in the X-ray structure, the geometry around the Mn and silicon atoms provides a strong argument for the formation of a manganese hydride. The coordination around the Mn appears to be that of a 4-legged piano stool with one of the legs missing where the hydrogen atom would be. This is evidenced by the large difference in Si-Mn-P bond angles, one of which is 86.4° while the other is 115.8°.

Without the presence of the extra phosphine ligand in place of CO, or the electron withdrawing groups on the phosphine, incomplete oxidative addition during the photolysis reactions can result in the formation of three-center two-electron bonds, as in

the compound $(MeCp)Mn(CO)(PMe_3)(H)(SiHPh_2)$ (Figure 38; **59**).[75] A neutron

diffraction study confirmed the locations of the hydrogen atoms and the appropriateness

of the delocalized bonding description.[97]
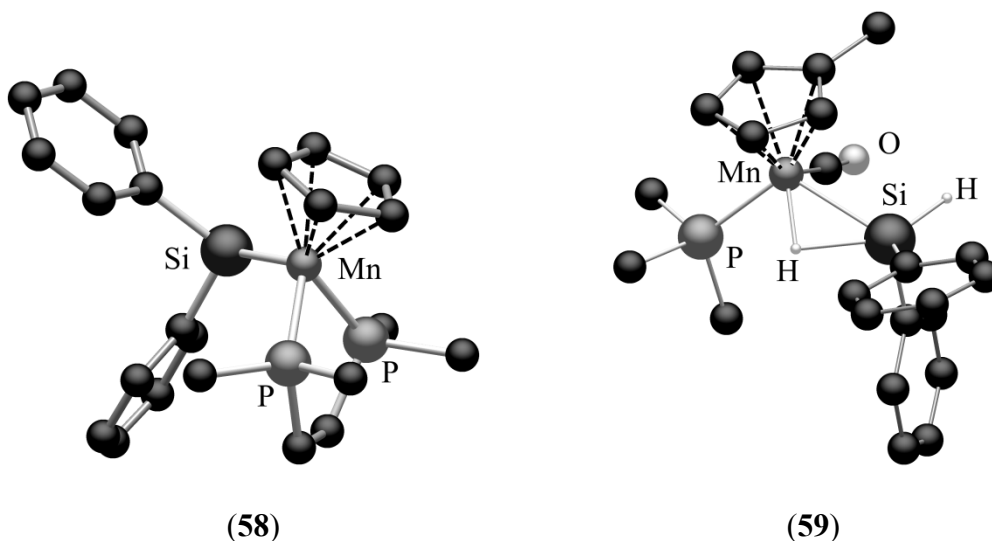
Figure 38. Solid state structures of (**58**) and (**59**).

Despite the vast amount of chemistry known for complexes of the form

[CpMnL$_x$], there are relatively few Mn compounds of the form [CpMnL$_y$X] for

comparison. Some early examples of these types of complexes were dimeric

CpMn(halide) complexes with coordinated bases. These compounds can be prepared by

allowing MnX_2 (X = Cl, Br, I) to react with [MeCp]$^-$ in the presence of a coordinating

base such as triethylphosphine.[98] The resulting complexes are dimeric with bridging

halides and a pseudotetrahedral geometry around the Mn centers, as observed in

[CpMnCl(PEt$_2$)]$_2$ (Figure 39; **60**). The most striking difference between these

compounds and those of the type CpMnL$_x$ is in the Mn-C and Mn-P distances. The

average Mn-C(Cp) bond length in (**60**) is 2.484 Å, considerably longer than any other

Mn-C bond lengths mentioned in this section, most of which are less than 2.2 Å. The

Mn-P bond length of 2.567 Å is also considerably longer than the average Mn-P bond in cymantrene-like compounds, where the average is only 2.22 Å. This may seem strange given that the manganese centers are not sterically crowded or coordinatively saturated, but makes sense when you consider we are now looking at a Mn^{II} species that is high spin. The 5 unpaired electrons distributed throughout the d orbitals prevent any ligand field stabilization, and lead to longer bonds. The bromine and iodine analogs of (**60**) have also been crystallographically characterized and are isostructural in their geometries and Mn-C and Mn-P bond distances.
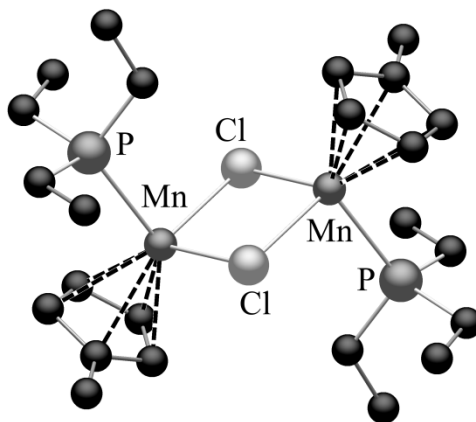
Figure 39. Solid state structure of (**60**).

Manganocenes and related compounds

Manganocenes

In comparison to the metallocenes of other first row transition metals, manganocenes are unique in that they can adopt either a high ($S = 5/2$) or low ($S = 1/2$) spin state based on the steric and electronic effects of the substituent(s) on the cyclopentadienyl ligand. The availability of two potential spin states produces distinct

structural characteristics with respect to Mn–C distances. Manganocenes with a $S = 5/2$ spin state possess longer M–C bonds than are typically seen for metallocenes, and with only a few exceptions are usually in the range 2.30–2.52 Å. The compounds at the short end of this range are typically triscyclopentadienyl manganese compounds or manganocenium ions. The bulk of unsolvated, substituted manganocenes display Mn–C bond lengths of 2.35-2.42 Å. In contrast, low spin compounds have considerably shorter Mn-C bonds that range from 2.09-2.25 Å. The histogram in Figure 40 illustrates the sharp division between high- and low-spin manganocenes; there are no known Mn-C distances in the range from 2.25–2.31 Å.
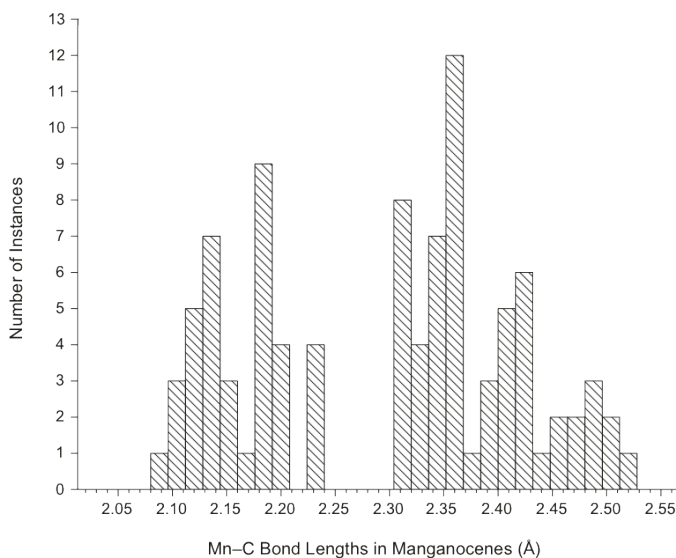
Figure 40. Spread of Mn-C distances in Cp_2Mn complexes.

These compounds are generally prepared by the salt metathesis reaction of $MnBr_2$ and the sodium or potassium salt of the desired substituted cyclopentadienyl ring (Equation 1).[29,99]

$$MnX_2 + 2\,MCp \rightarrow MnCp_2 + 2\,MX \quad (X = Cl, Br, I\,;\, M = K, Na) \qquad \text{(eq. 1)}$$
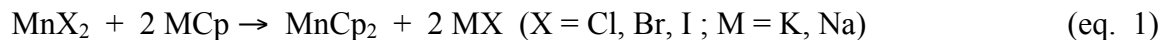
Manganocene, bis(cyclopentadienyl)manganese(II) (Figure 41; **61**) was not crystallographically characterized until 1978,[45] a consequence of its polymeric nature and the difficulty of obtaining suitable crystals.[100] Unlike other first row metallocenes, which have simple sandwich structures with parallel Cp rings, each Mn center in the unsubstituted manganocene is coordinated to 3 cyclopentadienyl ligands. One ligand is terminally bound in an η^5 fashion, with an average Mn-C bond distance of 2.411 Å. Each non-terminal Cp ligand is bridging between two Mn centers, with η^1-coordination to one Mn and η^2-coordination to the other Mn; this forms an infinite polymeric structure. The average Mn–C bond lengths are 2.441 Å and 2.438 Å for the η^1- and η^2-coordinated Mn–Cp interactions, respectively. The Mn$\cdots$Mn separation is relatively large at 5.38 Å. The compound has a high spin ground state ($^6A_{1g}$) with a magnetic moment of 5.97 μ_B at 19 °C, and displays antiferromagnetic behavior as a crystalline solid, the coupling arising from interactions between the polymeric chains.[100]
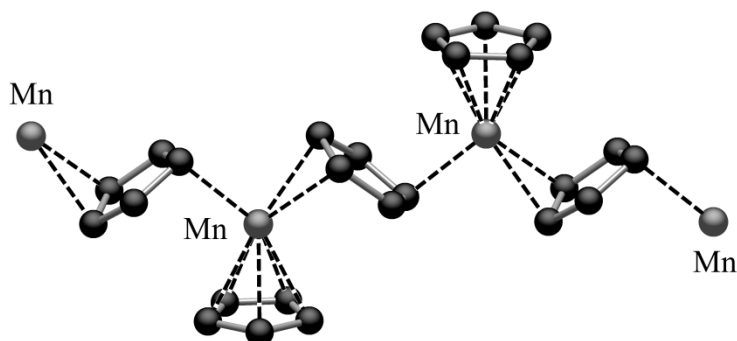
Figure 41. Solid state structure of (**61**).

The presence of a methyl group on each of the Cp ligands in 1,1´-dimethylmanganocene (Figure 42; **62**) produces a classic sandwich structure with two differing geometries, depending on the high- or low-spin state of the Mn^{II} center.[101] Both of these structures were resolved using gas phase electron diffraction;[102] the structural information supported previously acquired magnetic data that indicated that the two species were in a spin-state equilibrium at room temperature.[25] The high spin species exhibits an average Mn–C bond length of 2.433 Å, whereas the low-spin species displays an average of 2.144 Å. The large difference is driven by the ligand field stabilization energy and stronger covalent interaction present in the low spin species.
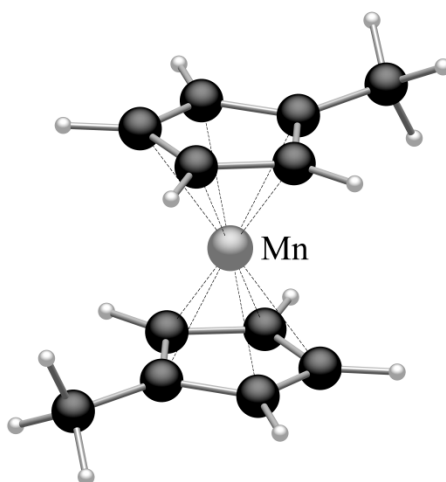
Figure 42. Gas-phase structure of dimethylmanganocene (**62**).

Decamethylmanganocene (Figure 43; **63**) is also a monomeric sandwich complex, but it is completely low spin at all temperatures.[103] It has an average Mn-C bond length of 2.112 Å, considerably shorter than the Mn-C distances in the high-spin form of the parent manganocene, but consistent with the superior donor properties of the Cp* ring compared to unsubstituted Cp.
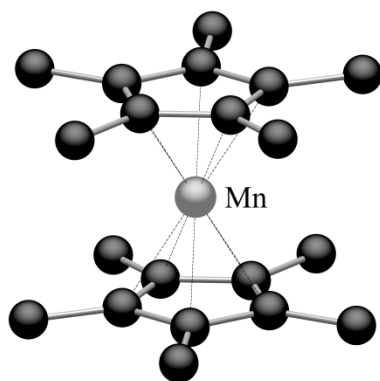
Figure 43. Solid state structure of decamethylmanganocene (**63**).

In general, the electronic properties of the cyclopentadienyl rings have a greater effect on the structures of substituted manganocenes than do possible steric effects provided by the ligands. The spin state of the complexes is usually determined by the donor abilities of the Cp ligands; more electron-donating groups favor the low spin state, even if the rings are somewhat more bulky (e.g., Cp* vs. Cp). There is a point, however, at which steric strain can overcome the donor properties of the Cp ligands by limiting the approach of the rings to the metal center. Examples of this and descriptions of both structures and magnetic properties for substituted manganocenes are discussed in detail in Chapter I.

The presence of coordinated solvents can strongly influence manganocene structures. For example, the polymeric structure of (**61**) can be disrupted by THF to yield the monomeric complex $Cp_2Mn(thf)$ (Figure 44; **64**).[104] There are now only two Cp rings coordinated to the Mn center, both in an η^5 fashion. The complex is high spin with a magnetic moment of 5.84 μ_B at 20 °C in the solid state and an average Mn-C distance of 2.462 Å, which is typical for a high spin manganocene. The Cp rings are bent at an angle of 138.1° owing to the steric congestion around the Mn center caused by the coordinated

THF. The relatively long Mn-O bond of 2.226 Å is similar to that in other Mn^{II} THF

complexes and suggests a mostly ionic interaction.
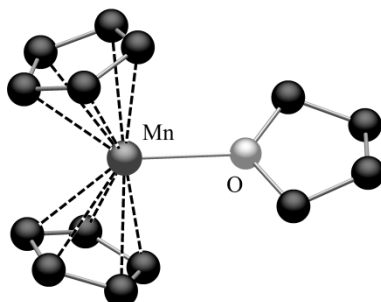
Figure 44. Solid state structure of THF solvated manganocene (**64**).

Other related structures can be obtained by allowing Cp$_2$Mn to react with neutral

coordinating ligands, such as phosphines or amines, at room temperature in an organic

solvent. Cp$_2$Mn(PMe$_3$) (Figure 45; **65**), Cp$_2$Mn(PPh$_2$Me) (Figure 45; **66**), Cp$_2$Mn(dmpe)

(Figure 46; **67**), and (MeCp)$_2$Mn(dmpe) (Figure 46; **68**) were all prepared using this

method.[87,105] Both (**65**) and (**66**) are similar to (**64**) in that the Cp rings are coordinated in

an η^5 manner and the rings are bent to give an almost trigonal planar arrangement around

the manganese, with Cp(centroid)–Mn–Cp(centroid) bond angles of 142.3° in (**65**) and

142.1° in (**66**). The C(centroid)–Mn–P bond angles are 108.1° and 109.6° in (**65**) and

110.6° and 106.8° in (**66**), making the sum of the C(centroid)–Mn–Cp(centroid) and

Cp(centroid)–Mn–P bond angles (360° for (**65**) and 359.5 for (**66**)) that expected for a

trigonal planar geometry around Mn. The average Mn–C bond distances of >2.5 Å are

slightly longer than that of normal high spin manganocenes, but this is likely a

consequence of the added bulk on the phosphine groups preventing the Cp rings from

approaching the metal center any more closely.

(**65**)   (**66**)
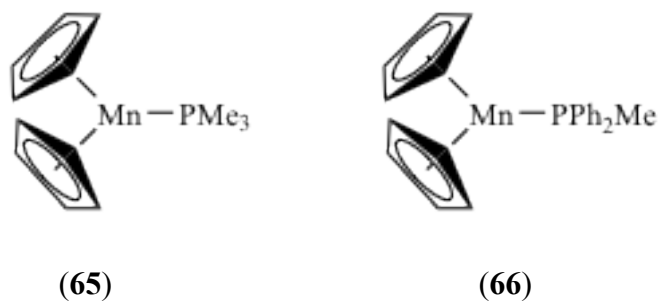
Figure 45. Structures of phosphine adducts of manganocene (**65**) and (**66**).

In the case of (**67**), a pseudotetrahedral geometry with C_2 symmetry is generated between the two Cp centroids and the two 2 phosphorus atoms. The steric bulk of the coordinating ligand is such that the Cp–Mn interaction has a tilt angle (τ) of 7.3º, meaning that while the Mn atom is still nearly centered above the ring in an apparent η^5 manner, the Mn–C distances vary greatly (2.492–2.742 Å). The Mn–Cp(centroid) distance is also relatively long at 2.334 Å, again due to the bulk of the dmpe ligand. Some of this lengthening could also stem from electronic effects, as the complex is formally a 21e⁻ species; it is consequently unsurprising that similarly bulky, yet stronger coordinating bases can cause ring slippage. Addition of a methyl substituent to each of the Cp rings to produce (**68**) is enough to cause the slippage of one ring to an η^2-coordination. Ring slippage is also observed when Cp$_2$Mn is allowed to react with TMEDA and bulky *N*-heterocyclic carbenes. Reaction with TMEDA to produce (C$_5$H$_5$)$_2$Mn(tmeda) results in the slippage of one ring to an η^1-mode while the other remains bound in an η^5 fashion.[106] The bulky *N*-heterocyclic carbenes 1,3-bis(2,6-dimethyl-4-bromophenyl)-imidazol-2-ylidene and 1,3-dimesitylimidazol-2-ylidene have also been found to react with Cp$_2$Mn to give similarly slipped species, in which neither ring remains coordinated in an η^5 manner.[107] Reaction of manganocene with the less bulky tetramethylimidazol-2-ylidene (Figure 46; **69**) yields (η^1-C$_5$H$_5$)(η^2-C$_5$H$_5$)Mn(**69**)$_2$

(Figure 46; **70**), a complex with distorted tetrahedral geometry. The latter is unique in comparison to cobaltocene, chromocene, and nickelocene, all of which react with (**69**) to give ion pair species of the form $[(\eta^5\text{-}C_5H_5)Mn(\mathbf{69})_2]^+[(C_5H_5)]^-$.[108]

(67)   (68)   (69)   (70)
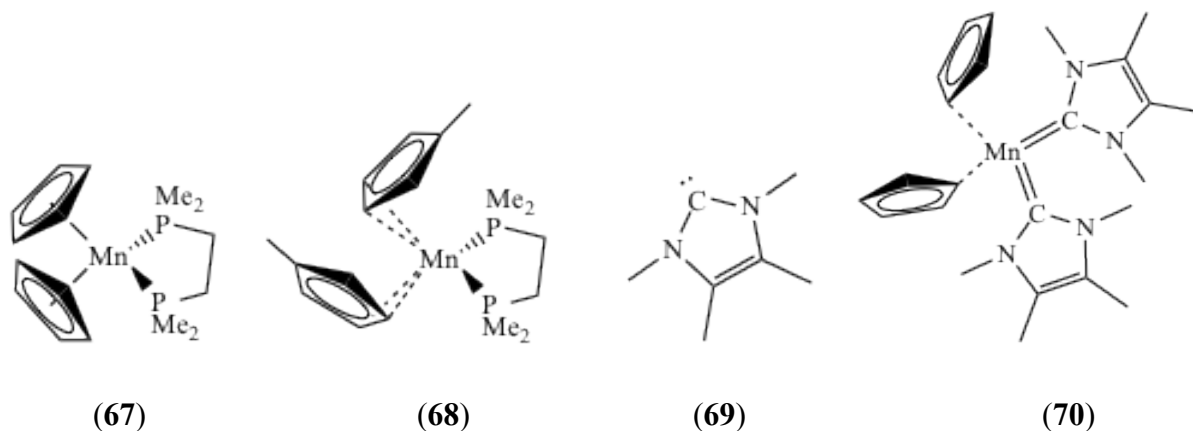
Figure 46. Structures of phosphine and carbene adducts of manganocenes (**67**)-(**70**).

There are only 9 known examples of manganocenium ions ($[Cp'_2Mn]^+$) that have been crystallographically characterized, all of which are in charge-transfer (CT) salts featuring (**63**) as the electron donor. The electron acceptor in each of the CT salts is planar in structure and most are of the metal-dichalcogolene variety,[109,110] although some contain purely organic acceptors such as 7,7,8,8-tetracyano-*p*-quinodimethanide (TCNQ)[111]. Structurally speaking, the $[Cp^*_2Mn]^+$ cation is very similar to low spin manganocene, as the Mn-C distances are all in the range of 2.08-2.15 Å. This is at the short end of the Mn-C distance range for low spin manganocenes, but reflects the presence of the more highly charged Mn[III] centers in the cations. The only difference between the crystallographically characterized $[Cp^*_2Mn]^+$ ions is that not all of the cations have the staggered ring structure found in (**63**). Instead, many of the CT salts

57

feature an eclipsed ring structure for the [Cp*$_2$Mn]$^+$ cation, a result likely due to the

packing effects of the charge transfer salt upon crystallization. The first of these charge-

transfer compounds was made by treating (**63**) with TCNQ to produce the CT salt

[Cp*$_2$Mn]$^+$[TCNQ]$^-$ (Figure 47; **71**), which is a bulk ferromagnet with a Curie

temperature of 6.2 K and coercive field of 3.6 x 10^3 gauss.[111] More recent efforts to

synthesize ferromagnetically ordered molecular charge-transfer salts have used metal-

dithiolate or diselenolate acceptors, such as decamethylmanganocenium

bis[bis(trifluoromethyl)ethylene diselenolato]metalate(III) (M = Ni (Figure 47, **72**),

Pt).[112]

(**71**)   (**72**)
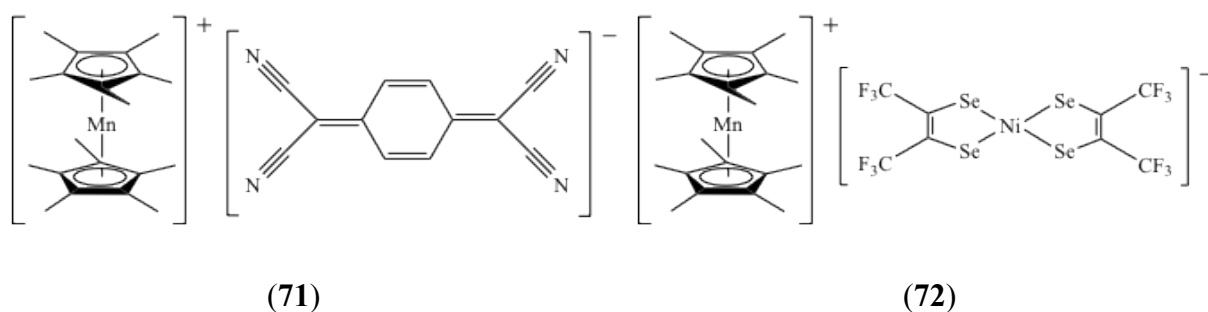
Figure 47. Schematics for the CT salts (**71**) and (**72**).

Metal triscyclopentadienyl anions ([Cp′$_3$M]$^-$) are relatively rare; the first known

transition metal examples (and the first to involve paramagnetic metal centers) were

synthesized with Mn^{II}.[113] The earliest versions were prepared in 2001 and made from the

reaction of Cp$_2$Mn with CpK or Cp$_2$Mg in a solution of THF. The structure of [(η^2-

Cp)$_3$MnK•1.5(thf)] (Figure 48; **73**) features three η^2-bound Cp ligands coordinating to

each Mn^{II} atom in a paddlewheel arrangement, which is then linked to other [Cp$_3$Mn]$^-$

anions by cation-π bonds between the potassium cation and the Cp ligands of neighboring

anions.[113] This allows for the formation of cyclic [(η^2-Cp)$_3$MnK]$_3$, which branches in

two dimensions to form a honeycomb sheet structure. The end result is a layered

structure similar to graphite, in which adjacent sheets are staggered in respect to one

another, with a large interlayer distance of ~9.5 Å. Despite considerable crystallographic

disorder from the presence of both right- and left-handed propeller-like arrangements, the

Mn–C distances can be determined to exist in the range of 2.36-2.41 Å, similar to the

distances commonly observed for high spin manganocenes. The range of Mn–C

distances (2.351-2.392 Å) in the ion-separated complex $[(\eta^2\text{-}Cp)_3Mn]_2[Mg(thf)_6]$ (Figure

48; **74**) are essentially identical to those of (**73**).[113] It is believed that the Cp rings all

coordinate in an η^2 manner in these types of complexes to avoid unfavorable electronic

arrangements, as three η^5-coordinated rings would lead to a formal electron count of 23e⁻

; with all of the rings η^2-coordinated, the anions are formally 14e⁻ species. Magnetic

measurements of both (**73**) and (**74**) demonstrate that the compounds that are in a spin

equilibrium favoring mostly the high spin state (μ_{eff} = 4.8 μ_B) at room temperature; both

display decreases in the moment as the temperature is lowered. The fact the compounds

are mostly high spin at room temperature is also consistent with their Mn-C distances.

(**81**)   (**82**)
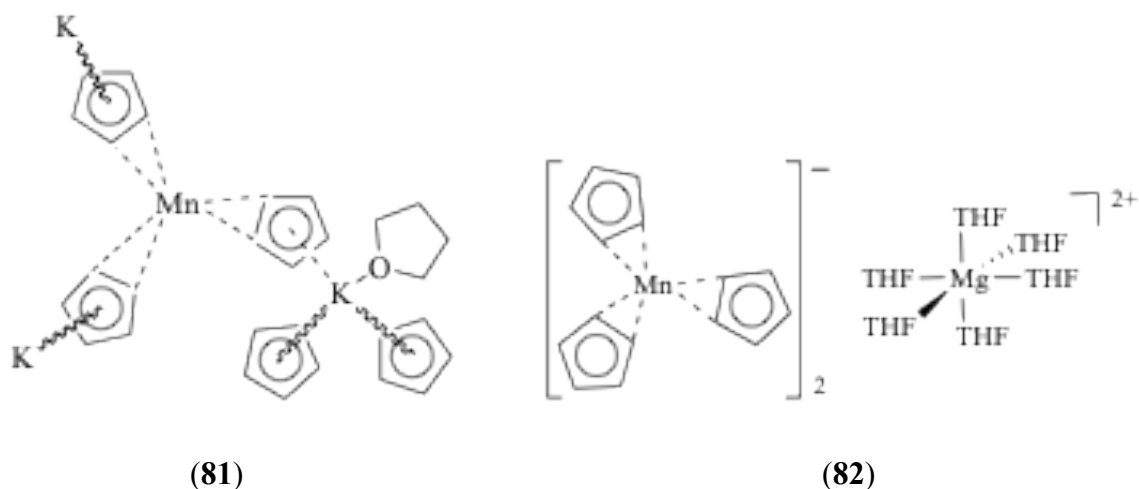
Figure 48. Structures of triscyclopentadienyl manganate anions (**81**) and (**82**).

Several additional triscyclopentadienyl manganate(II) anions have been isolated and structurally characterized.[87,114,115] All of them possess a similar same paddlewheel structure with three cyclopentadienyl rings η^2-bound to the Mn center. Not all of them possess the 3-dimensional layered structure of (**73**), but the immediate environment around the manganese centers is nearly identical.

Bis(indenyl) Manganese Complexes and Other Bis(Cyclopentadienyl) Derivatives

The indenyl ligand $[C_9H_7]^-$ is often considered an analogue of the cyclopentadienyl anion, in that both are 6-electron donors to metals and both can be functionalized to fit specific purposes. Although in many cases the indenyl ligand can replace cyclopentadienyl in a complex without materially changing the structure and reactivity, there are instances in transition metal complexes where the "indenyl effect" (the ability of the indenyl ligand to easily slip from $\eta^5 \rightarrow \eta^3 \rightarrow \eta^5$ coordination) can help enhance catalytic properties in transition metal complexes (Figure 49).

Figure 49. Rearrangements of the "indenyl effect".

In contrast to their first row transition metal counterparts containing V,[101] Cr,[116] and Fe–Ni,[117] many decades separated the appearance of bis(indenyl) complexes of Mn^{II} from the corresponding manganocenes. The first bis(indenyl)manganese(II) compounds were synthesized by allowing high purity anhydrous $MnCl_2$ to react with potassium indenide salts in THF.[118] One of the most noticeable features of these compounds is the

flexibility found for the Mn-indenyl interaction. This was evident during the attempted synthesis of the parent bis(indenyl)manganese,[112] which produced a THF solvate (**76**); the coordinated THF could not be removed by heating or vacuum.[118] The two indenyl ligands and the two THF molecules in (**76**) are arranged in a distorted tetrahedral fashion around the Mn center, with one indenyl ring coordinated in an η^1 fashion while the other is η^3-coordinated (Figure 97); magnetic measurements indicate that the compound is high spin. The Mn–C bond length for the η^1-coordinated indenyl is 2.222 Å to the carbon in the C1 position of the indene (**75**), which is longer than the typical Mn-C bond for low spin manganocenes, but is reasonable for a high-spin complex. The η^3-coordinated ring displays Mn–C distances ranging from 2.344 to 2.550 Å for the C1-C3 carbons on the indenyl ligand, whereas the bridgehead carbons display Mn-C separations of over 2.8 Å. The C–C distances in the two indenyl ligands show a noticeable difference based on their coordination mode. For the η^3-bound ring, the C–C distances on the 5-membered ring all range from 1.41-1.44 Å, which is typical for a mostly delocalized cyclopentadienyl or indenyl ligand. In contrast, the η^1-bound ring has C–C bonds that range from 1.38-1.45 Å, with the two bonds near the carbon bound to Mn at 1.44 and 1.45 Å in length, while the C2–C3 bond on the indenyl is 1.38 Å. This indicates a moderate localization of a double bond between the C2 and C3 carbons.
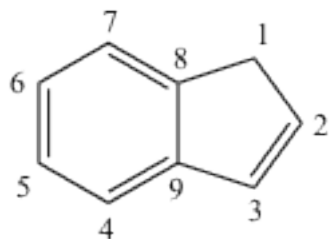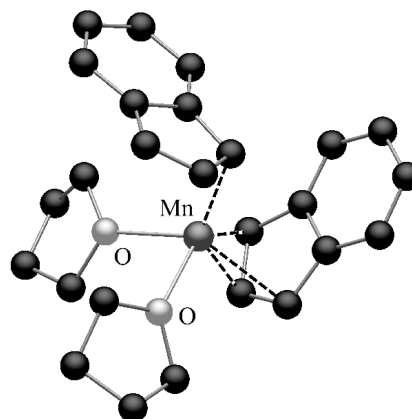
(75)   **(76)**

Figure 50. Numbering scheme for the indene ligand (**75**); Solid State structure of THF solvated bis(indenyl)manganese (**76**).

Unsolvated sandwich structures are found when sufficient bulk is added to the indenyl ligand to prevent THF coordination. In the case of bis[2-(trimethylsilyl)indenyl]manganese(II) (Figure 51; **77**), the result is a monomeric sandwich compound with η^5-bound rings in a staggered geometry.[118] The average Mn-C bond distance of 2.409 Å is similar to, but slightly longer than, that of typical high spin manganocenes. The rings can be considered to be η^5-bound despite a noticeable amount of slippage (Δ_{Mn-C} = 0.14 Å); similar displacements are encountered for bis(indenyl)chromium complexes,[119,120] and the η^3-coordinated rings in bis(indenyl)nickel have a much larger ring slip parameter (Δ_{Ni-C} = 0.44 Å).[117] Bis(1,3-diisopropylindenyl)manganese (Figure 51; **78**) has a staggered monomeric structure, and has an approximate average Mn-C bond distance of 2.4 Å.[118]

(77)   (78)
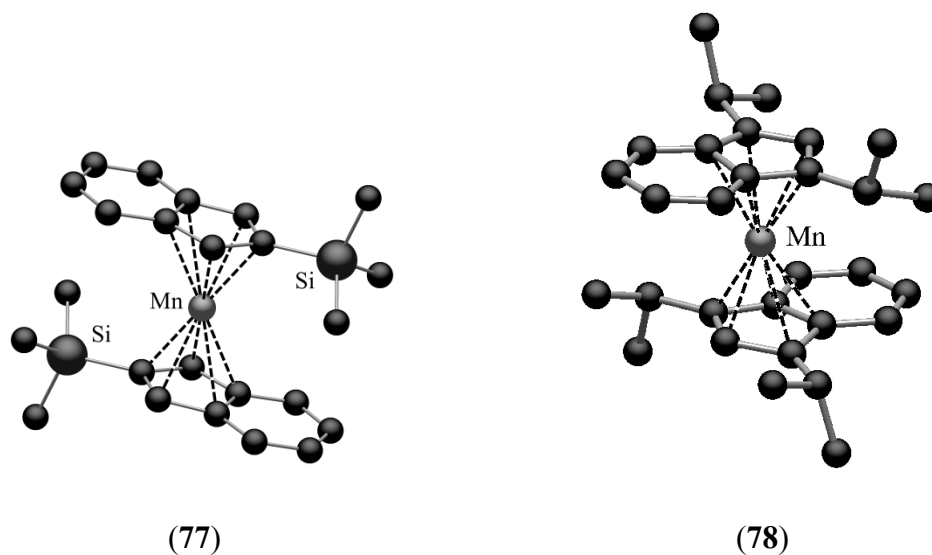
Figure 51. Solid state structures for bis(2-trymethylsilylindenyl)manganese (**85**) and bis(1,3-diisopropylindenyl)manganese (**86**).

Addition of a second trimethylsilyl group to the indenyl ligand to produce bis[1,3-bis(trimethylsilyl)indenyl]manganese(II) (Figure 52; **79**) results in a complex that is monomeric with a near gauche conformation (twist angle of 83.7° from eclipsed), and that is similar to the analogous compounds for Cr[119] and Fe.[118,121-123] The rings possess slightly distorted η^5-coordination, with an average Mn–C distance of 2.42 Å and a ring slip parameter ($\Delta_{Mn-C} = 0.12$ Å) close to that found for (**77**). The overall structure is slightly bent, with an angle between the C_5 rings on the indenyl ligands of 5.1°, which is significantly less than its Cr counterpart (11.5°) and slightly less than in the Fe analogue (5.8°). The long Mn-C distance in (**79**) helps to reduce much of the steric impact of the trimethylsilyl groups. The lowered steric strain can be gauged by the displacement of the silicon atom from C_5 ring plane of the indenyl ligand; the average displacement is 0.22 Å for (**87**), while it is 0.31 Å and 0.38 Å in Cr and Fe, respectively.

63
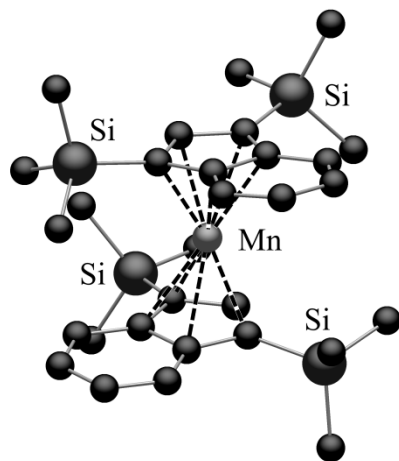
Figure 54. Solid state structure of bis(1,3-bistrimethylsilylindenyl)manganese (**87**).

CHAPTER III

SYNTHESES AND STRUCTURES OF SUBSTITUTED
BIS(INDENYL)MANGANESE(II) COMPLEXES

Introduction

As discussed previously at the end of Chapter II, the π indenyl anion $[C_9H_7]^-$ is often considered a close analogue of the cyclopentadienyl anion $[Cp]^-$. Both indenyl and cyclopentadienyl ligands are readily functionalized, and their complexes have found uses in a range of important applications, including polymerization and hydrosilylation chemistry.[124-132] Many of these properties, particularly those for catalysis, are often enhanced in the case of the indenyl compounds due to the previously mentioned indenyl effect.

Differences between indenyl and cyclopentadienyl ligands are also evident in the first-row transition metal sandwich complexes L_2M; the structures and properties of $(C_9H_7)_2M$ (M = V[133], Cr[134], Fe–Ni[135]) compounds diverge considerably from their $Cp´_2M$ counterparts. For example, in contrast to the orange, air-stable ferrocene, bis(indenyl)iron is a black solid and highly air-sensitive. Bis(indenyl)chromium is a diamagnetic metal-metal bonded dimer $\{(C_9H_7)_2Cr\}_2$,[134] unlike the monomeric, paramagnetic Cp_2Cr.[136] Until recently, when M = Mn, a comparison between cyclopentadienyl and indenyl-based species could not even made, as neither bis(indenyl)manganese, nor any substituted derivative of it, had been reported.[137-139]

 This was a curious omission, given that cyclopentadienyl complexes of Mn^{II} in the form of the well-studied manganocenes have been known for over 50 years.[60,140-142]

As mentioned in previous chapters, manganocenes are unique among first-row metallocenes for having two energetically accessible spin states that can be readily interconverted based on the substituents of the cyclopentadienyl ligands. In the absence of extreme steric congestion,[141,143] electron-donating substituents on the rings (e.g., alkyls) support a low-spin ($^2E_{2g}$) configuration, whereas less electropositive groups (e.g., H, SiMe$_3$) favor a high-spin ($^6A_{1g}$) state. Manganocenes have been used as one-electron donors in magnetically ordered charge-transfer salt complexes,[144-146] and given that bis(indenyl) complexes of iron have been explored as effective alternatives to metallocene donors in such compounds,[147] (Ind)$'_2$Mn(II) species would also be of interest.

We describe here methylated bis(indenyl) complexes of Mn^{II}, some of which were mentioned at the end of Chapter II. These new compounds focus on methylated indenyl ligands, and display substantial differences from structures seen previously for manganocenes owing to the greater bonding flexibility of the indenyl ligand.

Experimental

General Considerations. All manipulations were performed with the rigorous exclusion of air and moisture using Schlenk or glovebox techniques. Proton (^{1}H) NMR experiments were obtained on a Bruker DPX-300 spectrometer at 300 MHz, Bruker DPX-400 at 400 MHz or Bruker DRX-501 spectrometer at 500 MHz. Elemental analyses were performed by Desert Analytics (Tucson, AZ). Melting points were determined on a Laboratory Devices Mel-Temp apparatus in sealed capillaries. Mass spectra were obtained using a Hewlett-Packard 5890 Series II gas chromatograph/mass spectrometer.

Materials. Anhydrous manganese(II) chloride (99.999%) was purchased from Alfa Aesar and used as received. Indene, 2-methylindene, methacryloyl chloride, *p*-xylene, 3-chloropropionyl chloride, *n*-butyl lithium, potassium bis(trimethylsilyl)amide, *p*-toluenesulfonic acid, anhydrous pentane, and anhydrous, unstabilized tetrahydrofuran (THF) were purchased from Aldrich and used as received. Hexanes, toluene, and diethyl ether were distilled under nitrogen from potassium benzophenone ketyl. Toluene-d_8 (Aldrich) was vacuum distilled from Na/K (22/78) alloy and stored over type 4A molecular sieves prior to use.

Magnetic Measurements. Solution magnetic susceptibility measurements were performed on a Bruker DRX-400 spectrometer using the Evans' NMR method.[148] The paramagnetic material (5–10 mg) was dissolved in toluene-d_8 in a 1.0 mL volumetric flask. The solution was thoroughly mixed, and approximately 0.5 mL was placed in an NMR tube containing a toluene-d_8 capillary. The calculations required to determine the number of unpaired electrons based on the data collected have been described elsewhere.[149]

General Procedures for X-ray Crystallography. A suitable crystal of each sample was located, attached to a glass fiber, and mounted on a Bruker SMART APEX II CCD Platform diffractometer for data collection at 173(2) K or 100(2) K. Data collection and structure solutions for all molecules were conducted at the X-ray Crystallography Facility at the University of Rochester by Dr. William W. Brennessel or at the University of California, San Diego by Dr. Arnold L. Rheingold. Data resolution of 0.84 Å were considered in the data reduction (SAINT 7.53A, Bruker Analytical Systems, Madison, WI).

The intensity data were corrected for absorption and decay (SADABS). All calculations were performed using the current SHELXTL suite of programs.[150] Final cell constants were calculated from a set of strong reflections measured during the actual data collection.

The space groups were determined based on systematic absences (where applicable) and intensity statistics. A direct-methods solution was calculated that provided most of the non-hydrogen atoms from the E-map. Several full-matrix least squares/difference Fourier cycles were performed that located the remainder of the non-hydrogen atoms. All non-hydrogen atoms were refined with anisotropic displacement parameters. All hydrogen atoms were placed in ideal positions and refined as riding atoms with relative isotropic displacement parameters.

Synthesis of 2,4,7-trimethylindene, HInd$^{3Me-2,4,7}$. AlCl$_3$ (62.82 g, 0.47 mol) was slurried in 250 mL of CS$_2$ in a 500 mL Schlenk flask that had been flushed with N$_2$. Methacryloyl chloride (49.25 g, 0.47 mol) and *p*-xylene (50.07 g, 0.47 mol) were added to an addition funnel along with ~20 mL of CS$_2$ and the funnel was attached to the Schlenk flask. The methacryloyl chloride and *p*-xylene were added dropwise at 0 ºC under nitrogen, gradually turning the solution dark red. The reaction was stirred overnight while gradually warming to room temperature. The solution was refluxed the following day for 4 h at 55-60 ºC. The solution was cooled to room temperature and poured slowly over ~500 g of ice that had been slurried with concentrated HCl (200 mL), turning the solution yellow. The solution was allowed to stir until it had warmed to room temperature, then the organic layer was separated and neutralized with aqueous NaHCO$_3$. The remaining organic solution was dried with MgSO$_4$ and the solvent removed by rotary

evaporation to yield 69.47 g of an orange-red oil. The oil was distilled at 70 ºC and 200 mTorr for 4 h to produce 13.03 g (16%) of the pale yellow indenone oil that was characterized by GC/MS (m/e = 174).

The indenone was dissolved in anhydrous diethyl ether (75 mL) and chilled to 0 ºC in a 250 mL Schlenk flask before adding lithium aluminum hydride (44 mL of 1.0 M diethyl ether solution, 0.044 mol) dropwise through a syringe. The reaction was stirred overnight under nitrogen before refluxing at 65 ºC for 4 h. The solution was cooled to room temperature before being neutralized by the slow addition of cold water (~4 mL), aqueous $NaHCO_3$ (~8 mL), and more cold water (~30 mL). The white precipitate that formed was filtered off and the remaining solution neutralized with dilute $NaHCO_3$. The organic solution was dried with $MgSO_4$ and the solvent removed by rotary evaporation to leave the indenol product as a white crystalline solid (11.85 g, 90%). MS: m/e = 176.

The 2,4,7-trimethylindenol (11.85 g, 67 mmol) was dissolved in toluene (150 mL) and added to a 250 mL round-bottom flask. A few crystals of *p*-toluenesulfonic acid were added to a solution and the flask was fitted with a Dean-Stark trap and condenser. The solution was refluxed until 1.2 mL of water was collected. The remaining golden colored solution was neutralized with aqueous $NaHCO_3$ and water before drying with $MgSO_4$ and removing the solvent by rotary evaporation. The remaining orange oil was then added to a sublimation apparatus where the indene was obtained as a white crystalline solid (7.30 g, 69%) by fractional sublimation at 60 ºC and 300 mTorr over 3 hours. MS: m/e = 158. ^{1}H NMR (500 MHz, ppm in $CDCl_3$): δ 6.9 (doublet, 1 H), 6.8 (doublet, 1 H), 6.5 (singlet, 1 H), 3.2 (singlet, 2 H), 2.4 (singlet, 3H), 2.3 (singlet, 3H), 2.2 (singlet, 3H).

Synthesis of Potassium 2,4,7-trimethylindenide, K[Ind$^{\text{3Me-2,4,7}}$]. 2,4,7-
trimethylindene (2.96 g, 18.7 mmol) was dissolved in toluene (40 mL) in a 250 mL
Erlenmeyer flask. Potassium bis(trimethylsilyl)amide, K[N(SiMe$_3$)$_2$] (3.55 g, 17.8
mmol), was dissolved in toluene (30 mL) and added dropwise to the indene solution
while stirring. The solution immediately turned pale yellow upon the onset of addition,
but after stirring for 24 h at room temperature, the solution became yellow-green.
Hexanes were added (175 mL) to fully precipitate the potassium indenide salt, which was
then filtered over a medium-porosity frit, washed with hexanes (2 x 25 mL), and dried
under vacuum to yield 2.60 g (74%) of a blue-gray powder that was confirmed to be the
indenide salt by ^{1}H NMR (300 MHz) in toluene-d_8: δ 2.24(singlet, 3H, CH$_3$ in the 2-
position); 2.34 (singlet, 6H, CH$_3$ in the 4,7-positions); 6.56 (multiplet, 3H, CH in the
1,2,3-positions); 7.20 (doublet, 2H, CH in the 5,6-positions).

Synthesis of 4,7-dimethylindene, HInd$^{\text{2Me-4,7}}$. 200 mL of CS$_2$ was added to a 500
mL Schlenk flask containing AlCl$_3$ (31.51 g, 0.2363 mol) and cooled to 0 °C in an ice
bath. A solution containing *p*-xylene (25.01 g, 0.2356 mol) and 3-chloropropionyl
chloride (29.896 g, 0.2355 mol) was added dropwise through an addition funnel, and the
resulting reaction solution allowed to warm to room temperature. The solution was then
refluxed at 55 °C for 2.5 h with a drying tube attached. After cooling to room
temperature, the now red solution was poured over ~500 g of ice and stirred until the
whole solution turned light yellow. The organic layer was neutralized with NaHCO$_3$ and
dried with MgSO$_4$ before removing the remaining CS$_2$ by rotary evaporation. The
remaining orange-yellow oil (~45 mL) was added dropwise to excess H$_2$SO$_4$ at 0 °C,
turning the solution dark red. The solution was then warmed to room temperature before

refluxing at 80 °C for 1 hour, at which point the evolution of HCl gas had stopped. The solution was poured over ice and the slurry was allowed to stir while warming to room temperature, resulting in an orange solution. The product was extracted with diethyl ether and the solution was neutralized with NaHCO$_3$ before being dried with MgSO$_4$. Removal of the solvent by rotary evaporation yielded a mixture of white and yellow crystals that was purified by redissolving the product in warm methanol and placing in a freezer overnight at -20 °C. The resulting white crystals of 4,7-dimethy-1-indanone were isolated by filtration to yield 23.48 g (62%) of product whose identity was confirmed by GC/MS (m/e = 160).

The indanone (23.48 g, 0.1468 mol) was dissolved in anhydrous diethyl ether (250 mL) under nitrogen and chilled to 0 °C in a 500 mL Schlenk flask. 50 mL of 2.0 M Li[AlH$_4$] in diethyl ether was added dropwise through an addition funnel and the resulting solution stirred overnight at room temperature. The solution was refluxed at 55-60 °C the following day for 5 h. The mixture was then cooled to 0 °C and quenched by adding 3 mL of cold water, 5 mL of dilute NaOH and another 15 mL of cold water. The white precipitate that formed was filtered and the remaining organic solution was dried with MgSO$_4$. Removal of the solvent by rotary evaporation yielded 14.10 g (59%) of white, crystalline 4,7-dimethyl-1-indanol, confirmed by GC/MS (m/e = 162).

The indanol was dissolved in 150 mL of toluene and added to a 250 mL round-bottom flask with a Dean-Stark trap and condenser attached. A few crystals of *p*-toluenesulfonic acid were added to the solution and the solution was refluxed for 2.5 h until approximately 1.5 mL of water had been collected in the trap. The solution was then cooled to room temperature and neutralized with NaHCO$_3$ before being dried with

MgSO$_4$. Rotary evaporation to remove the remaining toluene gave 11.93 g (95%) of a

yellow oil that was then distilled at 35 °C and 50 mTorr to yield 8.22 g of a clear liquid

that was confirmed to be 4,7-dimethylindene by GC/MS (m/e = 144) and ^{1}H NMR: δ 2.3

(s, 3H), 2.4 (s, 3H), 3.2 (t, 2H), 6.5 (dt, 1H), 6.8-7.2 (m, 3H).

Synthesis of Potassium 4,7-dimethylindenide, K[Ind$^{2Me-4,7}$]. 4,7-

Dimethylindene (3.724 g, 25.9 mmol) was dissolved in toluene (50 mL) in a 250 mL

Erlenmeyer flask. Potassium bis(trimethylsilyl)amide, K[N(SiMe$_3$)$_2$] (4.300 g, 21.6

mmol), was dissolved in toluene (30 mL) and added dropwise to the indene solution

while stirring. The solution immediately turned yellow upon the onset of addition, but

after stirring for 24 h at room temperature, the solution became an opaque gray color.

Hexanes (125 mL) were added to fully precipitate the potassium indenide salt, which was

then filtered over a medium-porosity frit, where it was washed with hexanes (2 x 20 mL)

and dried under vacuum to yield 3.794 g (95%) of a gray powder. The powder was

confirmed to be the indenide salt by ^{1}H NMR (300 MHz) in toluene-d_8: δ 2.34 (singlet,

6H, CH$_3$ in the 4,7-positions); 6.56 (multiplet, 3H, CH in the 1,2,3-positions); 7.20

(doublet, 2H, CH in the 5,6-positions).

Synthesis of Bis(2,4,7-trimethylindenyl)manganese(II), (Ind$^{3Me-2,4,7}$)$_2$Mn.

MnCl$_2$ (0.126 g, 1.00 mmol) and a stir bar were added to a 125 mL Erlenmeyer flask.

THF (50 mL) was added to the flask and the MnCl$_2$ was dispersed by stirring for 1 h.

Potassium 2,4,7-trimethylindenide, K[Ind$^{3Me-2,4,7}$], (0.404 g, 2.06 mmol) was dissolved in

30 mL of THF and added to a 60 mL addition funnel. The K[Ind$^{3Me-2,4,7}$] was added

dropwise over 30 min into the flask containing MnCl$_2$ and allowed to stir overnight;

removal of the solvent by vacuum left behind an orange oil. The product was then

extracted with pentane (5 x 30 mL) and filtered to remove the KCl precipitate. The orange pentane filtrates were combined and most of the solvent was then removed under vacuum. The remaining solvent was then allowed to evaporate at room temperature over 2 days, affording a dark orange solid, mp 146–150 °C (0.252 g, 67%). Crystals suitable for crystal structure determination were eventually obtained from a sealed solution of [(Ind$^{3Me-2,4,7}$)MnCl(thf)]$_2$ dissolved in toluene that remained at room temperature for 10 days. Anal. Calcd. for C$_{24}$H$_{26}$Mn: C, 78.03; H, 7.09; Mn, 14.87. Found: C, 78.64; H, 7.31; Mn, 14.9. Solution magnetic susceptibility (μ_{eff}^{298K}): 5.68 μ_B.

Synthesis of Bis(4,7-dimethylindenyl)manganese(II), (Ind$^{2Me-4,7}$)$_2$Mn. MnCl$_2$ (0.344 g, 2.73 mmol) was added to a 125 mL Erlenmeyer flask fitted with a stir bar and 30 mL of THF. The flask was stirred at room temperature for 1 h to disperse the MnCl$_2$. Potassium 4,7-dimethylindenide (1.001 g, 5.11 mmol) was dissolved in THF (20 mL) and added dropwise to the flask containing MnCl$_2$. The reaction was allowed to stir overnight at room temperature before the removal of the solvent under vacuum left an orange residue. Three extractions with pentane (20 mL each) were performed yielding a lightly colored solution; only an orange oil remained when the solvent was removed. The remaining orange product that was not extracted into pentane was then extracted with 40 mL of toluene, and 30 mL of this solution was placed in the freezer at –20 °C for 3 days. Dark orange crystalline blocks grew from the solution (58 mg, 26% yield), mp 260-265 °C. Anal. Calcd. for C$_{22}$H$_{22}$Mn: C, 77.41; H, 6.50. Found: C, 78.86; H, 6.72. Solution magnetic susceptibility was not obtained owing to the lack of solubility in toluene once the crystals had formed.

Synthesis of Potassium Tris(4,7-dimethylindenyl)manganate-(II),

[K(dioxane)$_{1.5}$][Mn(Ind$^{2Me-4,7}$)$_3$]. MnCl$_2$ (0.217 g, 1.72 mmol) was added to a 125 mL

Erlenmeyer flask fitted with a magnetic stirring bar and 30 mL of THF. The flask fitted

with a magnetic stirring bar and 30 mL of THF. The flask was stirred at room

temperature for 1 to disperse the MnCl$_2$. Potassium 4,7-dimethylindenide (0.917 g, 5.03

mmol) was dissolved in THF (20 mL) and added dropwise to the flask containing MnCl$_2$.

The reaction mixture was stirred overnight at room temperature; removal of the solvent

under vacuum left a red solid. The residue was then extracted with 1,4-dioxane (2 x 30

mL), and the solvent was removed under vacuum to yield 0.323 g (29%) of a red powder.

Crystals were grown by dissolving the product in a 1,4-dioxane/toluene mixture (3:1) and

allowing the solvent to evaporate slowly at room temperature, mp 308-312 °C (dec).

Anal. Calcd for C$_{39}$H$_{45}$KMnO$_3$: K, 5.96; Mn, 8.38. Found: K, 5.15, Mn 8.07.

Attempted synthesis of Bis(2-methylindenyl)manganese(II), (Ind^{Me-2})$_2$Mn.

MnCl$_2$ (0.388 g, 3.08 mmol) was added to a 250 mL Erlenmeyer flask fitted with a stir

bar. THF (20 mL) was added and the flask was stirred at room temperature for 1 h to

disperse the MnCl$_2$. Potassium 2-methylindenide (1.014 g, 6.04 mmol) was dissolved in

THF (25 mL) at room temperature and added dropwise into the flask containing MnCl$_2$,

yielding an orange solution. The solution was allowed to stir overnight at room

temperature before the solvent was removed under vacuum, leaving a light yellow solid.

Pentane (20 mL) was added to the flask and the liquid was decanted into a medium

porosity glass frit, but the solution came through colorless, indicating that no product had

been extracted. Toluene (3 × 20 mL) was used instead to extract the expected

bis(indenyl) product and the extract filtered over a medium porosity frit. The orange

toluene filtrate was collected and used in an attempt to grow crystals by various methods, including slow cooling in a toluene solution, slow removal of solvent under vacuum, and diffusion of aliphatic solvents. Unfortunately, only an orange oil was ever isolated. There were a few crystals that grew above the oil when hexanes were allowed to evaporate at room temperature; however, there were only enough to acquire a crystal structure, and these crystals were not of the expected bis(2-methylindenyl)manganese(II) compound. Instead the crystal structure proved to be of the aryloxide containing complex (Ind^{Me-2})$_3$Mn$_2$(BHT). Butylatedhydroxytoluene (BHT) is used in trace amounts in THF as an inhibitor, but in this case reacted with the Mn center(s). Further attempts to use BHT-free THF in order to obtain the desired bis(indenyl) complex have been unsuccessful. Attempts to remake (Ind^{Me-2})$_3$Mn$_2$(BHT) are described in detail in Chapter V.

Results

Ligand Synthesis. An extensive library of substituted indenes is available either by direct reaction with indenide salts,[151,152] or by Friedel-Crafts-assisted ring assembly from substituted benzenes.[153] The indenes used in this study were readily deprotonated by *n*-BuLi or K[N(SiMe$_3$)$_2$] in hexanes or toluene, and the resulting air-sensitive salts were isolated in moderate to high yield.

Ligand and Metal Complex Synthesis. Bis(indenyl)manganese(II) complexes were synthesized by salt metathesis elimination reactions of the appropriate indenide salts with MnCl$_2$ in THF (eq 1).
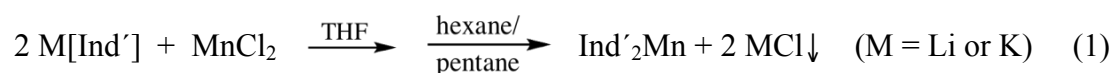
$$2 \text{ M[Ind}'] + \text{MnCl}_2 \xrightarrow[\text{pentane}]{\text{THF} \quad \text{hexane/}} \text{Ind}'_2\text{Mn} + 2 \text{ MCl}\downarrow \quad (M = \text{Li or K}) \quad (1)$$

After the removal of THF under vacuum, addition of pentane or toluene served to extract the manganese complexes, allowing for the removal of the alkali metal chloride by-products. The purified (indenyl)manganese complexes were crystallized either by slow evaporation of a saturated solution, or by cooling of a concentrated solution to approximately -30 °C. They vary in color from bright orange to dark red-orange, and all are highly air- and moisture-sensitive.

It should be noted that the preparation of the indenyl complexes requires chemicals and reagents of very high quality in order to achieve consistent results. In particular, the purity of the manganese chloride has proven critical; initial experiments with commercially available anhydrous $MnCl_2$ (specified with 97% purity, and satisfactory for the preparation of manganocenes[25]) led to the formation of intractable red-orange oils that decomposed to brown materials over the course of several days. The use of $MnCl_2$ beads of >99.99% purity led to consistently reproducible reactions and to compounds that are indefinitely stable under an inert atmosphere.

Butylhydroxytoluene (BHT) is a stabilizer used in small quantities (0.025%) in anhydrous THF. In cases where large volumes of THF are used, the butylhydroxytoluene anion is likely formed from the deprotonation of BHT with various potassium indenide ligands. This can be a problem as the BHT anion can react and coordinate to Mn^{II} centers. This was seen when a product containing a bridging BHT as an aryloxide was isolated while trying to synthesize $(Ind^{Me-2})_2Mn$. This result generated interest in intentionally synthesizing additional Mn^{II} aryloxide compounds. These compounds were subsequently explored and are discussed in Chapter V.

Manganese complexes of the $[4,7\text{-}Me_2C_9H_5]^-$ anion were obtained in two forms; crystals of the toluene-solvated $(4,7\text{-}Me_2C_9H_5)_2Mn$ were only marginally acceptable for single-crystal X-ray study, but proved to form a cyclic octomer (see below). As the bis(indenyl) compound accounted for only 26% of the theoretical reaction yield, a separate extraction was performed using 1,4-dioxane to obtain additional manganese-containing product. After the extraction, the $[K(dioxane)_{1.5}][(Mn(Ind^{2Me\text{-}4,7})_3]$ salt was isolated; its formation likely occurred due to the reaction of previously unreacted potassium indenide salt with $(4,7\text{-}Me_2C_9H_5)_2Mn$. This compound can be prepared in moderate to good yield by allowing 3 equivalents of the potassium indenide salt to react with 1 equivalent of $MnCl_2$. This reaction is represented by eq 2.

$$3\ K[Ind^{2Me\text{-}4,7}]\ +\ MnCl_2\ \xrightarrow{\text{dioxane}}\ [K(dioxane)_{1.5}][(Mn(Ind^{2Me\text{-}4,7})_3]\ +\ 2\ KCl\downarrow \quad (2)$$
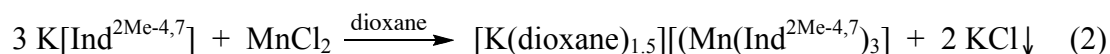
Except for the poorly soluble $(Ind^{2Me\text{-}4,7})_2Mn$, the solution magnetic susceptibilities of the other crystalline compounds were measured with Evans' method.[148] In all cases, a room temperature value consistent with high spin Mn(II) (cf. 5.92 μ_B for the spin-only value for $S = 5/2$) was obtained.

Crystallographic Results

$\{(Ind^{2Me\text{-}4,7})_2Mn\}_8.$ Crystals of $(Ind^{2Me\text{-}4,7})_2Mn$ were isolated from a toluene solution as dark orange blocks. The presence of multiple, extensively disordered solvent molecules in the unit cell lowered the resolution of the structure, so that bond lengths and angles cannot be discussed in detail.[154] Repeated attempts to grow more satisfactory crystals were not successful.

The structure is constructed of an octameric ring of manganese atoms with a crystallographically imposed 2-fold axis (Figure 53). The ring is puckered, with the metal atoms separated by distances of 5.1–5.2 Å; they alternate above and below the mean M_8 plane by maximum distances of 1.2 and 1.1 Å. Each manganese center is associated with three 4,7-dimethylindenyl ligands. One of these ligands is terminal, and although appearing somewhat slipped, is approximately η^5-bound to the manganese centers. The bridging ligands display η^1-coordination to the manganese atoms at an average distance of 2.3 Å, and alternate their positions above and below the Mn_8 ring.
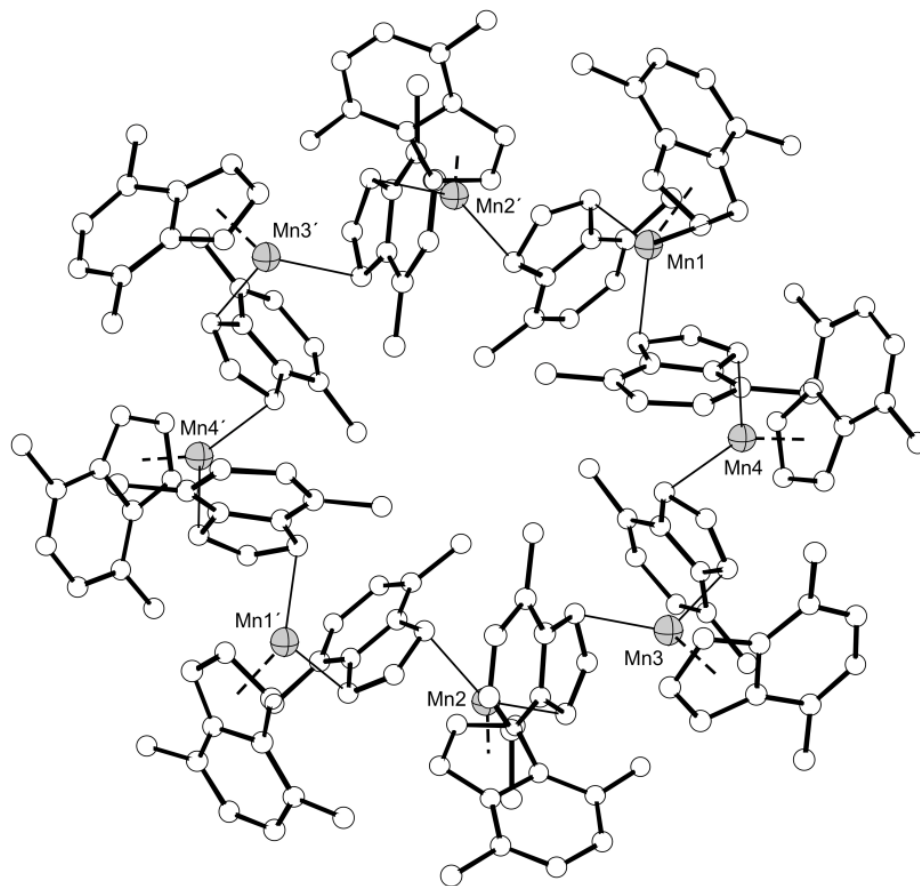
Figure 53. Plot of the non-hydrogen atoms of $\{(Ind^{2Me-4,7})_2Mn\}_8$.

[K(dioxane)$_{1.5}$][(Mn(Ind$^{2Me-4,7}$)$_3$]. Extraction of the residue of the reaction to

form (Ind$^{2Me-4,7}$)$_2$Mn with 1,4-dioxane produced a solution that deposited yellow

hexagonal plates. An ORTEP of the molecule is shown in Figure 54, which gives the

numbering scheme that is referred to in the text. Figure 55 shows a projection of the

three-dimensional structure and Table 2 gives selected bond lengths.

There are six crystallographically independent manganese atoms in the

asymmetric unit, although all six have very similar carbon bonding distances and

arrangements of the indenyl ligands. The general coordination geometry around each

manganese atom is a paddlewheel of three η^2-bound 4,7-dimethylindenyl ligands. The

average Mn–C contacts are at 2.337(5) and 2.404(5) Å for C1 and C2, respectively, and

the other Mn$\cdots$C contacts are >2.75 Å, and are considered to be nonbonding. The

indenyl ligands are involved in cation–π bonding to the potassium through either the 5-

membered rings in one half of the molecules (K–C distances range from 3.00 Å to 3.24

Å), or the 6-membered rings in the other half (K–C distances range from 3.00 Å to 3.47

Å). Every potassium cation is coordinated by a 6-membered ring, a 5-membered ring,

and one oxygen atom on each of two dioxane molecules. This coordination extends in

two-dimensions, forming a layer of cations and anions. One of the two dioxane

molecules bound to the potassium cation is bridging to a separate potassium cation of

another layer, essentially creating a bilayer system held together with the bridging

dioxane molecules, with no interactions between separate bilayers.

The η^2-coordination is established from the range of manganese bond distances to

C(1) and C(2) (Mn–C(1) = 2.29 Å to 2.34 Å, Mn–C(2) = 2.37 Å to 2.42 Å) which are

significantly shorter than the distances to C(3) and C(8) (Mn–C(3) = 2.86 Å to 2.91 Å,

Mn–C(8) = 2.78 Å to 2.84 Å). There are few other compounds known to exhibit η^2-coordination of a Cp to a manganese center,[155] yet one of these is the manganocene polymer. Those distances for η^2-coordination (2.44 Å and 2.62 Å) are much longer than the distances reported here. The structure of [K(dioxane)$_{1.5}$][(Mn(Ind$^{2Me-4,7}$)$_3$] is very similar to that of [(η^2-Cp)$_3$MnK(thf)$_{1.5}$],[155] in which the three Cp ligands are arranged in a paddlewheel around each Mn center, and each Cp is cation-π bound to a potassium counter ion. With THF as the solvent molecule, the structure forms a single layer with *ca.* 9.5 Å between sheets. As a comparison, a single sheet of the bilayer in the indenyl complex is *ca.* 8.1 Å, and the distance between bilayers is 16.0 Å, making the crystals fragile in two dimensions.

Table 2. Select bond distances and averages for [K(dioxane)$_{1.5}$][(Mn(Ind$^{2Me-4,7}$)$_3$].

Atoms	Distance (Å)	Atoms	Distance (Å)
Mn(1)–C(1)	2.337(4)	Mn(1)–C(2)	2.405
Mn(2)–C(1)	2.330(5)	Mn(2)–C(2)	2.375
Mn(3)−C(1)	2.332(5)	Mn(3)−C(2)	2.419
Mn(4)−C(1)	2.298(5)	Mn(4)−C(2)	2.397
Mn(5)−C(1)	2.311(5)	Mn(5)−C(2)	2.418
Mn(6)−C(1)	2.285(5)	Mn(6)−C(2)	2.413
Avg. Mn–C(1)	2.32(1)	Avg. Mn–C(2)	2.40(1)
Avg. K−C(η^5)	3.09(1)	Mn(1)−C(3),C(4),C(5) Mn(2)−C(3),C(4),C(5)	> 2.72
Avg. K−C(η^6)	3.27(1)		
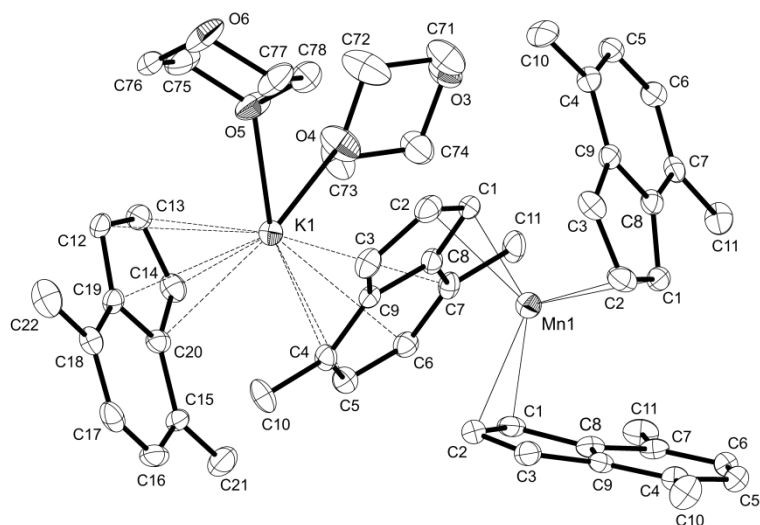
Figure 54. ORTEP of the non-hydrogen atoms of $[K(dioxane)_{1.5}][(Mn(Ind^{2Me-4,7})_3]$, illustrating the numbering scheme used in the text. Thermal ellipsoids are shown at the 50% level.
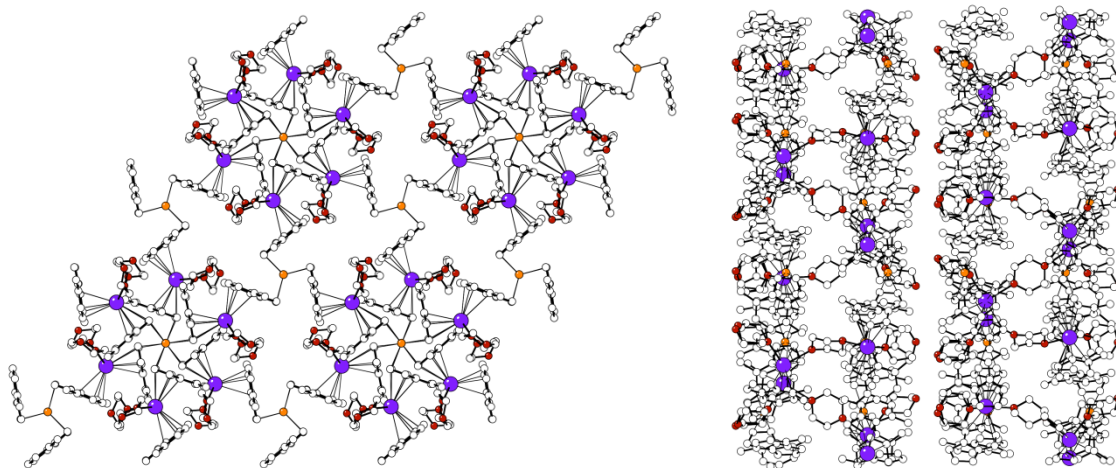
Figure 55. Projections down the crystallographic c (left) and a (right) axes of $[K(dioxane)_{1.5}][(Mn(Ind^{2Me-4,7})_3]$; manganese atoms are in orange; potassium in purple. The c projection shows only one-half a bilayer; the a projection shows the two adjacent bilayers

(Ind$^{3Me-2,4,7}$)$_2$Mn. Orange needles were extracted from a solution of $[(Ind^{3Me-2,4,7})MnCl(thf)]_2$ in pentane. An ORTEP of an expanded asymmetric unit for the

81

polymeric molecule is shown in Figure 56, which gives the numbering scheme that is referred to in the text. Selected bond lengths and angles are shown in Table 3.

The asymmetric unit contains one manganese atom and two indenyl ligands, one that is η^1 and one that is η^5 bound. Each manganese atom is also coordinated to a third indenyl ligand that is symmetry equivalent to the η^1 bound species, creating an overall structure that is polymeric in one dimension. The general coordination geometry around each manganese is very similar to that seen in $\{(\text{Ind}^{2\text{Me-4,7}})_2\text{Mn}\}_8$. The ligand hapticities can be identified in this complex from their bond distances. For the η^1 bound indenyl, the Mn-C bond is 2.323(3) Å for C13 and C15a. The bond lengths to the other carbons on each ligand are all >2.8 Å. The η^5 bound ring is significantly slipped, as the $\Delta_{\text{Mn-C}}$ value of 0.32 Å is large enough to potentially be considered η^3 bound; however, the average Mn-C distance of 2.459(7) is still within the range of what is considered to be η^5 bound. Additionally, since $\{(\text{Ind}^{3\text{Me-2,4,7}})_2\text{Mn}\}_n$ is polymeric, there is steric crowding from the indenyl ligands, with C⋯C contacts approaching 3.5 Å between the benzo methyl groups (C24) of the bridging indenyl ligands to the benzo carbons (C6 and C7) of the terminal η^5 bound ligand. Ligand contortions on a monomeric species would likely be far less given the relatively small size of the methyl group ligand substituents.

Table 3. Selected bond distances of (Ind$^{3Me-2,4,7}$)$_2$Mn.

Atoms	Distance (Å)	Atoms	Distance (Å)
Mn(1)–C(1)	2.522(3)	C(1)–C(2)	1.406
Mn(1)–C(2)	2.377(3)	C(2)–C(3)	1.423
Mn(1)−C(3)	2.300(3)	C(3)−C(9)	1.437
Mn(1)−C(9)	2.475(3)	C(9)−C(8)	1.442
Mn(1)−C(8)	2.620(3)	C(8)−C(1)	1.429
Avg. Mn–C(1)	2.456(7)		
Mn(1)−C(13)	2.291(3)		Δ_{Mn-C} =0.32
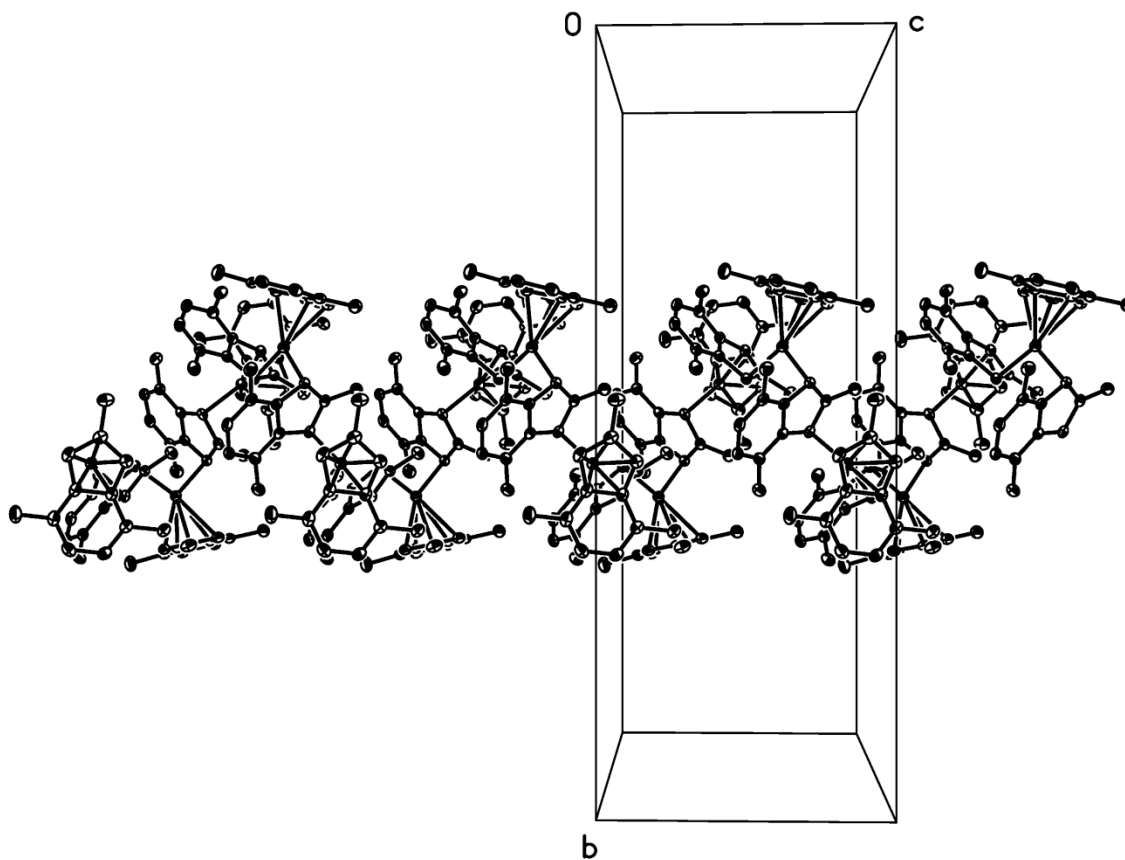
Figure 56. Polymeric structure of (Ind$^{3Me-2,4,7}$)$_2$Mn.
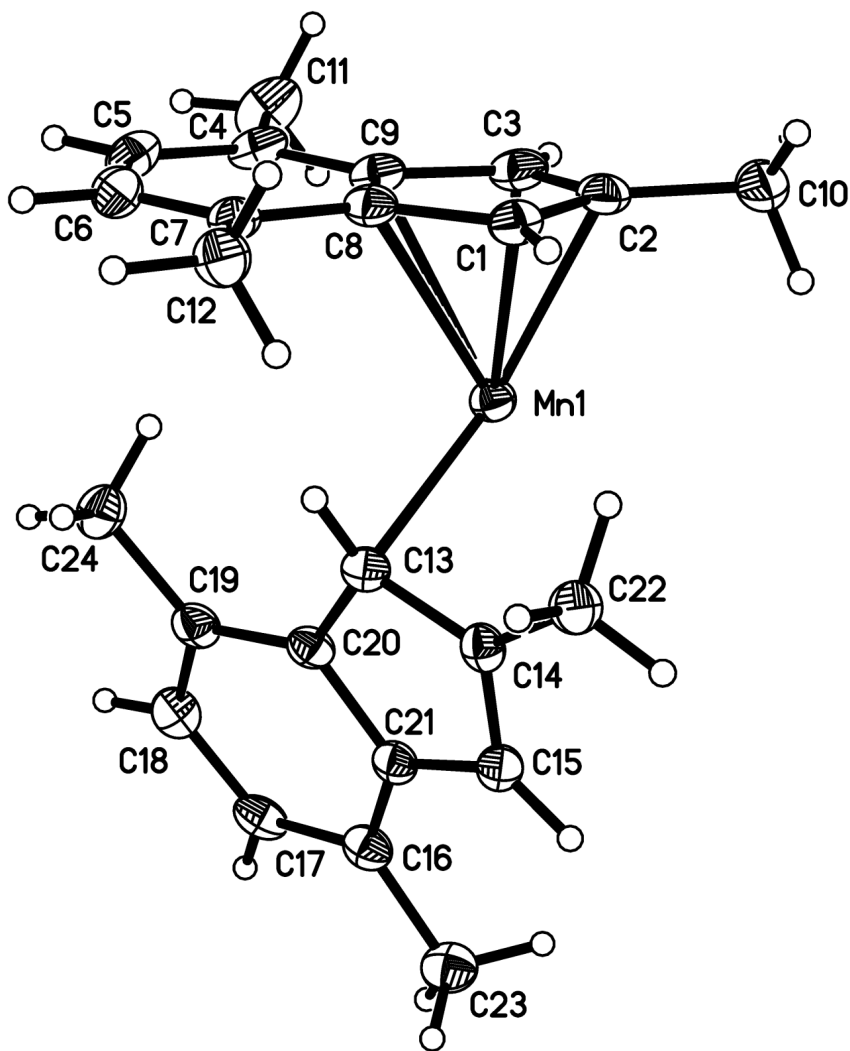
Figure 57. Asymmetric unit of $(Ind^{3Me-2,4,7})_2Mn$.

Discussion

In contrast to the low-spin or spin crossover behavior observed in methyl substituted cyclopentadienyl compounds,[27,156,157] bis(indenyl)manganese(II) complexes have all been found to be high spin. This is confirmed both by magnetic susceptibility measurements (spin-only value of $S = 5/2$ is 5.92 μ_B) as well as the length of Mn−C bonds in the crystal structures. High spin Cp'$_2$Mn complexes have an average Mn−C

bond distance near 2.4 Å, whereas the average is around 2.1 Å for low spin complexes.[27] The average length of the Mn−C bond is over 2.4 Å for all bis(indenyl) complexes. These distances alone are suggestive of a high spin Mn(II) center, the assignment of which has been supported by all available magnetic data.

The high spin nature of the bis(indenyl)manganese(II) complexes is also different from similar complexes of Cr^{II}, in which the complexes with $Ind^{2Me-4,7}$ or $Ind^{3Me-2,4,7}$ showed spin crossover behavior.[35,36] This difference can be explained by the fact Mn^{II} has 5 unpaired d- electrons, which require more spin-pairing energy to leave only 1 electron in the low-spin state than do the 4 d electrons of Cr^{II}, whose conformation changes from 4 to 2 unpaired electrons. Also, some of the structures are quite different; $(Ind^{2Me-4,7})_2Mn$ is an octomer in the solid state, for example, as opposed to the monomeric sandwich structure of its chromium counterparts, which also influences the spin state of the molecule.

An increase in the donor character of the Cp ligand is afforded by the addition of alkyl donating groups, such as those in 1,1′-dimethylmanganocene.[25] This simple modification from the parent Cp_2Mn is enough to lower the HOMO–LUMO gap to an energy that supports a spin-crossover state. As an adjunct to this work, methylation of the C_5 ring on the indenyl ligand and the subsequent incorporation of the modified ligands into Mn^{II} complexes was pursued. The tendency of these compounds to form orange to red oils that show signs of decomposition after a day initially hindered characterization. However, more recently it has been discovered that the use of higher purity $MnCl_2$ sources, solvents without added stabilizers, and less than two full

equivalents of the methylated indenide per manganese atom, produces complexes that do not decompose upon standing.

Given the need for a stronger donating ligand, a more heavily methylated indene, 2,4,7-trimethylindene, was synthesized and deprotonated. The reaction of two equivalents of the ligand with one equivalent of $MnCl_2$ produced bright-orange, highly branched crystals that were unsuitable for x-ray crystallography. Crystals of this compound were eventually obtained from a solution of the mono(indenyl)manganese(II) halide that underwent Schlenk-type equilibrium to produce the bis(indenyl)manganese complex (a process explained and discussed in Chapter IV). Elemental analysis of C, H, and Mn confirmed the composition of $(Ind^{3Me-2,4,7})_2Mn$, and this compound was established to be high-spin by solution magnetic susceptibility methods (5.68 μ_B). This result would suggest the need for even stronger donor substituents such as isopropyl or *t*-butyl groups to promote a spin-crossover or low-spin complex; however, there is evidence *t*-butyl groups can paradoxically support a high-spin state due to their steric bulk,[33] and there has been a report of the high-spin complex bis(1,3-diisopropylindenyl)manganese(II).[158]

Conclusions

We have synthesized the first indenyl manganese(II) systems. As anticipated from manganocene and its derivatives, bis(indenyl)manganese(II) complexes display a wide range of Mn–C bond distances, as well as various hapticities of the indenyl ligand. This makes direct comparisons of the reactivity among the metal centers difficult due to their different coordination environments.

Indenyl ligands with only methyl substituents do not provide enough steric hindrance to prevent access to the manganese center. The divergence from the typical sandwich compounds observed in transition metal complexes is unexpected, although not unreasonable due to the larger metal radius and the fact that in high-spin d^5 complexes there is no ligand field stabilization energy. Manganese centers bound to two or more indenyl ligands favor the high-spin state regardless of the coordination environment, as seen from the magnetic properties of the trimethylsilylated, isopropylated, and methylated species. In the cases of methyl substitution on the indenyl ring, the ease of ring slippage combined with the lack of steric bulk allows for more than two ligands (indenyl, solvent, or otherwise) to bind the metal center. The generation of low-spin or spin-crossover complexes may be more likely with the use of more heavily methylated ligands. Alternative substituents which have been investigated include ethyl and isopropyl groups.[158] Bulkier groups, such as t-butyl or trimethylsilyl, may be less capable of supporting the shorter Mn–C bond distances of the low-spin state due to the steric repulsion of the opposing ring. In comparison, shorter metal–carbon bond distances do appear in the complexes (Ind$^{2Si-1,3}$)$_2$M (M = V, Cr,[33] or Fe[159]), giving further evidence that manganese requires a higher ligand field strength to produce low-spin complexes than do other first row metals.

CHAPTER IV

SYNTHESES, STRUCTURES, AND REACTIVITIES OF MONO(INDENYL)MANGANESE(II) HALIDES

Introduction

Along with the synthesis of the new methylated bis(indenyl) complexes of Mn^{II}

discussed in Chapter III, a series of dimeric indenyl manganese(II) halides (halide =

chloride or iodide) have also been synthesized. Unlike what has been found for some of

the bis(indenyl) complexes, the dimeric mono(indenyl)manganese halides show

remarkable structural similarity to their Cp analogs.[98] Figure 39 in Chapter II shows an

example of one of these Cp compounds, which features Cp^{Me-1}, bridging chlorides, and

triethylphosphine ligands. Both the Cp and indenyl complexes feature the same dimeric

bridging halide structure, as well as being high spin with antiferromagnetically coupled

Mn centers.

The indenyl and Cp manganese halides are also both observed to exhibit Schlenk

equilibrium in solution. Schlenk equilibrium is a phenomenon most often associated with

magnesium and other group II metals, and in particular, Grignard reagents.[160] Grignard

reagents are alkylmagnesium halides (MgRX), which in solution undergo constant

rearrangement to form the magnesium halide and dialkyl magnesium compounds as

shown below.[160]   While this behavior is not often seen with manganese compounds,

high-spin Mn^{II} does share similarities with Mg^{II}, so this parallel reactivity should not be

completely unexpected. The two metals are very similar in size, as mentioned in Chapter

II ($r_{Mn^{II}}$ = 0.81 Å; $r_{Mg^{II}}$ = 0.86 Å)[50,51]. In addition, high-spin Mn^{II} lacks any ligand field

stabilization energy due to its 5 unpaired electrons. This is part of the reason Mn^{II} will display very ionic behavior in some of its compounds, a feature that is much more similar to magnesium than is the case other transition metals.

$$2 \text{ MgRX} \quad \longleftrightarrow \quad \text{MnR}_2 + \text{MnX}_2 \tag{3}$$

This series of indenyl compounds is unique, however, due to the reactivity observed with molecular oxygen while in solution, a feature not shared with the Cp analogs. At low temperature (-78 °C) and very low concentrations of oxygen (single ppm level), several $[\text{MnIndX(thf)}]_2$ compounds undergo a dramatic color change from yellow-orange to dark blue. This has been attributed to the coordination of the trace amounts of oxygen to form a superoxoide or peroxide species.

Reactions of manganese with both molecular oxygen and superoxide have been of interest for some time due to their relevance in manganese containing enzyme functions, particularly manganese superoxide dismutase and catalase, as well as the oxygen-evolving complex (OEC) in photosystem II.[161-165] However, the exact mechanisms of some of these processes are not fully understood, making reactions of manganese with oxygen of particular interest for helping to design useful models of biological systems.

There are a few different forms oxygen can take when it coordinates to metal centers: it can stay a neutral ligand and coordinate as dioxygen, it can be reduced once to O_2^- and become superoxide, or it can be reduced twice to O_2^{2-} and become peroxide. The identity of these species is usually identifiable through various methods of spectroscopy, which will be described below.

There have been a small number of dioxygen, superoxide- and peroxide complexes of manganese documented,[166-170] but few have actually been derived by

reaction with molecular oxygen.[171,172] Instead, nearly all are formed by either a direct

reaction with a superoxide source, or more commonly, by reaction with hydrogen

peroxide. The other Mn complexes capable of binding molecular oxygen are not air-

sensitive, and are able to be pressurized with oxygen to help facilitate coordination. The

fact that the organometallic compounds discussed in this chapter are highly air-sensitive,

and cannot simply be pressurized with oxygen, makes isolation of the oxygenated species

difficult and full quantification of the reactivity almost impossible. The sensitivity of

these compounds, down to low (< 5ppm) levels of O_2, is a major source of the interest in

their behavior. While the effective limit of detection of oxygen for these compounds is

extremely low, the upper window of oxygen concentration needed to decompose the

compounds is almost equally as low, causing challenges throughout the characterization

process.

Characterization of dioxygen adducts of manganese and peroxo- and

superoxomanganese compounds is typically done with a combination of methods

including UV-vis, infrared, Raman (and resonance Raman), and EPR (electron

paramagnetic resonance) spectroscopy, as well as mass spectrometry and X-ray

diffraction. For both peroxo and superoxo compounds of manganese, UV-vis serves as a

method to confirm the presence of the oxo species by the observation of two peaks in the

absorption spectrum: a narrower band in the range between 400-450 nm and a broader

band between 575-650 nm.[170,171] While this technique is not effective in differentiating

between a superoxide and peroxide species, infrared spectroscopy and X-ray

crystallography (when applicable) can be used to do so. Superoxides will generally have

an O−O stretch in the range of 950-1200 cm^{-1} and will have O−O bond lengths in the

neighborhood of 1.20-1.35 Å.[173] Peroxides, on the other hand, will usually have O−O

stretches in the range of 650-950 cm^{-1} and bond lengths around 1.38-1.55 Å.[173] [18]O

labeling experiments are helpful for IR characterization because a clear shift can be seen

in the IR spectra for the O−O stretch. Isotopically labeled [18]O experiments are also useful

with mass spectrometry to prove the presence of a coordinated O_2 by observing a shift of

4 m/z units in the mass spectrum.[171] The isotopically labeled experiments for IR and

mass spectrometry were not performed for the compounds in this study due to a lack of

[18]O availability.

Resonance Raman spectroscopy can also be used to identify the mode of oxygen

coordination and give insight into the M−O and O−O bonding in metal-O_2 compounds.[174]

The last major characterization technique that can help to give insight onto the nature of

the metal-O_2 bonding is electron paramagnetic resonance spectroscopy (EPR). This

technique can give information about the spin state, and consequently oxidation state, of

the metal center. For Mn ($I = 5/2$ for [55]Mn), the hyperfine splitting can potentially

indicate whether a compound is Mn^{II} (A = 75-90 G) or Mn^{III} (A = 50-65 G).[175,176] These

trends hold true for monomeric species of coordination compounds that typically have

very defined (usually octahedral) geometries. Due to our complexes being

organometallic and also dimeric, at least in solution, the generic assignment of oxidation

state based on hyperfine splitting may not be applicable. However, an EPR spectrum

should still be able to indicate a change in the manganese environment, as well as the

presence of superoxide if it is formed.

We report here the preparation and characterization of a series of substituted

mono(indenyl)manganese(II) halides that display reactivity with molecular oxygen at low

concentrations to form what is tentatively assigned as a superoxide complex. Due to the characterization challenges presented by the oxo-compounds, reactions with a number of other potential oxidizing molecules were also examined.

Experimental

General Considerations. All manipulations were performed with the rigorous exclusion of air and moisture using Schlenk or glovebox techniques. Proton (^{1}H) NMR experiments were obtained on a Bruker DPX-300 spectrometer at 300 MHz, Bruker DPX-400 at 400 MHz or Bruker DRX-501 spectrometer at 500 MHz. Elemental analyses were performed by Desert Analytics (Tucson, AZ). Melting points were determined on a Laboratory Devices Mel-Temp apparatus in sealed capillaries. Mass spectra were obtained using a Hewlett-Packard 5890 Series II gas chromatograph/mass spectrometer.

Materials. Anhydrous manganese(II) chloride (99.999%) was purchased from Alfa Aesar and used as received. Indene, 2-methylindene, methacryloyl chloride, *p*-xylene, 3-chloropropionyl chloride, *n*-butyl lithium, potassium bis(trimethylsilyl)amide, *p*-toluenesulfonic acid, anhydrous pentane, and anhydrous, unstabilized tetrahydrofuran (THF) were purchased from Aldrich and used as received. Hexanes, toluene, and diethyl ether were distilled under nitrogen from potassium benzophenone ketyl. Toluene-d_8 (Aldrich) was vacuum distilled from Na/K (22/78) alloy and stored over type 4A molecular sieves prior to use. Substituted indene ligands prepared as described in Chapter III.

Magnetic Measurements. Solution magnetic susceptibility measurements were performed on a Bruker DRX-400 spectrometer using the Evans' NMR method.[148] The

paramagnetic material (5–10 mg) was dissolved in toluene-d_8 in a 1.0 mL volumetric flask. The solution was thoroughly mixed, and approximately 0.5 mL was placed in an NMR tube containing a toluene-d_8 capillary. The calculations required to determine the number of unpaired electrons based on the data collected have been described elsewhere.[149]

UV-Vis Spectroscopy. Electronic absorption spectra experiments were run in the Que lab at the University of Minnesota. The experiments were run on a Hewlett-Packard (Agilent) 8453 diode array spectrophotometer (190-1100 nm range) in quartz cuvettes cooled using a liquid nitrogen cooled cryostat from Unisoku Scientific Instruments (Osaka, Japan).

Electron Paramagnetic Resonance (EPR). X-band (9.62 GHz) EPR spectra were recorded on a Bruker 300 spectrometer equipped with an Oxford ESR 910 cryostat for low temperature measurements. The microwave frequency was calibrated with a frequency counter and the magnetic field with an NMR gaussmeter. The temperature was calibrated with a carbon-glass resistor temperature probe (CGR-1-1000, Lake Shore Cryotronics).

Resonance Raman Spectroscopy. Resonance Raman spectra were collected on an ACTON AM-506M3 monochromator with a Princeton LN/CCD data collection system (LN-1100PB) using a Spectra Physics Model 2060 krypton laser or a Spectra Physics Beamlok 2065-7S argon laser, and Kaiser Optical holographic super-notch filters. Samples were frozen onto a gold-plated copper cold finger in thermal contact with a Dewar flask containing liquid nitrogen. The Raman frequencies were referenced to indene.

IR Spectroscopy. Solution IR spectra were recorded on a Thermo-Nicolet FT-IR module instrument Magna 760 spectrometer at 4 cm^{-1} resolution. 10 mM samples in toluene were run in an International Crystal Labs solution cell. Room temperature samples were loaded in a glove bag under an argon atmosphere. For low temperature experiments, the cell was brought into the glove box where it was cooled to -40 °C along with the blue oxo-species. The sample was then loaded in the cell and immediately transported out of the box and into the instrument while in a plastic bag to avoid water condensation. The sample chamber of the instrument had been cooled with dry ice and was purged with argon in attempt to keep the chamber both cold and dry.

General Procedures for X-ray Crystallography. A suitable crystal of each sample was located, attached to a glass fiber, and mounted on a Bruker SMART APEX II CCD Platform diffractometer for data collection at 173(2) K or 100(2) K. Data collection and structure solutions for all molecules were conducted at the X-ray Crystallography Facility at the University of Rochester by Dr. William W. Brennessel or at the University of California, San Diego by Dr. Arnold L. Rheingold. Data resolution of 0.84 Å were considered in the data reduction (SAINT 7.53A, Bruker Analytical Systems, Madison, WI).

The intensity data were corrected for absorption and decay (SADABS). All calculations were performed using the current SHELXTL suite of programs.[150] Final cell constants were calculated from a set of strong reflections measured during the actual data collection.

The space groups were determined based on systematic absences (where applicable) and intensity statistics. A direct-methods solution was calculated that

provided most of the non-hydrogen atoms from the E-map. Several full-matrix least squares/difference Fourier cycles were performed that located the remainder of the non-hydrogen atoms. All non-hydrogen atoms were refined with anisotropic displacement parameters. All hydrogen atoms were placed in ideal positions and refined as riding atoms with relative isotropic displacement parameters.

Synthesis of {(2,4,7-trimethylindenyl)manganese(II)chloride(thf)}$_2$, {(Ind$^{3Me-2,4,7}$)MnCl(thf)}$_2$. MnCl$_2$ (0.302 g, 2.40 mmol) was slurried in THF (50 mL) in a 250 mL Erlenmeyer flask. After stirring for 45 min to disperse the MnCl$_2$, K[Ind$^{3Me-2,4,7}$] (0.475 g, 2.42 mmol) in THF (100 mL) was added dropwise to the MnCl$_2$, gradually turning the solution green-yellow. After stirring overnight, the THF was removed under vacuum, leaving a yellow solid. The product was extracted with pentane (3 x 30 mL) and filtered over a medium porosity frit to remove the KCl precipitate. During filtration, the filtrate turned dark green when passing through the frit, and remained that color for about one minute before returning to light yellow in color. The light yellow solution was then evaporated to dryness, leaving 0.321 g (43%) of a yellow-orange solid. The remaining product was redissolved in pentane, and was slowly cooled to -25 ºC to give green-yellow needles that were of X-ray quality. mp 130-133 °C. Anal. Calcd. for C$_{30}$H$_{42}$O$_2$Mn$_2$Cl$_2$: C, 60.10; H, 6.62; Mn, 17.18. Found: C, 60.10; H, 6.84; Mn, 17.2. Solution magnetic susceptibility: μ_{eff} (298 K): 7.27 μ_B.

Synthesis of {(2-methylindenyl)manganese(II)iodide(thf)}$_2$, {(Ind^{Me-2})MnI(thf)}$_2$. MnI$_2$ (0.703 g, 2.28 mmol) dissolved in THF (50 mL) in a 250 mL Erlenmeyer flask. After stirring for 1 h at room temperature to allow for dispersion of the MnI$_2$, a solution of potassium 2-methylindenide (0.383 g, 2.28 mmol) in THF (75 mL)

was added dropwise, resulting in an immediate change in color to golden yellow. After stirring overnight, the THF was removed under vacuum, leaving an orange powder. An attempted extraction with pentane did not remove any product. A second and third extraction using toluene (20 mL) produced an orange solution, which turned green upon passing through a medium porosity frit before changing back to orange upon standing. The toluene extractions were then combined and the solution was concentrated by removal of some of the solvent under vacuum. Hexanes were then added to the solution to make approximately a 2:1 ratio of toluene to hexanes solution, and then slowly cooled to – 10 °C for 3 days to produce 0.317 g (38%) of green crystalline blocks, mp 160-165 (dec). Anal. Calcd for $C_{28}H_{34}O_2Mn_2I_2$: C, 43.87; H, 4.47; Mn, 14.35; I, 33.1. Found: C, 43.71; H, 4.54; Mn, 13.68; I, 34.4.

Attempted synthesis of {(2-methylindenyl)manganese(II)chloride(thf)}$_2$, {(Ind^{Me-2})MnCl(thf)}$_2$. MnCl$_2$ (0.279 g, 2.22 mmol) was added to a 250 mL Erlenmeyer flask and dispersed in THF (50 mL) by stirring at room temperature for 1 h. Potassium 2-methylindenide (0.379 g, 2.25 mmol) was then dissolved in 75 mL of THF and added dropwise through an addition funnel to the MnCl$_2$ solution. The bright yellow solution was allowed to stir overnight at room temperature, turning orange overnight. The solvent was removed under vacuum to leave a yellow-orange residue. The product was extracted first with pentane (3 x 30 mL), but it was not very soluble. The pale yellow solution was then passed through a medium porosity glass frit, where the filtrate came through dark blue; the color persisted about a minute before turning back to pale yellow. Toluene was then used to extract the product (4 x 30 mL) and the extract was also filtered through a medium porosity frit to remove any KCl. Like the pentane extract, the solution turned

blue coming through the frit and remained that color for a few minutes before returning to a yellow-orange color. Removal of solvent from the pentane and toluene extracts (done separately) produced a total yield of 0.134 g (22%) of an oily orange-yellow product. Attempts to concentrate the solution and grow crystals were unsuccessful.

Attempted synthesis of {(indenyl)manganese(II)chloride(thf)}₂,

{(Ind)MnCl(thf)}₂. $MnCl_2$ (0.200 g, 1.59 mmol) was added to a 250 mL Erlenmeyer flask and dispersed in THF (30 mL) by stirring at room temperature for 1 h. Lithium indenide (0.188 g, 1.54 mmol) was dissolved in THF (50 mL) and added dropwise through an addition funnel to the flask with $MnCl_2$. The solution turned yellow after a few drops and gradually turned dark orange after complete addition. The solution was stirred overnight at room temperature before removal of the solvent under vacuum left a dark red-orange solid. Pentane was added (20 mL) to extract the product, but the product was insoluble in pentane and the colorless pentane extract was evaporated to yield a colorless oil that was likely the coupled indene. An attempt to extract with toluene yielded a very dark orange solution that produced 0.261 g of an oily orange-red solid when the toluene extract was filtered and solvent removed under vacuum. Crystallization attempts were unsuccessful.

Alternate method: $MnCl_2$ (0.297 g, 2.36 mmol) was added to a 250 mL Erlenmeyer flask and dispersed in THF (50 mL) by stirring at room temperature for 1 h. Potassium indenide (0.268 g, 2.39 mmol) was dissolved in THF (70 mL) and added dropwise through an addition funnel to the flask with $MnCl_2$. The orange solution was allowed to stir overnight at room temperature before removal of the solvent under vacuum yielded an orange powder. Pentane was added to extract the product, but the

product was insoluble in pentane and the colorless pentane extract was evaporated to yield a colorless oil that was likely the coupled indene. An attempt to extract with toluene (3 x 30 mL) yielded a dark orange solution that briefly turned green while filtering through a medium porosity frit, then changed back to orange upon standing. Attempts to crystallize and isolate the product produced only films and oils that could not be characterized.

Attempted synthesis of {(indenyl)manganese(II)iodide(thf)}$_2$, {(Ind)MnI(thf)}$_2$. MnI$_2$ (0.304 g, 0.99 mmol) was added to a 250 mL Erlenmeyer flask and dispersed in THF (40 mL) by stirring at room temperature for 1 hour. Potassium indenide (0.153 g, 0.99 mmol) was dissolved in THF (50 mL) and added dropwise through an addition funnel to the flask with MnI$_2$. The solution turned golden yellow and was allowed to stir overnight at room temperature. The next morning the solution had changed to red, and removal of the solvent under vacuum to yielded an orange-red solid. The product was not soluble in pentane, so it was extracted with toluene (3 x 30 mL) and filtered through a medium porosity frit (no color change was observed). The toluene was removed under vacuum to leave 0.280 g (40%) of an oily red solid that could not be successfully characterized.

Reactions of (indenyl)manganese(II) halides with various gases. Small amounts (~10 mL) of 10 mM to 50 mM (Ind$^{3Me-2,4,7}$)MnCl(thf) or (Ind^{Me-2})MnCl(thf) in toluene or pentane or a mixture of the two were added to a 300 mL pressure vessel inside a drybox. The vessel was then brought out of the box and put on a Schlenk line where it was degassed and cooled to -78 °C. The vessel was then pressurized with 20-40 psi of various laboratory-grade gases (N$_2$, CO, H$_2$, CO$_2$, Ar, and He were all tried) and in every

case, the yellow solution gradually turned dark green and eventually a deep royal blue after a few min. The time necessary to change color could be correlated with the identity of the gas, as the higher the O_2 impurity of the gas, the faster the solutions changed color. Regular NF grade N_2 (<100 ppm O_2) displays the fastest change (< 30 sec), followed by CO (< 10 ppm O_2; < 1 min), UHP Ar (< 2 ppm O_2; 2-3 min), and eventually Research Grade N_2 (< 0.5 ppm O_2; 5 min). Solutions remained blue as long as they were kept below -20°. Upon warming, the blue color dissipates and the solution usually returns to its initial color. This can usually be repeated anywhere from 1-6 times before the color change can no longer be induced by cooling.

The solutions could be opened to vacuum at -78 °C and the blue color would remain, but upon warming to room temperature, the solutions returned to their initial yellow color. Attempts to grow crystals of the blue compound at these temperatures by the removal of solvent produced the original compounds as yellow or orange solids. The only gas that did not produce this color was O_2 itself, which instead turned the solution brown within seconds of pressurizing with O_2 at -78 °C. However, when a degassed solution was pressurized with a minimal amount of O_2 (5 mmol) a color change was observed in the solution, as a blue color slowly descended from the top of the solution while the very top of the solution turned brown. The solution exposed to pure O_2 does not remain blue indefinitely, as eventually the solution slowly turns brown after a couple minutes, even at low temperature. Other attempts to add stoichiometric quantities of O_2 have been met with similar results, making it nearly impossible to quantify the amount of O_2 that is actually coordinated at any point in time. One additional feature of these experiments is that when they are done in THF instead of pentane or toluene, no color

99

changes are observed, suggesting that THF blocks the open coordination site where O_2 likely binds.

Reactions of {(Ind$^{3Me-2,4,7}$)MnCl(thf)}$_2$ with bipyridine, NOBF$_4$, azobenzene, and tetrathiafulvalene. 1 mM to 10 mM solutions of {(Ind$^{3Me-2,4,7}$)MnCl(thf)}$_2$ in pentane or toluene were exposed both to the solid forms of bipyridine (bipy), NOBF$_4$, azobenzene and tetrathiafulvalene. Bipy, azobenzene and tetrathiofulvalene were also added dropwise as a solution in toluene or pentane. In the case of bipy, a brown solid was produced that was soluble in toluene and THF, but could not be characterized. It is possible that this compound is simply a bipy solvate, where bipy has replaced THF, and likely taken up any remaining coordination sites on the Mn, or caused the indenyl ligand to slip to accommodate its coordination. The NOBF$_4$ salt was not soluble in any available organic solvents, so it was added directly to the solution of {(Ind$^{3Me-2,4,7}$)MnCl(thf)}$_2$, and it caused an immediate color change to a deep blue-green color. This color only persisted for a couple of minutes before the solution turned black and precipitated out an intractable black tar. This process was repeated at cold temperature (-30 °C), but the same result was obtained. Addition of azobenzene and tetrathiafulvalene had no visible or measureable effect on the compound in solution.

Reaction of {(Ind$^{3Me-2,4,7}$)MnCl(thf)}$_2$ with CO. In order to expose {(Ind$^{3Me-2,4,7}$)MnCl(thf)}$_2$ to CO without having O_2 present to contaminate the reaction, a method other than direct CO pressurization had to be attempted. To do this, 20 mL of a 0.10 mM solution of {(Ind$^{3Me-2,4,7}$)MnCl(thf)}$_2$ in a 50/50 mix of toluene and pentane was degassed and cooled to -78 °C in a Schlenk flask. The Schlenk flask was connected to a separate sealed Schlenk tube that had also been put under partial vacuum and contained solid

Co_2CO_8 (0.189 g, 1.1 mmol). The Co_2CO_8 was then heated to 50°C, causing it to decompose into Co_4CO_{12} and CO gas. Excess of CO was used to try and encourage reactivity. Upon opening the cooled solution of $\{(Ind^{3Me-2,4,7})MnCl(thf)\}_2$ to the CO source, the yellow solution slowly turned a dark maroon color. As with the pressurization experiments, the color dissipated upon warming. An IR spectrum of the maroon solution appeared the same as $\{(Ind^{3Me-2,4,7})MnCl(thf)\}_2$; there was no evidence for a CO stretch.

Results

Mono(indenyl)manganese(II) halide complexes were synthesized by salt metathesis elimination reactions of the appropriate indenide salts with MnX_2 in THF (5).

$$2 \ K[Ind'] \ + \ 2 \ MnX_2 \xrightarrow{\text{THF}} \{Ind'MnX(thf)\}_2 + 2 \ KX\downarrow \quad (X = Cl \text{ or } I) \quad (5)$$

After the removal of THF under vacuum, addition of pentane or toluene served to extract the manganese complexes, allowing for the removal of the alkali metal chloride by-products. The purified (indenyl)manganese complexes were crystallized by cooling of a concentrated solution to approximately -30 °C. They are lighter in color than their bis(indenyl) counterparts and tend to be green-yellow in color for the chlorides, and dark green for the iodide. Again, it should be stressed that the preparation of the indenyl complexes requires chemicals and reagents of very high quality (e.g. $MnCl_2$ beads of >99.99% purity) in order to yield consistent results. These compounds are also highly air- and moisture-sensitive, like their bis(indenyl) counterparts. For $\{(Ind^{3Me-2,4,7})MnCl(thf)\}_2$, the solid-state magnetic moment was also determined by SQUID magnetometry, and was fit to an extension of the Bleaney-Bowers equation.[177,178] The

data obtained was consistent with anti-ferromagnetic coupling between two high-spin Mn(II) (S = 5/2) centers (g = 2.04, J/k_B = -17.7 K). The magnetic moment in toluene d_8 is 7.3 µB, which is consistent with the room temperature magnetic susceptibility obtained by SQUID magnetometry (7.74 µB).

Crystallographic Results

[(Ind$^{3Me-2,4,7}$)MnCl(thf)]$_2$. Crystals of [(Ind$^{3Me-2,4,7}$)MnCl(thf)]$_2$ were harvested as green-yellow rods from a cold pentane solution. An ORTEP of an expanded asymmetric unit for the polymeric molecule is shown in Figure 58, which gives the numbering scheme that is referred to in the text. Selected bond lengths and angles are shown in Table 4.

There is an inversion center between the two manganese centers, making only half of the molecule unique. Cp analogues of this dimeric structure are known, [1,2,4-(tBu)$_3$CpMnCl(thf)]$_2$[42] and [(CH$_3$C$_5$H$_4$)MnCl(PEt$_3$)]$_2$.[62] Like these compounds, the indenyl compound features bridging chlorides with Mn-Cl distances of 2.483 Å and 2.424 Å for each manganese to the two chloride atoms. These distances are comparable to those in the Cp analogues. The Mn···Mn distance is noticeably shorter (3.386 Å compared to 3.514 Å), but is still outside of usual Mn···Mn bonding distances.[20] The indenyl ligand appears to show a slipped η^2 interaction, but the rest of the ring is still within range of what has previously been considered bonding. When viewed orthogonally to the C$_5$ plane, the Mn atom is shifted towards the C1 carbon of the ring, as opposed to the C2 carbon as is often expected when slippage occurs. Despite appearing

to be an η^2 interaction, the ring is still clearly delocalized, as the C-C distances of the

five-membered ring are all within 0.03 Å of one another.

Table 4. Selected bond distances for $[(Ind^{3Me-2,4,7})MnCl(thf)]_2$.

Atoms	Distance (Å)	Atoms	Distance (Å)
Mn(2)–C(19)	2.325(2)	C(18)–C(19)	1.409
Mn(2)–C(18)	2.382(2)	C(19)–C(25)	1.432
Mn(2)−C(17)	2.525(2)	C(25)−C(24)	1.437
Mn(2)−C(24)	2.624(2)	C(24)−C(17)	1.418
Mn(2)−C(25)	2.492(2)	C(17)−C(18)	1.400
Avg. Mn–C	2.470(5)	Mn(2)−Cl(2)	2.4237(5)
Mn⋯Mn	3.380(2)	Mn(2)−Cl(2b)	2.4832(6)
		Δ_{Mn-C} = 0.299	
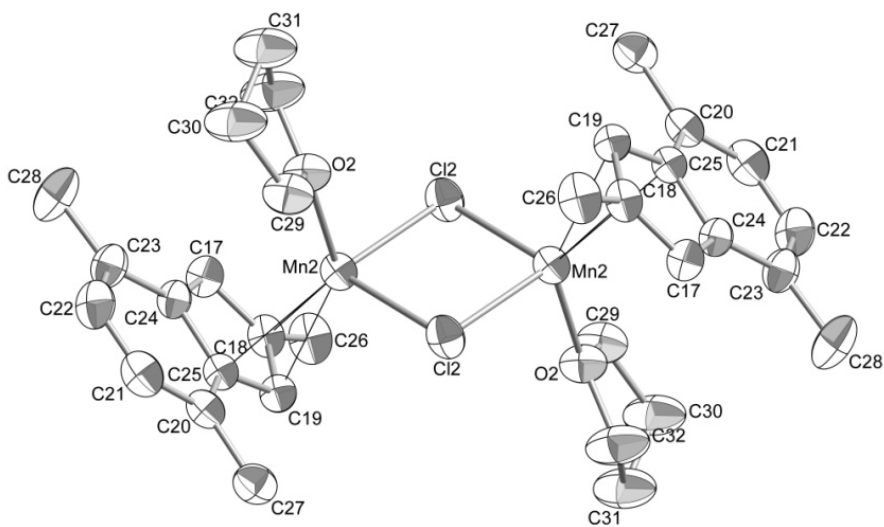
Figure 58. Diagram of the non-hydrogen atoms of $[(Ind^{3Me-2,4,7})MnCl(thf)]_2$ with the numbering scheme used in the text. Thermal ellipsoids are shown at the 50% probability level.

[(Ind^{Me-2})MnI(thf)]₂. Crystals of $[(\text{Ind}^{\text{Me-2}})\text{MnI}(\text{thf})]_2$ were harvested as dark green blocks from a cold mixture of toluene and hexanes (2:1). An ORTEP of an expanded asymmetric unit for the dimeric molecule is shown in Figure 59, which gives the numbering scheme that is referred to in the text. Selected bond lengths and angles are shown in Table 5.

As with the structure of $[(\text{Ind}^{3\text{Me-2,4,7}})\text{MnCl}(\text{thf})]_2$, the compound has an inversion center that makes only half of the molecule unique, but instead of the two bridging chlorides, the compound contains two bridging iodides. The Mn···Mn distance has increased to 3.668 Å from the 3.386 Å in $[(\text{Ind}^{3\text{Me-2,4,7}})\text{MnCl}(\text{thf})]_2$, but that is to be expected due to the increased size of the bridging iodine atoms. A similar increase is observed in the change in the Mn-X bond distances, as the Mn-I distances are 2.792(3) Å and 2.831(3) Å compared to the 2.424(1) Å and 2.483(1) Å observed in the chloride-bridged complex. There is only one previous example of a similar organometallic Mn$^{\text{II}}$ complex with bridging iodides, $[\text{MeCpMnI}(\text{PEt}_3)]_2$, and it displays both longer Mn-I (2.865 Å) and Mn···Mn (3.952 Å) distances. However, this difference is consistent with the difference in ligand sets between $[\text{MeCpMnCl}(\text{PEt}_3)]_2$ and $[\text{Ind}^{3\text{Me-2,4,7}}\text{MnCl}(\text{thf})]_2$.

The indenyl ligands appear to display an unusual type of η^3 coordination. The Mn center is usually bound to the carbons in the 1-, 2-, and 3-postitions of the indenyl ring and is centered roughly over C(2) when the indenyl group is η^3 coordinated. However, in this case, the Mn center is clearly shifted towards C(1) with a bond distance of 2.331(2) Å, almost a full 0.1 Å shorter than the distance to C(2) (2.427(2) Å). As a further indication of an η^3 interaction, the difference in Mn-C distances between the average of these 3 carbons and the remaining 2 carbons is about 0.18 Å. To our knowledge this

would be the first time an indenyl group has shown this type of side-on η^3 conformation. However, despite the difference in Mn-C bond lengths, the Mn-C(3) and Mn-C(9) distances are still both within distances previously considered to be bonding for other η^5 bound Mn(II) complexes.

Table 5. Selected bond distances for [(Ind^{Me-2})MnI(thf)]$_2$.

| Atoms	Distance (Å)	Atoms	Distance (Å)
Mn(1)–C(1)	2.331(2)	C(1)–C(2)	1.422
Mn(1)–C(2)	2.427(2)	C(2)–C(3)	1.411
Mn(1)−C(3)	2.553(2)	C(3)−C(9)	1.426
Mn(1)−C(9)	2.618(2)	C(9)−C(8)	1.442
Mn(1)−C(8)	2.467(2)	C(8)−C(1)	1.435
Avg. Mn–C	2.479(5)	Mn(1)−Cl(1)	2.792(1)
Mn⋯Mn	2.291(3)	Mn(1)−Cl(1a)	2.831(1)
			$\Delta_{Mn-C} = 0.287$
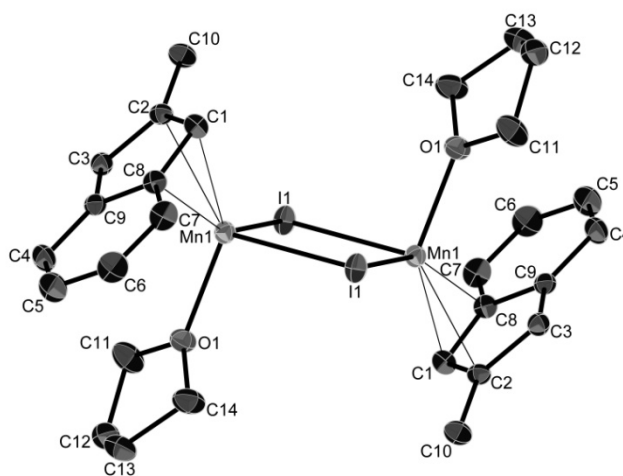
Figure 59. Diagram of the non-hydrogen atoms of $[(Ind^{Me-2})MnI(thf)]_2$ with the numbering scheme used in the text. Thermal ellipsoids are shown at the 50% probability level.

Spectroscopic Results

FTIR Spectroscopy

In an effort to observe the presumed oxygen-bound species of $[Ind^{Me-2}MnCl(thf)]_2$, solution IR spectra were collected for a 10 mM solution of the yellow $[Ind^{Me-2}MnCl(thf)]_2$, and for the same solution after having turned dark blue when cooled to -45 °C in the glovebox freezer (Figure 60). The spectrum of the cold $[Ind^{Me-2}MnCl(thf)]_2$ solution shows a slight change from the initial room temperature spectrum of $[Ind^{Me-2}MnCl(thf)]_2$, with the major difference being the formation of a new peak at 1119 cm^{-1} (Figure 62). This is in the range commonly associated with superoxide O−O stretches, suggesting the oxidation of Mn^{II} to Mn^{III}. Due to the fact that the initial complex is a dimer, it is also possible that the IR band at 1119 cm^{-1} corresponds to a peroxo species where the O_2^{2-} group is bridging between the two manganese centers, both of which have oxidized to Mn^{III}. This experiment was attempted for $[Ind^{3Me-}$

^{2,4,7}MnCl(thf)]$_2$, but the blue species would not persist long enough in solution to transport the solution cell from the glovebox freezer to the instrument, despite several precautions that were taken to prevent this.
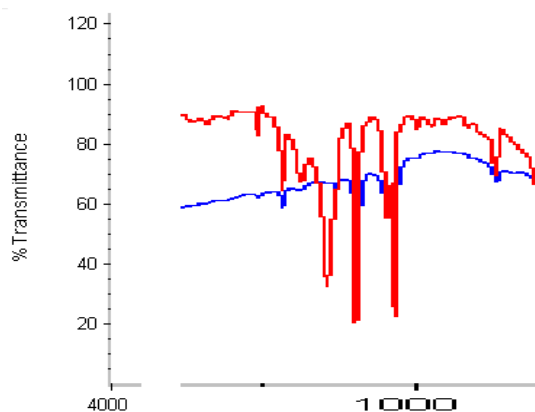
Figure 60. Comparison of IR spectra for [Ind^{Me-2}MnCl(thf)]$_2$ at room temperature (blue spectrum) and the presumed oxo-species at cold temperature (red spectrum)

UV-vis Spectroscopy

To monitor and attempt to quantify the vivid color change that occurs upon cooling [Ind$^{3Me-2,4,7}$MnCl(thf)]$_2$ in the presence of trace levels of oxygen, electronic absorption spectroscopy (UV-vis) was performed. To do this, a 10 mM sample of [Ind$^{3Me-2,4,7}$MnCl(thf)]$_2$ was prepared in toluene and then sealed in a quartz cuvette inside a nitrogen atmosphere glovebox. The sample was then brought outside the box and placed in a UV-vis spectrophotometer with a cryostat to regulate the temperature. Two different experiments were conducted; in the first, the sample was slowly cooled from room temperature to -60 °C in 10° C intervals every 5 minutes while monitoring the corresponding change in the UV-vis spectrum. In the second experiment, the complex was immediately placed in the cryostat that was cooled to -60 °C and the UV-vis

spectrum of the solution was collected every 5 minutes until the absorbance stopped rising (Figure 61). This figure shows the slow increase in absorbance at 643 nm over time (showing spectra from 20 minute intervals) while the solution remains cooled at – 60 °C. The increase in intensity of this peak indicates an increase of the oxygen containing species present in solution.

The only major problem with interpreting these spectra is that there is no way to quantify how much of the initial manganese complex is binding O_2. The first problem encountered in trying to do so involves attempting to fully degas the solution once inside the cuvette, as even a supposedly clean nitrogen atmosphere glove box possesses the requisite oxygen concentrations to initiate the color transition at low temperatures. The cuvettes cannot be freeze-pump thawed, and pulling a vacuum on the non frozen solution will eventually pull off solvent, changing the solution concentration, and hence preventing accurate calculations of observable electronic properties such as molar absorptivity. Attempts were made to syringe in controlled amounts of both air and O_2, but in both instances, the complex quickly turned blue and then brown and the blue color did not persist. If the molar absorptivity were calculated for this compound, assuming all of the Mn had bound oxygen, it would be 250 M^{-1} cm^{-1}. The real value is likely slightly higher, given that not all of the initial complex may have reacted to form the colored species. Other manganese superoxide and peroxide systems have shown similar values for the extinction coefficient ranging anywhere from 70 M^{-1} cm^{-1} to 700 M^{-1} cm^{-1}. [175]

UV-vis Spectra of 10 mmol {Mn(2,4,7-Me$_3$C$_9$H$_4$)Cl(thf)}$_2$ at -60 °C

3

2.5

2

Absorbance

1.5

1

0.5

0

Spectra collected every 20 min
λ$_{max}$ ≈ 643 nm

300   400   500   600   700   800   900   1000   1100

Wavelength (nm)
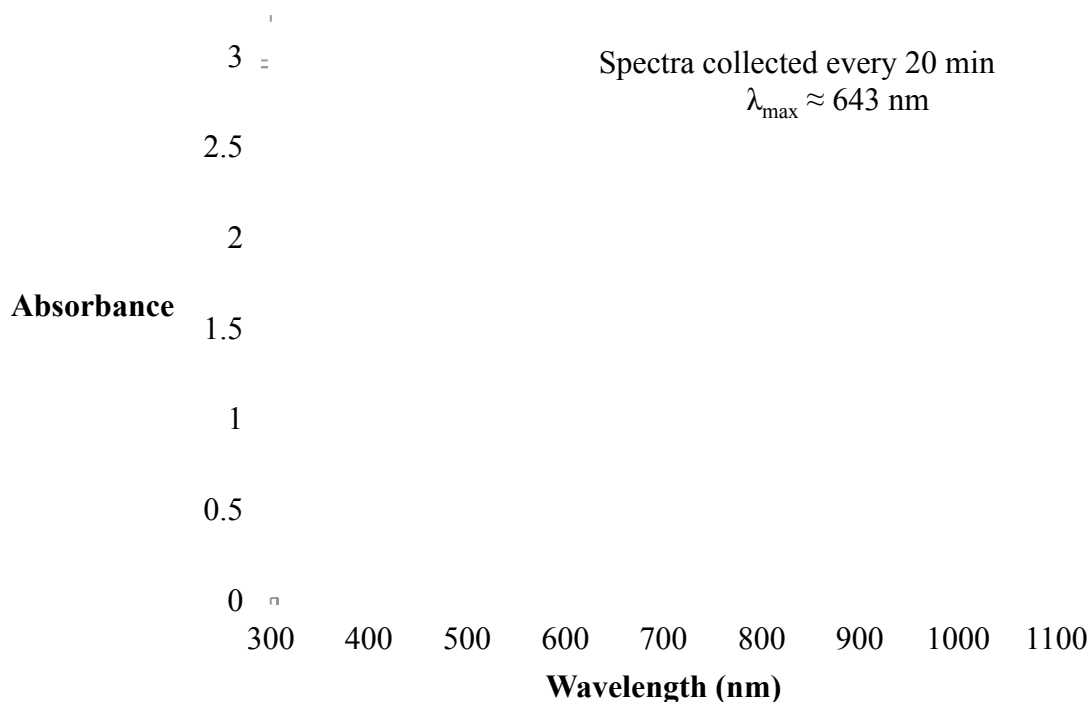
Figure 61. UV-vis spectra for [Ind$^{3Me-2,4,7}$MnCl(thf)]$_2$. Observed λ$_{max}$ at 643 nm consistent with either a superoxido- or a peroxidomangnaese compound.

Resonance Raman

Resonance Raman (rR) studies were performed on [Ind$^{3Me-2,4,7}$MnCl(thf)]$_2$ and its resulting blue oxo-species formed at low temperature. A full excitation profile has been done on both the starting material and the blue oxo-species it forms. Thus far the only results that have been sent to us from our collaborators at the Que lab at the University of Minnesota are for the spectra collected from the excitations at 647 nm. This is near the λ$_{max}$ observed for the oxo species in the UV-vis.

The rR of the oxo-species is very rich, but the fact that there are so many peaks when comparing the blue complex to the starting material (Figure 62) suggests that most

of the peaks are likely to be ligand-based. Had ^{18}O been available to do ^{18}O labeling studies, it would be possible to easily determine which peaks are ligand based and which are O−O and Mn−O based. All spectra were normalized to toluene at 621 cm^{-1}. More definitive information on the oxo-species should be available once the excitation profile is fully analyzed, and the Mn−O peak frequencies should give an indication of the type of Mn−O bonding present.
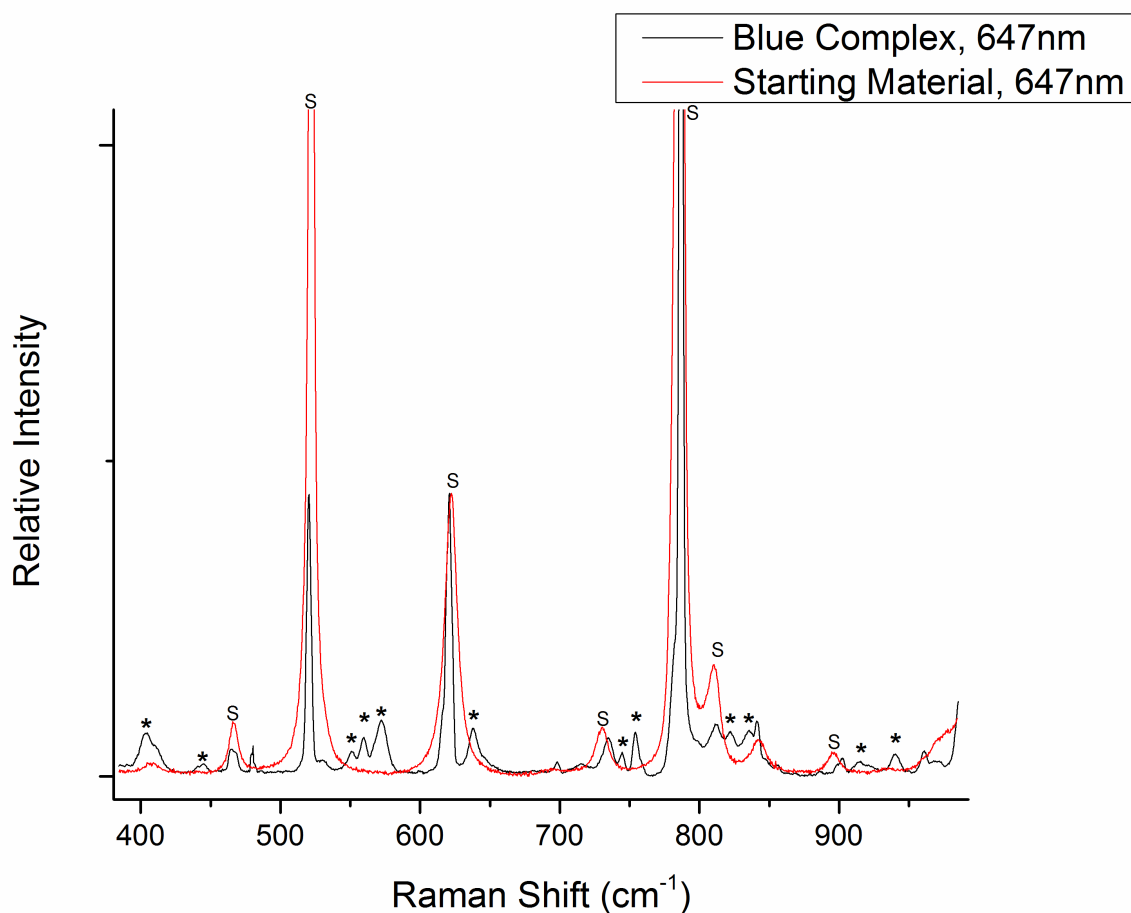
Figure 62. Resonance Raman spectra for the blue oxo-species and the [Ind$^{3Me-2,4,7}$MnCl(thf)]$_2$ starting material at an excitation wavelength of 647nm. Peaks labeled "S" are those of the solvent toluene. Asterisks (*) indicate peaks unique to the oxo-species.

EPR Spectroscopy

      Low temperature X-band EPR spectroscopy was performed on [Ind$^{3Me-2,4,7}$MnCl(thf)]$_2$ (Figure 63), its associated blue oxo-species (Figures 64 and 65), and the decomposition products formed when the oxo-species is warmed (causing the solution to turn brown before being refrozen). There is a stark difference in the spectrum of the blue oxo-species in comparison to the initial [Ind$^{3Me-2,4,7}$MnCl(thf)]$_2$ starting compound (Figure 64). The spectrum of the starting compound is shown below (Figure 63) and contains multiple signals, the clearest two of which have g-values of 4.439 and 3.264. The hyperfine splitting in these signals is exceptionally complicated, as [Ind$^{3Me-2,4,7}$MnCl(thf)]$_2$ contains two $I = 5/2$ ^{55}Mn centers. However, the fact the compound is dimeric with two antiferromagnetically coupled Mn^{II} centers makes it surprising [Ind$^{3Me-2,4,7}$MnCl(thf)]$_2$ even has an EPR signal a low temperature (10 K). The signal centered at $g = 4.439$ is less defined than the one centered at 3.264, which shows much clearer hyperfine splitting; however, it appears as though there are two sets of overlapping six-line hyperfine splitting, each with A $\approx$ 60 G. It is more difficult to decipher the hyperfine of the signal at $g = 4.439$, as it appears there are multiple six-line splittings present as with the signal at $g = 3.264$, but it could also be a slightly distorted eleven-line spectrum, which one might expect for a compound with 2 $I = 5/2$ ^{55}Mn centers.
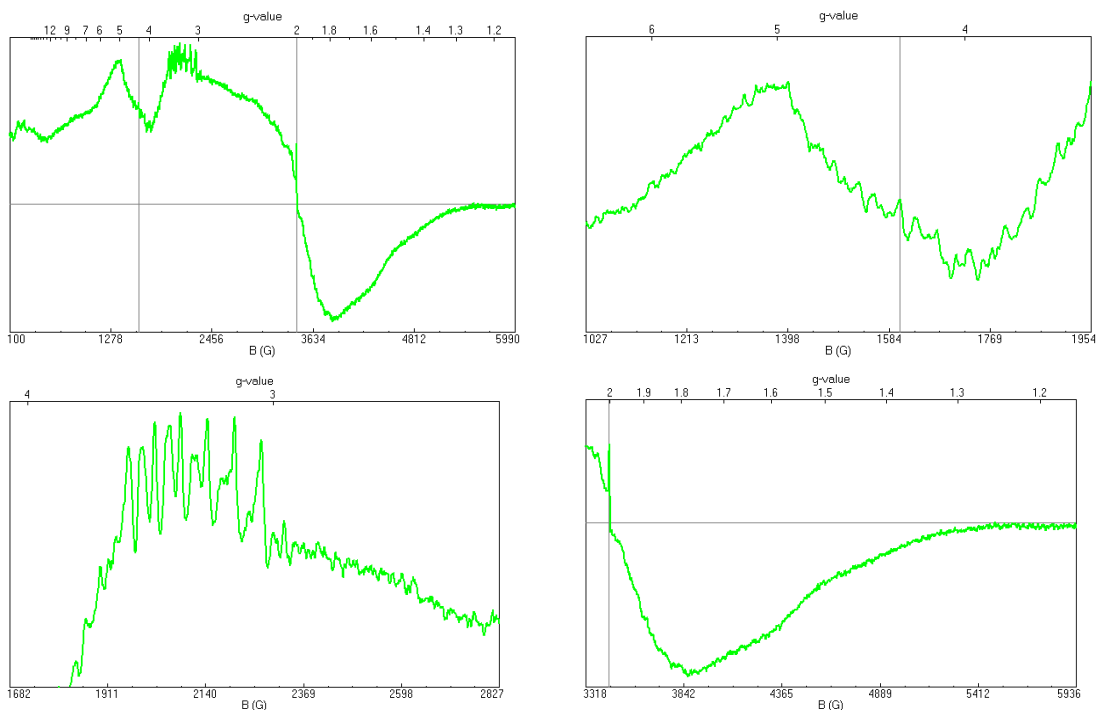
Figure 63. EPR spectrum of [Ind$^{3Me-2,4,7}$MnCl(thf)]$_2$. *T* = 10 K, Freq = 9.65 GHz, Power = 0.2 mW. Full spectrum (top left) and enlarged views of the signals at g = 4.439 (top right), g = 3.264 (bottom left), and potential signals with g < 2.

It is possible that since the signal for [Ind$^{3Me-2,4,7}$MnCl(thf)]$_2$ is relatively weak, that the complex responsible for the EPR signal is not [Ind$^{3Me-2,4,7}$MnCl(thf)]$_2$, but instead (Ind$^{3Me-2,4,7}$)$_2$Mn, which as mentioned in the introduction, is also present in a solution of [Ind$^{3Me-2,4,7}$MnCl(thf)]$_2$.

The spectrum of the oxo-species is much more intense, and has more defined hyperfine splitting. There are signals centered at g = 9.367, g = 4.405, and g = 3.675 that all display hyperfine splitting. The first and last of these display six-line hyperfine splitting patterns with A values of 49 G and 54 G for the signals at g = 9.367 and g = 3.675, respectively. This slight decrease in the hyperfine splitting compared to the initial compound could potentially indicate an oxidation state change in the Mn center from

Mn^{II} to Mn^{III}. The signal at g = 4.405, on the other hand, shows a very complicated, potentially eleven-line, hyperfine pattern that has an approximate A value of 26 G. This is extremely small for a manganese system, suggesting maybe this is actually two overlapping six-line patterns, as in the initial compound. The problem with this assignment is the peak intensities do not seem consistent with what would be expected for two overlapping six-line splitting patterns, which is what appears to be the case for the signal near g = 3.264 for the initial compound. There is may be additional signals with g < 1.8, but they are not strong and do not display any noticeable hyperfine splitting. The last major feature in the spectrum is the presence of a signal that is not associated with Mn, observed near g = 2. This likely corresponds to the presence of a superoxide. There was no ^{17}O available to try and generate an isotopically labeled oxo-species to observe a splitting on this signal from the $I = 5/2$ ^{17}O center.
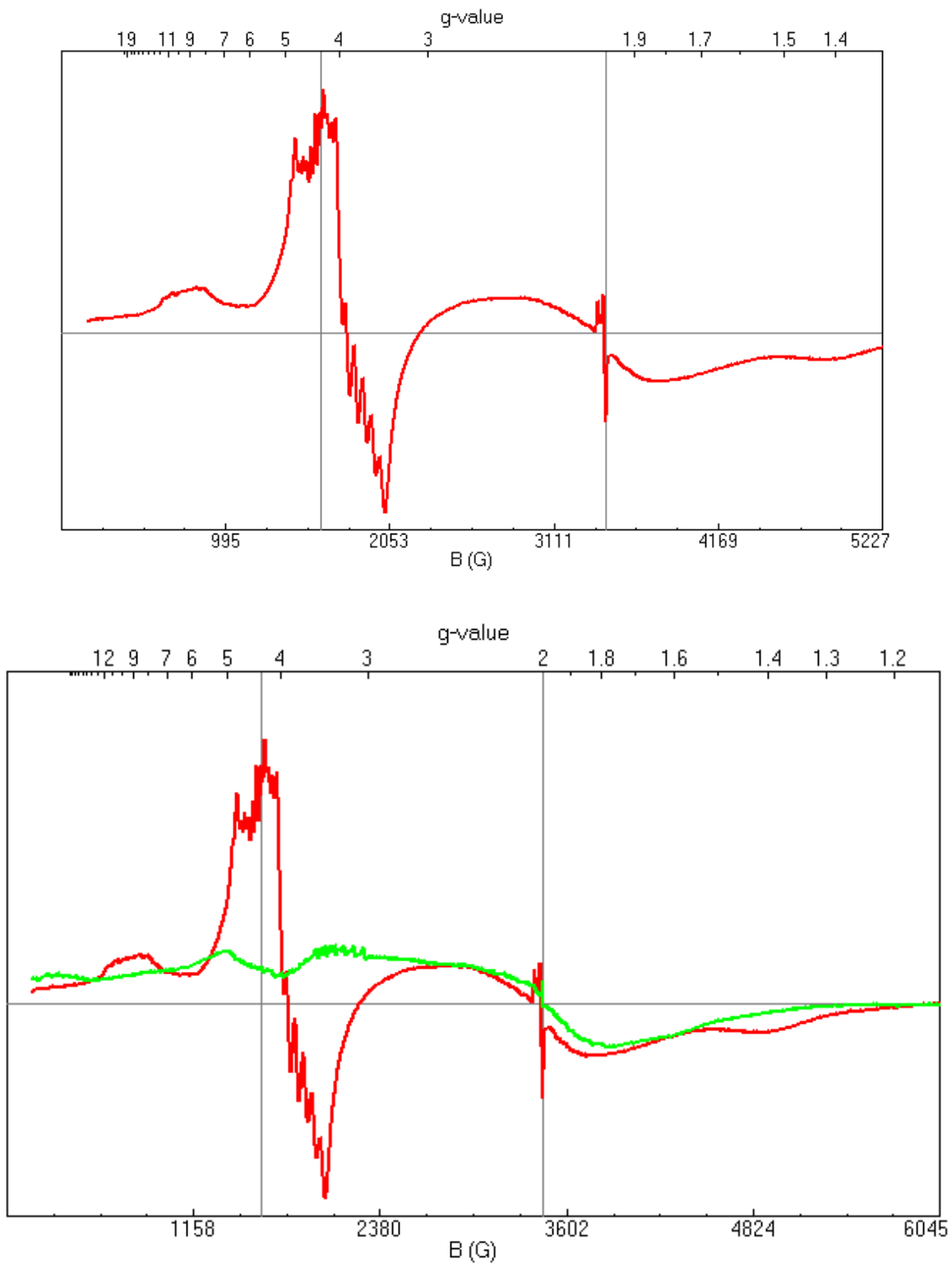
Figure 64. EPR spectrum of oxo-species of [Ind$^{3Me-2,4,7}$MnCl(thf)]$_2$ (top) and a comparison of the oxo- (red) and initial species (green) (bottom). $T = 10$ K, Freq = 9.65 GHz, Power = 0.2 mW.
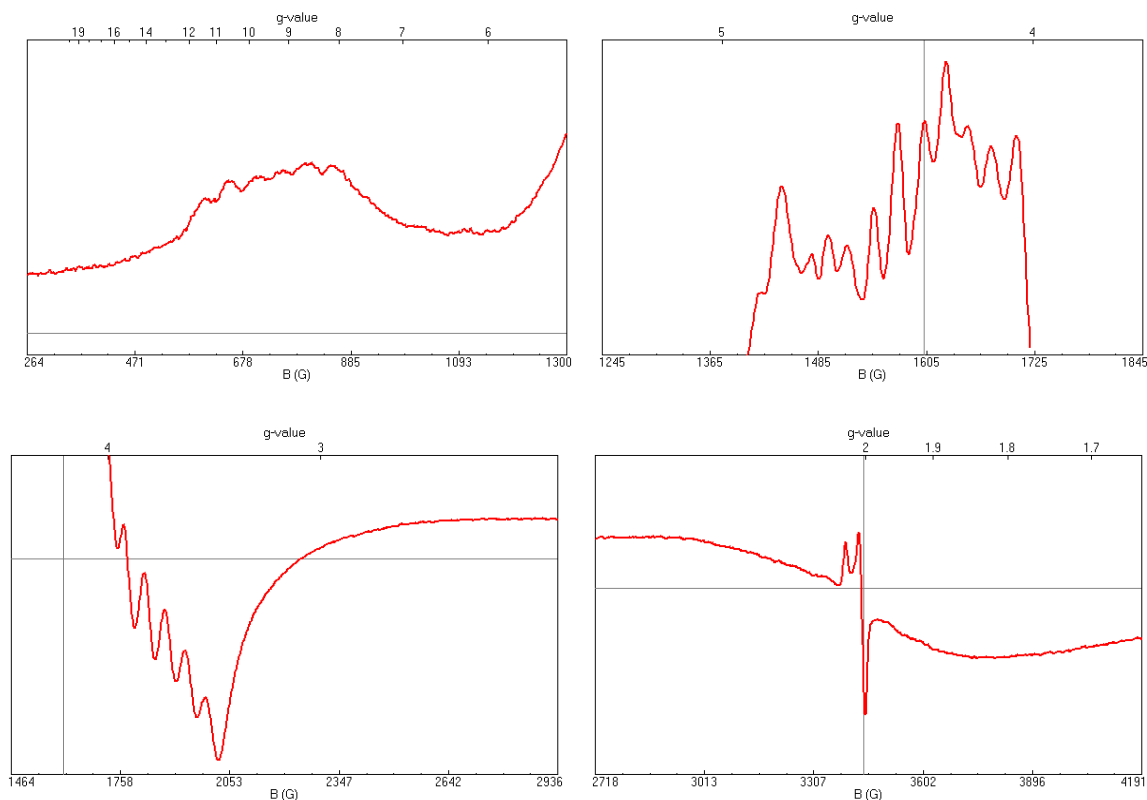
Figure 65. Enlarged views of the EPR signals of blue oxo-species of [Ind$^{3Me-2,4,7}$MnCl(thf)]$_2$ centered at g = 9.367 (top left), g = 4.405 (top right), g = 3.675 (bottom left), and g ≈ 2 (bottom left).

Discussion

Despite [Ind$^{3Me-2,4,7}$MnCl(thf)]$_2$ originally being isolated as a by-product while trying to make the bis(indenyl)manganese compound, substituted (indenyl)manganese(II) halides have provided a rich amount of interesting solution chemistry in the presence of trace quantities of oxygen.

This chemistry was first witnessed while attempting to crystallize a sample of [Ind$^{3Me-2,4,7}$MnCl(thf)]$_2$.   A small amount of the yellow/orange solid that had been cooled to -10 °C was redissolved in pentane at room temperature, only to have the resulting

solution instantly turn dark green; upon warming the green color changed back to yellow. Various hypothesis for the color change were proposed and tested along several lines.

The first possibility to be explored involved the potential for a spin-crossover compound as a cause for the observed color change. However, the possibility of a spin-state change being the cause was diminished when SQUID based magnetic data revealed there was no spin crossover occurring in the compound's solid state. Spin-crossover behavior would be even less likely to occur in solution as it is easier for intermolecular interactions to occur between atoms/molecules in the solid state. This result rendered unlikely the hypothesis that the color change was due to a spin-crossover phenomenon. Evan's method was used to measure the magnetic susceptibility in solution, and while the compound still appeared to be in the high spin state at room temperature, variable temperature (VT) experiments gave very peculiar results. They indicated a potential increase in magnetic moment with decreased temperature. However, these results were later proved erroneous as the sample had its spectra taken at low temperature first, and the compound decomposed as the temperature was raised. EPR data would later show the decomposition products are EPR silent, potentially suggesting a reduced number of unpaired electrons, and offering an explanation for the confusing VT NMR results.

The second possible cause that was examined was that the compound was simply thermochromic. Degassing a solution of $[Ind^{3Me-2,4,7}MnCl(thf)]_2$ and then cooling it to -78 °C showed that thermochromism was not the cause of the color change, however. This result, coupled with the previous one ruling out a spin state change, combined to suggest that a chemical reaction causes the color change. Further evidence for this was found when a solution of $[Ind^{3Me-2,4,7}MnCl(thf)]_2$ in THF was cooled to -78 °C without being

degassed, and failed to show a color change. If the cause of the color change were a chemical reaction, then this result can be explained by the THF solvent coordinating to any accessible sites on the Mn centers, preventing any reactive species from subsequently binding to the metal center.

The possibility that $[Ind^{3Me-2,4,7}MnCl(thf)]_2$ might reversibly bind the dinitrogen gas of the glove box atmosphere was then considered. A solution of $(Ind^{3Me-2,4,7})MnCl(thf)$ in toluene was degassed and pressurized with N_2 at room temperature, resulting in a slight color change at the solution's surface from yellow to green. Upon further cooling in an ice bath at 0 °C the solution turned dark green, and further cooling to -78 °C turned the solution a deep royal blue color. Whether the color change was unique to N_2 binding was examined by testing a series of gases under similar conditions. After repeating the same experiment with CO, H_2, N_2O, CO_2, Ar, and He and achieving the same color change each time, it was concluded there was likely a common contaminant responsible for the color change, probably elemental oxygen. This should not be too surprising as carbonyl complexes of Mn^{II} are unknown, as are dinitrogen compounds of Mn^{II}. This is a consequence of the absence of an empty orbital in high-spin Mn^{II} to accept a lone pair of electrons from N_2 or CO, making binding unlikely without a spin state change, which the SQUID data had already ruled out.

Once it became evident that oxygen was the likely cause, an FTIR experiment was conducted to see if an O−O band could be seen. When spectra of the initially yellow $[Ind^{3Me-2,4,7}MnCl(thf)]_2$ and its presumed blue oxo-species were taken and compared, there was an additional peak at 1119 cm^{-1} in the spectrum of the blue solution. This value is consistent with transition metal superoxide compounds, which are generally found

117

between 950-1200 cm^{-1}.[173] In addition, previously documented superoxido- and peroxo-manganese complexes have been reported as being green and blue in color.[171,175] This is of importance because it should be noted that blue and green are not common colors for Mn^{II} organometallic complexes, which tend to be yellow or orange in color. A charge transfer between O$_2$ and a Mn^{II} center to form a superoxide and Mn^{III} metal center would explain the intense color change.

Further characterization of the oxo-species proved exceedingly difficult due to the strict conditions required for the compound to form, but not immediately decompose. It was found that the complex only persisted at low temperatures (below -40 °C), but more importantly, that slightly increased oxygen levels caused decomposition, even at low temperature. Having a finite window of oxygen concentrations (on the single ppm scale) where this phenomenon could be observed made for challenging characterization due to the difficulty in handling and manipulating the compounds. Thus, a collaboration with the Que lab at the University of Minnesota was sought to help with further characterization. With the aid of the Que lab, UV-vis, resonance Raman and EPR experiments were conducted in attempt to better characterize the oxo-species being formed by [Ind$^{3Me-2,4,7}$MnCl(thf)]$_2$.

Electronic absorption spectroscopy showed the formation of a new peak with λ_{max} = 643 nm. This is similar to what is seen for other peroxide and superoxide compounds of manganese, which also typically display an additional feature near 400-450 nm.[170,171] This second feature was not observed in this case due to the presence of strong absorbance in this region from indenyl ligand, which absorbs heavily in that region. The approximate extinction coefficient observed for the blue oxo-species is 250 M^{-1} cm^{-1}.

This is consistent with what has been observed for other superoxo and peroxo species of manganese.[175]

The EPR spectra of both the initial complex and the oxo-species are fairly complex, but there is clear evidence of a drastic electronic change. Specifically, it appears that the initial compound, which is initially dimeric, has become monomeric in the new oxo-species. This is evidenced by the very clear six-line hyperfine structures with average splittings of 49 G and 54 G, which, coupled with the resonance locations, suggest a monomeric $^{55}Mn^{III}$ center. There is also the presence of a signal near $g = 2$ that is not from unpaired electron density on manganese, as it lacks any hyperfine splitting. The only possible spots for this unpaired electron density to be found if it is not located on Mn are the indenyl ligand or newly formed superoxide. The assignment of a superoxide for this EPR signal matches what is observed for the O−O stretch in the IR. For full characterization, however, EPR spectral simulations will be required to confirm this assignment.

Full resonance Raman interpretation is still forthcoming, as the substituted indenyl ligand has a large number of vibrations that show up in the spectra and must be accounted for. Without the benefit of an ^{18}O labeled experiment, it is very difficult to identify the exact peaks corresponding to a Mn−O interaction. The preliminary Raman data from excitation at 647 nm was given in the results section, but without the rest of the excitation profile, an assignment of the Mn−O bond is not possible. Since $[Ind^{3Me-2,4,7}MnCl(thf)]_2$ does not absorb at 647 nm (based on its UV-vis spectrum), the full extent of ligand vibrations is not obvious, requiring that a full excitation profile over the visible spectrum be obtained.

Conclusions

In addition to having synthesized the bis(indenyl)manganese(II) compounds described in Chapter III, mono(indenyl)manganese(II) halides can also be synthesized. While possessing some similarities to the analogous bis(indenyl) complexes, the mono(indenyl)manganese halides show a marked difference in their chemical behavior. In particular is the fact that $[Ind^{3Me-2,4,7}MnCl(thf)]_2$, $[Ind^{Me-2}MnCl(thf)]_2$, $[IndMnCl(thf)]_2$, and $[Ind^{Me-2}MnI(thf)]_2$ all display reactivity with elemental oxygen that be observed in the presence of only single ppm levels of O_2. It should be noted that attempts to form $[Ind^{2Me-4,7}MnCl(thf)]_2$ were unsuccessful, as only the bis(indenyl) complex was formed. Additionally, complexes with larger frontside steric bulk on the indenyl ligand, such as in $[Ind^{3Me-1,2,3}MnCl(thf)]_2$ or with any trimethylsilylated species, do not display this type of behavior with oxygen.

The sensitivity of these complexes to elemental oxygen is of specific interest, as the interaction can be observed even under normal glove box conditions. That kind of sensitivity lends itself to use as a potential oxygen sensor, as neither trimethylaluminum nor diethyl zinc react with such levels of oxygen. The nature of the interaction can at this point best be described as the formation of a Mn^{III} superoxide compound. The final results of the resonance Raman, coupled with EPR simulations, will help to either confirm this assignment or offer new evidence of another assignment.

CHAPTER V

SYNTHESIS AND CHARACTERIZATION OF MANGANGESE(II) COMPLEXES OF BULKY ARYLOXIDES

Introduction

While metal alkoxides have been known for over a century, dating from the first synthesized alkoxides of aluminum in the late 1800s,[179] metal alkoxides attracted increasing attention starting in the 1980s. It was at this time they were observed as intermediates in processes such as hydrogenation of aldehydes and ketones and the carbonylation of olefins.[180,181] In addition, these compounds have been recognized for their potential use as precursors for chemical vapor deposition (MOCVD) of metal oxide films.[182-184] However, applications of these compounds are limited by their air and moisture sensitivity. One way to address these sensitivity issues involves the use of bulkier aryloxide ligands to block decomposition pathways.

In the case of manganese, there are only a few of these aryloxide compounds that have been synthesized and structurally characterized that do not possess chelating functional groups on the aryl ring.[185-189] Often, the chelating atom is not C, H, or O, which can potentially restrict use in MOCVD due to the impurities that could be left behind by heteroatoms. However, there are additional uses for aryloxide compounds. In the case of simple phenoxides, there is interest in their ability to assist the conversion of acylmanganese to alkoxy carbonyl derivatives via treatment with syn gas. Additionally, bipy solvated manganese(II) aryloxide dimers display both intramolecular and intermolecular ferromagnetism in the solid state.[185] There are even some pyridyl substituted phenoxides of manganese that are capable of enzymatic-like behavior.[189]

121

There are a variety of ways to prepare metal alkoxides and aryloxides, most of them involving the reactions of alcohols, phenols, or phenoxide ions with metal amides or halides. A newer approach, introduced by Deacon et al,[187] synthesizes monomeric manganese phenoxides via the reaction of manganese powder, $Hg(C_6F_5)_2$, and substituted phenols in the presence of trace mercury in dimethoxyethane (DME). This reaction is claimed to be an efficient one-pot synthesis that takes place via protolytic ligand exchange and gives the monomeric manganese phenoxides in moderate to good yields (40-70%). Despite the reasonable yields, the toxicity associated with both perfluorophenyl mercury(II) and mercury itself make this a less than desirable route.

The preparation of aryloxide complexes of Mn^{II} became of interest in our lab upon the isolation of a dimeric (indenyl)manganese compound that contained a deprotonated bridging butylhydroxytoluene (BHT) group, $(Ind^{Me-2})_2(\mu\text{-}Ind^{Me-2})Mn_2(\mu\text{-}BHT)$. This was only the second example of an organometallic species that also contained an aryloxide coordinated to the same metal center. While attempts to make additional aryloxide-containing organometallic complexes were unsuccessful, we report the synthesis of new manganese(II) phenoxides that can be prepared by a simple salt metathesis reaction between a manganese(II) halide and the potassium salt of the substituted aryloxide.

Experimental

General Considerations. All manipulations were performed with the rigorous exclusion of air and moisture using Schlenk or glovebox techniques. Proton (^{1}H) NMR experiments were obtained on a Bruker DPX-300 spectrometer at 300 MHz, Bruker

DPX-400 at 400 MHz or Bruker DRX-501 spectrometer at 500 MHz. Elemental analyses were performed by Desert Analytics (Tucson, AZ). Melting points were determined on a Laboratory Devices Mel-Temp apparatus in sealed capillaries. Mass spectra were obtained using a Hewlett-Packard 5890 Series II gas chromatograph/mass spectrometer.

Materials. Anhydrous manganese(II) chloride (99.999%) was purchased from Alfa Aesar and used as received. 2-methylindene, *n*-butyl lithium, potassium bis(trimethylsilyl)amide, 2,6-diisopropylphenol, butylhydroxytoluene, anhydrous pentane, and anhydrous, unstabilized tetrahydrofuran (THF) were purchased from Aldrich and used as received. Hexanes, toluene, and diethyl ether were distilled under nitrogen from potassium benzophenone ketyl. Toluene-d_8 (Aldrich) was vacuum distilled from Na/K (22/78) alloy and stored over type 4A molecular sieves prior to use.

Magnetic Measurements. Solution magnetic susceptibility measurements were performed on a Bruker DRX-400 spectrometer using the Evans' NMR method.[148] The paramagnetic material (5–10 mg) was dissolved in toluene-d_8 in a 1.0 mL volumetric flask. The solution was thoroughly mixed, and approximately 0.5 mL was placed in an NMR tube containing a toluene-d_8 capillary. The calculations required to determine the number of unpaired electrons based on the data collected have been described elsewhere.[149]

General Procedures for X-ray Crystallography. A suitable crystal of each sample was located, attached to a glass fiber, and mounted on a Bruker SMART APEX II CCD Platform diffractometer for data collection at 173(2) K or 100(2) K. Data collection and structure solutions for all molecules were conducted at the X-ray Crystallography Facility at the University of Rochester by Dr. William W. Brennessel or at the

University of California, San Diego by Dr. Arnold L. Rheingold. Data resolution of 0.84 Å were considered in the data reduction (SAINT 7.53A, Bruker Analytical Systems, Madison, WI).

The intensity data were corrected for absorption and decay (SADABS). All calculations were performed using the current SHELXTL suite of programs.[150] Final cell constants were calculated from a set of strong reflections measured during the actual data collection.

The space groups were determined based on systematic absences (where applicable) and intensity statistics. A direct-methods solution was calculated that provided most of the non-hydrogen atoms from the E-map. Several full-matrix least squares/difference Fourier cycles were performed that located the remainder of the non-hydrogen atoms. All non-hydrogen atoms were refined with anisotropic displacement parameters. All hydrogen atoms were placed in ideal positions and refined as riding atoms with relative isotropic displacement parameters.

Synthesis of potassium 2,6-di-*tert*-butyl-4-methylphenoxide, K[2,6-(C(Me$_3$)$_2$)-4-Me-C$_6$H$_2$-2-O], KBHT. 2,6-di-*tert*-butyl-4-methylphenol (1.049 g, 4.76 mmol) was dissolved in toluene (30 mL) in a 250 mL Erlenmeyer flask. Potassium bis(trimethylsilyl)amide, K[N(SiMe$_3$)$_2$], (0.908 g, 4.55 mmol) was dissolved in toluene (20 mL) and added dropwise to the phenol solution while stirring. The solution immediately slowly turned to an opaque milky white color upon the addition of the potassium bis(trimethylsilyl)amide. After stirring for 24 h at room temperature, the solution became yellow-green. Hexanes (150 mL) were then added to fully precipitate the potassium phenoxide salt, which was then filtered over a medium-porosity frit,

washed with hexanes, and dried under vacuum to yield 0.849 g (72.2%) of a white powder that confirmed to be the phenoxide salt by ^{1}H NMR (300 MHz) in C_6D_6: δ 1.38 (singlet, 18H, $C(CH_3)_3$); 2.07 (singlet, 3H, CH_3); 6.62 (singlet, 2H, CH in 3,5-position).

Synthesis of potassium 2,6-diisopropylphenoxide, K[2,6-(CH(Me$_2$)$_2$)-C$_6$H$_3$-2-O], KODipp. 2,6-diispropylphenol (3.061 g, 17.1 mmol) was dissolved in toluene (25 mL) in a 250 mL Erlenmeyer flask. Potassium bis(trimethylsilyl)amide, K[N(SiMe$_3$)$_2$], (3.261 g, 16.3 mmol) was dissolved in toluene (20 mL) and added dropwise to the phenol solution while stirring. The solution slowly darkened to a grayish color, and became very thick. The rate of addition had to be slowed to prevent stirring from being stopped. Additional toluene (15 mL) was added to keep solution stirring overnight at room temperature. By the next morning, the solution was still thick and gray in color, but with the addition of hexanes (175 mL) it became more white and much less viscous. A white precipitate was formed and vacuum filtered to produce 3.208 g (86.7%) of a white powder that was confirmed to be the phenoxide salt by ^{1}H NMR (300 MHz) in THF-d_8: δ 1.12 (doublet, 12H, CH(CH_3)$_2$); 3.50 (quintet, 2 H, CH(CH$_3$)$_2$); 6.50 (triplet, 1H, CH in 4-position); 6.68 (doublet, 2H, CH in 3,5-positions).

Attempted synthesis of (Ind^{Me-2})$_2$(μ-Ind^{Me-2})Mn$_2$(μ-BHT). Multiple attempts were made to remake this compound intentionally and are described here. **Method I.** Anhydrous MnCl$_2$ (0.210 g, 1.67 mmol, 1 eq) was added to a 250 mL Erlenmeyer flask and stirred for 1 h in THF (50 mL) to disperse the MnCl$_2$. Potassium 2-methylindenide (0.425 g, 2.53 mmol, 1.5 eq) and BHT (0.184 g, 0.835 mmol, 0.5 eq) were dissolved in THF (85 mL) at room temperature and added dropwise into the flask containing MnCl$_2$. The resulting reaction mixture immediately turned yellow upon addition, and was

allowed to stir overnight at room temperature, after which the solution had turned bright

red. The solvent was then removed under vacuum, leaving a light yellow solid. The

product was extracted with pentane (3 x 30 mL) and decanted into a medium porosity

glass frit. The solution turned green upon filtering, indicating presence of the oxo species

of $[(Ind^{Me-2})MnCl(thf)]_2$. Pentane was then removed under vacuum to leave 0.335 g of a

yellow solid. This solid was redissolved in pentane and cooled to 0 °C, which caused the

crystallization of pale yellow needles. ^{1}H NMR of the needles contained only broad,

structurally uninformative, signals due to the presence of paramagnetic Mn^{II}. Crystals

likely desolvated before an X-ray structure could be obtained. Attempts to grow crystals

from pentane at 0 °C produced olive green blocks that did not diffract. **Method II.**

Anhydrous $MnCl_2$ (0.827 g, 6.57 mmol, 1 eq) was added to a 250 mL Erlenmeyer flask

and stirred for 1 h in THF (40 mL) to disperse the $MnCl_2$. Potassium 2-methylindenide

(1.659 g, 9.86 mmol, 1.5 eq) and KBHT (0.849 g, 3.29 mmol, 0.5 eq) were dissolved in

THF (40 mL) at room temperature and added dropwise into the flask containing $MnCl_2$.

The resulting reaction mixture immediately turned a brownish orange upon initial

addition, before becoming olive green after complete addition. The reaction mixture was

allowed to stir overnight at room temperature, after which the solution had turned bright

red. The solvent was then removed under vacuum, leaving a brown-orange solid. The

product was extracted with pentane (3 x 30 mL) and poured over a medium porosity glass

frit to filter off KCl. No color changes were observed upon filtration, and the filtrate was

a very dark orange color. After standing at room temperature for 72 hours, large, pale,

orange-yellow blocks (80 mg) crystallized that were suitable for single crystal X-ray

analysis. The resulting compound proved not to be the expected $(Ind^{Me-2})_3Mn_2(BHT)$, but

instead a dimeric manganese phenoxide that featured both bridging and terminal phenoxide groups, and a bridging chloride. Synthesis of this compound from the stoichiometric combination of appropriate reagents is described below. **Method III.** Bis(2-trimethylindenyl)manganese (0.184 g, 0.587 mmol) was dissolved in THF (30 mL) to give a red solution that was stirred while KBHT (0.077 g, 0.298 mmol) in THF (10 mL) was added dropwise via pipet over 5 min. No color change was visible during or immediately after addition. After 16 h the solution had darkened slightly in color, and the THF was removed under vacuum, leaving a pale pinkish-red solid. Pentane (1 x 30 mL) and toluene (2 x 30 mL) were used in attempt to extract the product, but the product did not appear to be soluble in pentane, and the dark orange filtrate of the toluene yielded only an intractable orange-red oil.

Synthesis of [Mn(BHT)(THF)]$_2$(µ-BHT)(µ-Cl). MnCl$_2$ (0.285 g, 2.27 mmol, 2 eq) was added to a 250 mL Erlenmeyer and dispersed in THF (75 mL) by magnetic stirring for 1 hour before adding KBHT (0.887 g, 3.43 mmol, 3 eq) in THF (50 mL) dropwise. The solution initially turned yellow-orange before becoming a dark rose color. After stirring overnight, the solvent was removed under vacuum to yield a red solid that was extracted with pentane (3 x 30 mL) and filtered over a medium porosity glass frit, producing a pale, rosy pink filtrate. The pentane filtrate was then removed under vacuum, leaving 0.880 g (76%) of a pale orange solid, mp 198-208 °C (dec). Anal. Calcd. for C$_{58}$H$_{97}$O$_5$Mn$_2$Cl: C, 67.16; H, 9.05; Mn, 11.60; Cl, 3.74. Found: C, 66.39; H, 9.09; Mn, 11.66; Cl, 3.95.

Attempted synthesis of bis(2,6-diisopropylphenoxy)-manganese(II), (KODiPP)$_2$Mn(thf)$_x$. MnCl$_2$ (0.257 g, 2.04 mmol) was added to a 250 mL Erlenmeyer

and dispersed in THF (40 mL) by magnetic stirring for 1 hour before adding KODIPP (0.864 g, 3.99 mmol) in THF (40 mL) dropwise. The solution initially turned light brown before ending up a greenish-gray color. After stirring overnight, the solvent was removed under vacuum to yield a brown-black solid that was extracted with pentane (2 x 30 mL) and then toluene (1 x 40 mL). Both fractions were filtered over a medium porosity glass frit, producing dark brown filtrates. The solvents were both removed under vacuum, leaving a total of 0.609 g (73%) of dark green-gray solid, mp 162-166 °C (dec).

Results and Discussion

New manganese(II) aryloxide species have been prepared by straightforward salt metathesis elimination reactions of $MnCl_2$ and the appropriate amounts of potassium phenoxide salts. These compounds can be extracted using pentane or toluene following the removal of THF and the alkali metal by-products. Purified solutions of the manganese aryloxide species in pentane gave crystals at room temperature upon slowly allowing the solvent to evaporate.

Crystallographic Results

$(Ind^{Me-2})_2(\mu\text{-}Ind^{Me-2})Mn_2(\mu\text{-}BHT)$. $(Ind^{Me-2})_2(\mu\text{-}Ind^{Me-2})Mn_2(\mu\text{-}BHT)$ was isolated from the reaction of $MnCl_2$ and 2 equivalents of Ind^{Me-2} in anhydrous THF containing BHT as an inhibitor. Yellow plate like crystals of $(Ind^{Me-2})_2(\mu\text{-}Ind^{Me-2})Mn_2(\mu\text{-}BHT)$ were obtained from a pentane solution. A plot of the molecule is shown below in Figure 66.

Deprotonated butylhydroxytoluene (BHT) is present in the molecule as a bridging ligand. The average Mn−O distance is 2.045(4) Å, which is on the low end for distances seen in similarly bridging aryloxide complexes of Mn^{II} (2.07-2.20 Å).[189-191] This distance is still considerably longer than the Mn−O bonds seen for terminally bound aryloxides, however, which typically range from 1.86-1.95 Å.[186,187]

The molecule also contains two terminal and one bridging 2-methyindenyl group. The terminal groups appear to have a slipped η^5-coordination, similar to what is observed for the methylated (indenyl)manganese halides from Chapter IV. The average distance is 2.48(2) Å for all 10 Mn-C bonds, which is only slightly longer than what is considered η^5 coordination in other compounds.[139] The amount of slippage (Δ(Mn-C) = 0.198 Å) is also slightly less than that usually expected for an η^3-C_5 ring.[19] The visible centering of the manganese atom is towards the front portion of the ring when looking from a view orthogonal to the C_5 plane, suggesting possible η^3-coordination.

The bridging 2-methylindenyl ligand is clearly η^1-bound to both manganese atoms. The distances of the 1- and 3-positions to the metal centers to which each is coordinated are 2.259^{192} and 2.282^{192} Å, while the distances to the bridgehead carbons or the carbon in the 2-position are all greater than 2.95 Å from both metal centers. The Mn(1)-Mn(2) distance in the complex is 3.56 Å, which is well beyond the range of metal-metal bonding.[20]

Table 6. Selected bond distances for $(Ind^{Me-2})_2(\mu\text{-}Ind^{Me-2})Mn_2(\mu\text{-}BHT)$.

Atoms	Distance (Å)	Atoms	Distance (Å)
Terminal		Bridging	
Mn(1)–C(1)	2.390(1)	Mn(1)–C(19)	2.259(1)
Mn(1)–C(2)	2.353(1)	Mn(2)–C(21)	2.282(2)
Mn(1)−C(3)	2.413(1)	C(1)−C(2)	1.412(1)
Mn(1)−C(9)	2.576(2)	C(2)−C(3)	1.413(1)
Mn(1)−C(8)	2.558(2)	C(3)−C(9)	1.427(1)
Avg. Mn(1)–C	2.458(3)	C(9)−C(8)	1.435(1)
Mn(2)–C(10)	2.416(2)	C(8)−C(1)	1.436(1)
Mn(2)–C(11)	2.385(3)	C(10)−C(11)	1.409(1)
Mn(2)−C(12)	2.448(1)	C(11)−C(12)	1.408(1)
Mn(2)−C(18)	2.637(1)	C(12)−C(18)	1.437(1)
Mn(2)−C(17)	2.625(1)	C(18)−C(17)	1.446(1)
Avg. Mn(2)–C	2.502(4)	C(17)−C(10)	1.460(1)
$\Delta_{Mn(1)-Cterm}$	0.252	C(19)−C(20)	1.415(1)
$\Delta_{Mn(2)-Cterm}$	0.223	C(20)−C(21)	1.405(1)
Mn$\cdots$Mn	3.557(1)	C(21)−C(26)	1.452(1)
Mn(1)−O(1)	2.037(2)	C(26)−C(25)	1.426(1)
Mn(2)−O(1)	2.053(1)	C(25)−C(1)	1.445(1)
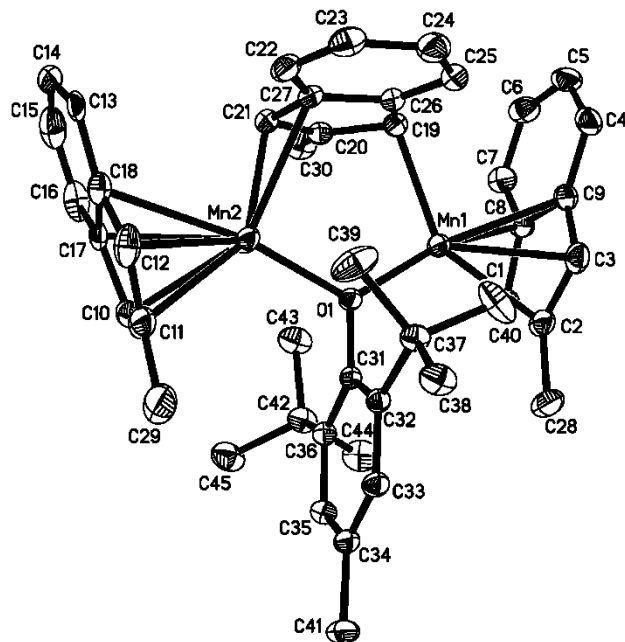
Figure 66. Diagram of the non-hydrogen atoms of $(Ind^{Me-2})_2(\mu\text{-}Ind^{Me-2})Mn_2(\mu\text{-}BHT)$ with the numbering scheme used in the text. Thermal ellipsoids are shown at the 50% probability level.

[Mn(BHT)(THF)]$_2$(μ-BHT)(μ-Cl). Crystals of $(BHT)_2(\mu\text{-}BHT)Mn_2(\mu\text{-}Cl)$ were harvested as pale yellow blocks from a room temperature solution of pentane. An ORTEP of the unit cell is shown in Figure 67, which gives the numbering scheme that is referred to in the text. Selected bond lengths and angles are shown in Table 6.

There are two types of BHT present in the molecule, as a bridging ligand between the two Mn centers and as a terminal ligand on both Mn centers. The geometry around each manganese is a slightly distorted tetrahedral with a near planar Mn_2O_2 core despite having no crystallographically imposed symmetry. The structure is unique among structurally characterized aryloxides of Mn^{II}, as this is the first compound to contain both a bridging halide and aryloxide in addition to terminal aryloxides. This fact is surprising given that attempts to make the compound with a 2:1 ratio of aryloxide ligand to Mn have produced the same compound, suggesting an unusual stability of this particular complex.

131

The terminal Mn−O bonds have an average length of 1.902(4) Å, which falls in

the typical range for terminal Mn^{II} aryloxides (1.86-1.95 Å).[186,187] The Mn−O−C angles

for the terminal aryloxide ligands average 162.6° (160.50 and 164.70), which is much

closer to linear than should be expected around an oxygen atom with sp^3 hybridization.

This suggests a large amount of ionic character in this interaction, similar to what is

proposed by Bartlett et al in their homoleptic compounds from the early 1990s.[186] More

recent compounds prepared by Deacon et al show a much smaller Mn−O−C angle for

terminal aryloxide ligands, but this is likely adopted to help alleviate steric strain of the

bulky aryloxide ligands that are crowded around a monomeric Mn^{II} center with a

tetrahedral geometry from coordinated DME.[187]

The bridging BHT group has an average Mn−O bond length of 2.060(5) Å, which

is very similar to the distance in (Ind^{Me-2})$_2$(μ-Ind^{Me-2})Mn$_2$(μ-BHT) for the same bridging

aryloxide group (2.04(1) Å). The Mn−Cl distances of 2.449(6) and 2.442(6) Å for the

bridging halide are also very close to those present for the chlorides in {(Ind^{3Me-}

^{2,4,7})MnCl(thf)}$_2$. The Mn---Mn distance of 3.282(3) Å is shorter than what is reported

for other dimeric Mn phenoxide compounds, but is still well outside the range typically

considered for metal−metal bonding.

Table 7. Selected bond distances for (BHT)$_2$(μ-BHT)Mn$_2$(μ-Cl).

Atoms	Distance (Å)	Atoms	Distance (Å)
Terminal		Bridging	
Mn(1)–O(1)	2.060(5)	Mn(1)–Cl(1)	2.259(1)
Mn(1)–O(2)	2.353(1)	Mn(2)–C(1)	2.282(2)
Mn(2)−O(1)	2.413(1)	Mn(1)−O(2)−C(16) <	164.8°
Mn(2)−O(3)	2.576(2)	Mn(2)−O(3)−C(31) <	160.5°
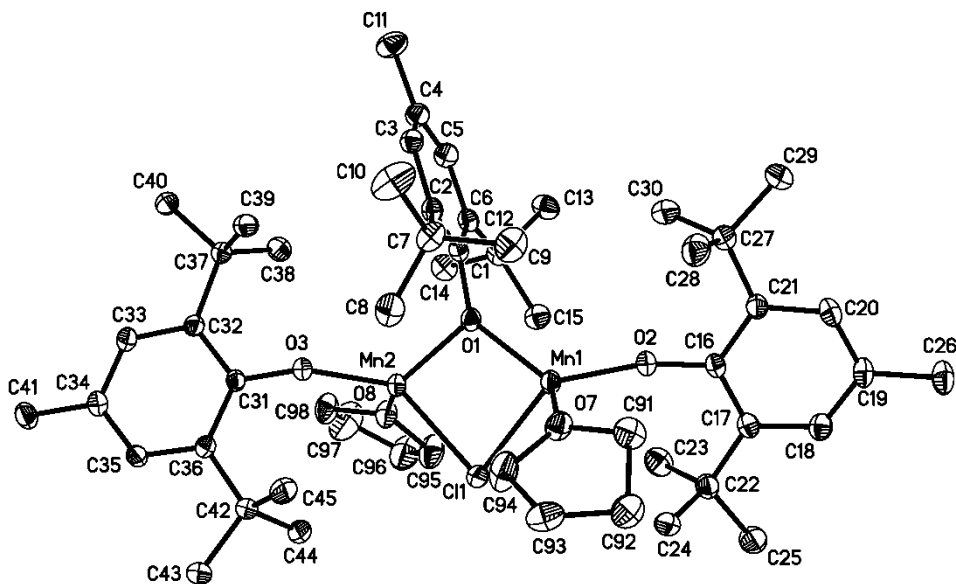
Figure 67. Diagram of the non-hydrogen atoms of $(BHT)_2(\mu\text{-}BHT)Mn_2(\mu\text{-}Cl)$ with the numbering scheme used in the text. Thermal ellipsoids are shown at the 50% probability level.

Conclusions

Interest in aryloxide complexes of Mn^{II} came about from the isolation of $(Ind^{Me\text{-}2})_2(\mu\text{-}Ind^{Me\text{-}2})Mn_2(\mu\text{-}BHT)$ as an unexpected side product from the preparation of the bis(indenyl)manganese compound. BHT was present as an inhibitor in the anhydrous THF used for the reaction, and was deprotonated and then scavenged by the oxophilic manganese center. The oxophilicity of Mn^{II} has been evidenced throughout this dissertation, ranging from the inability to remove THF from the parent bis(indenyl)manganese to the oxygen reactivity witnessed with mono(indenyl)manganese halides. Additional evidence of its oxophilicity is provided by the multiple attempts to remake the previously isolated $(Ind^{Me\text{-}2})_2(\mu\text{-}Ind^{Me\text{-}2})Mn_2(\mu\text{-}BHT)$, only to instead obtain $(BHT)_2(\mu\text{-}BHT)Mn_2(\mu\text{-}Cl)$ and other compounds that lacked the presence of the indenyl

133

ligand. This indicates a strong preference of the Mn to coordinate phenoxide ligands over the indenyl ligands, given that indenyl ligand was present in a 3:1 abundance compared to the phenoxide.

Manganese(II) aryloxides are relatively rare, with fewer than 20 having been reported in the literature. The synthesis routes proposed in this work represent a straightforward method towards making these compounds in relatively high yields (> 70%) without having to use toxic reagents such as aryl mercury compounds during synthesis. If monomeric complexes are desired, routes using slightly a bulkier coordinating solvent such as DME could be attempted, and these methods are currently under further investigation.

CHAPTER VI

PROJECT SUMMARY AND FUTURE RESEARCH

Summary

The indenyl ligand, while similar to the cyclopentadienyl ring, has greater

flexibility in its interactions with metal centers, which is reflected by the greater variety

of chemical bonding modes in the ligands for organometallic indenyl compounds in

comparison to analogous ones featuring Cp. This contrast can be seen in the case of

methyl substituted bis(indenyl)manganese complexes relative to their manganocene

counterparts, especially when there is only substitution on the benzo position of the

indenyl ligand, as the lack of steric bulk around the Mn center results in oligomeric or

polymeric structures. Additionally, there is a measureable difference in physical

properties between the two families of complexes, as manganocenes have access to both

low and high spin states, and their magnetic properties can be tuned by the electronic

properties of the Cp substituents. For the bis(indenyl)manganese compounds, there has

been no evidence of an accessible low spin state, and all compounds have been shown to

be high spin at all temperatures.

Methylated mono(indenyl)manganese halides also demonstrate that even in cases

where the structures of the indenyl compounds are very similar to that of their Cp

analogs, there can be stark differences in the chemical behavior between the species. The

mono(indenyl)manganese halides coordinate oxygen at low temperature and very low

concentrations, something that is not observed in the Cp compounds. Current analysis of

this interaction has lead to the conclusion that a Mn^{III} superoxide is formed, but the full excitation profile for the resonance Raman spectra, coupled with EPR simulations for the proposed superoxide, will be needed to fully confirm this assignment.

A consistent trend seen with both the bis(indenyl)manganese complexes and the mono(indenyl)manganese halides is the relatively high oxophilicity of the Mn^{II} center. This is shown in the bis(indenyl) compounds by the inability to isolate THF-free bis(indenyl)manganese, as once THF is coordinated to the metal center, it is difficult to remove unless there is sufficient steric bulk on the indenyl ligand. The oxophilicity is further displayed by the mono(indenyl) halide compounds, which will react with trace quantities (< 5 ppm) of molecular oxygen. These observations, coupled with the isolation of $(Ind^{Me-2})_2(\mu\text{-}Ind^{Me-2})Mn_2(\mu\text{-}BHT)$, prompted attempts to synthesize Mn^{II} aryloxide complexes, a relatively rare type of compound for manganese. These compounds could be prepared from straightforward salt-metathesis elimination reactions, which represent a marked improvement on previous synthetic routes involving aryl mercury reagents.[187]

Future Work

There are still several avenues for continued research on manganese(II) indenyl compounds. For the bis(indenyl) compounds, synthesis of a monomeric methylated bis(indenyl) species has not been achieved. This compound would be of interest for its magnetic properties (e.g. its potential for assuming a low-spin state) and its incorporation into a charge-transfer (CT) salt. Currently, the oligomeric and polymeric bis(indenyl)manganese complexes do not favorably lend themselves to making magnetically ordered CT salts due to their lack of a classic sandwich structure that

enables π stacking, a physical trait that has been linked to magnetic ordering. A monomeric, methyl-substituted bis(indenyl)manganese compound could make such a CT salt possible. Previous studies on the trimethylsilyl-substituted compounds indicated no magnetic ordering in the associated CT salts, but methyl groups may be better suited for this purpose.

For the methyl-substituted mono(indenyl)manganese halides, further analysis of the resonance Raman and EPR data is needed to confirm the assignment of the oxo-species as a Mn^{III} superoxide compound. EPR can also be used in an attempt to quantify the reactivity, and determine just how much oxygen is being coordinated. This can be done using internal standards, but may be complicated if the EPR active species is actually the bis(indenyl) complex formed from Schlenk-type rearrangement. This is another reason why simulations to help confirm EPR assignments should be pursued.

Further investigation on the structural and electronic requirements for enabling oxygen reactivity should also be examined. Thus far, it is observed for only $[Ind^{3Me-2,4,7}MnCl(thf)]_2$, $[Ind^{Me-2}MnCl(thf)]_2$, $[IndMnCl(thf)]_2$, and $[Ind^{Me-2}MnI(thf)]_2$, and forms the most stable oxo-species with the chlorides, specifically $[Ind^{Me-2}MnCl(thf)]_2$. Preliminary results for $[Ind^{3Me-1,2,3}MnCl(thf)]_2$ suggest this compound does not react with oxygen at the ppm levels, indicating that sufficient steric bulk on the front side of the indenyl ligand may block oxygen access to the Mn center. This is counterintuitive when electronics are considered, as the stronger donating trimethylindenyl ligand should be expected to help promote superoxide formation relative to the methylindenyl ligand. However, since this is not observed, it is likely that the steric bulk of the ligand has a greater impact on reactivity than the electron donating effects of the ligand.

The Mn^{II} aryloxide chemistry can still benefit from optimizztion of the syntheses and the development of both homoleptic and monomeric species. Use of bulkier coordinating solvents may help to form monomeric species, as is found for some DME solvates.[187] Additional synthetic attempts using a larger excess of the phenoxide salts may help to form homoleptic species, instead of the chloride-containing species currently known. SQUID magnetometry may prove informative, as there is precedent for Mn^{II} aryloxide compounds with ferromagnetic behavior.[191] Further tests investigating their potential to serve as hydrogenation or carbonylation catalysts can also be considered, as metal alkoxides and aryloxides are presumed to be key components in the mechanisms of both of these processes.

Appendix A

CRYSTAL DATA AND ATOMIC FRACTIONAL COORDINATES FOR X-RAY
STRUCTURAL DETERMINTIONS

Table 8. Crystal data and structure refinement for [K(dioxane)$_{1.5}$][(Mn(Ind$^{2Me-4,7}$)$_3$].

_____

Empirical formula	C234 H270 K6 Mn6 O18
Formula weight	3934.74
Temperature	100.0(1) K
Wavelength	0.71073 Å
Crystal system	Hexagonal
Space group	$P6_3$
Unit cell dimensions	a = 19.125(5) Å α = 90°
	b = 19.125(5) Å β = 90°
	c = 32.076(8) Å γ = 120°
Volume	10160(4) Å^3
Z	2
Density (calculated)	1.286 Mg/m^3
Absorption coefficient	0.549 mm^{-1}
F(000)	4164
Crystal color, morphology	yellow, hexagonal plate
Crystal size	0.28 x 0.16 x 0.06 mm^3
Theta range for data collection	1.77 to 31.51°
Index ranges	-28 ≤ h ≤ 28, -28 ≤ k ≤ 28, -47 ≤ l ≤ 47
Reflections collected	132350
Independent reflections	22576 [R(int) = 0.1435]
Observed reflections	13455
Completeness to theta = 31.51°	100.0%
Absorption correction	Multi-scan
Max. and min. transmission	0.9678 and 0.8616
Refinement method	Full-matrix least-squares on F^2
Data / restraints / parameters	22576 / 14 / 822
Goodness-of-fit on F^2	1.012
Final R indices [I>2sigma(I)]	$R1$ = 0.0758, $wR2$ = 0.1770
R indices (all data)	$R1$ = 0.1425, $wR2$ = 0.2191
Absolute structure parameter	0.21(2)
Largest diff. peak and hole	4.709 and -0.541 e.Å^{-3}

Table 9. Atomic coordinates (x 10^4) and equivalent isotropic displacement parameters (Å^2x 10^3) for [K(dioxane)$_{1.5}$][(Mn(Ind$^{2\text{Me-4,7}}$)$_3$]. U$_{eq}$ is defined as one third of the trace of the orthogonalized U$_{ij}$ tensor.

	x	y	z	U$_{eq}$
Mn1	6667	3333	6577(1)	20(1)
C1	5713(3)	3686(3)	6367(2)	21(1)
C2	5682(3)	3676(3)	6813(2)	25(1)
C3	5142(3)	2890(3)	6954(2)	22(1)
C4	4292(3)	1544(3)	6558(1)	18(1)
C5	4128(3)	1228(3)	6161(1)	21(1)
C6	4462(3)	1718(3)	5801(1)	20(1)
C7	4971(3)	2538(3)	5830(1)	18(1)
C8	5163(3)	2885(3)	6231(1)	19(1)
C9	4816(2)	2387(3)	6596(1)	18(1)
C10	3957(3)	1029(3)	6940(2)	28(1)
C11	5342(3)	3078(3)	5458(2)	26(1)
Mn2	0	0	6016(1)	21(1)
C12	1251(3)	1044(3)	6234(2)	23(1)
C13	1251(3)	1097(3)	5788(2)	22(1)
C14	1518(3)	595(3)	5621(2)	23(1)
C15	1974(3)	-337(3)	5960(2)	22(1)
C16	2099(3)	-573(3)	6339(2)	26(1)
C17	1973(3)	-269(3)	6719(2)	25(1)
C18	1695(3)	268(3)	6727(2)	21(1)
C19	1541(3)	522(3)	6335(2)	18(1)
C20	1704(3)	228(3)	5954(1)	19(1)
C21	2121(3)	-651(3)	5562(2)	34(1)
C22	1554(3)	594(3)	7124(2)	32(1)
Mn3	3333	6667	3474(1)	21(1)
C23	2969(3)	5357(3)	3676(2)	24(1)
C24	2999(3)	5340(3)	3227(2)	26(1)
C25	3786(3)	5595(3)	3100(2)	22(1)
C26	5121(3)	6086(3)	3509(2)	20(1)

C27	5424(3)	6243(3)	3908(2)	22(1)
C28	4916(3)	6080(3)	4263(2)	21(1)
C29	4091(3)	5752(3)	4226(1)	20(1)
C30	3766(3)	5604(3)	3818(1)	18(1)
C31	4269(3)	5756(2)	3459(1)	18(1)
C32	5637(3)	6262(3)	3132(2)	26(1)
C33	3549(3)	5589(3)	4596(2)	27(1)
Mn4	6667	3333	4079(1)	18(1)
C34	5655(3)	3568(3)	3867(1)	20(1)
C35	5579(3)	3523(3)	4306(2)	23(1)
C36	6064(3)	4295(3)	4479(1)	18(1)
C37	6984(3)	5690(3)	4141(2)	22(1)
C38	7244(3)	6056(3)	3752(2)	27(1)
C39	6979(3)	5617(3)	3381(2)	26(1)
C40	6449(3)	4797(3)	3371(2)	22(1)
C41	6185(3)	4413(3)	3763(2)	18(1)
C42	6440(3)	4844(3)	4143(2)	19(1)
C43	7243(3)	6160(3)	4544(2)	31(1)
C44	6141(4)	4318(4)	2974(2)	32(1)
Mn5	3333	6667	5998(1)	19(1)
C45	3065(3)	5394(3)	6195(2)	22(1)
C46	3063(3)	5361(3)	5749(2)	23(1)
C47	2279(3)	5123(3)	5607(2)	24(1)
C48	958(3)	4777(3)	5990(2)	24(1)
C49	642(3)	4696(3)	6380(2)	29(1)
C50	1113(3)	4822(3)	6747(2)	24(1)
C51	1915(3)	5058(3)	6728(2)	20(1)
C52	2266(3)	5141(2)	6327(2)	15(1)
C53	1781(3)	4981(3)	5955(2)	20(1)
C54	459(3)	4638(3)	5605(2)	36(1)
C55	2433(3)	5228(3)	7110(2)	26(1)
Mn6	0	0	4033(1)	25(1)
C56	1306(3)	938(3)	3879(2)	33(1)
C57	1324(3)	874(4)	4320(2)	41(1)
C58	1507(3)	275(4)	4431(2)	38(1)
C59	1815(3)	-655(3)	3983(2)	27(1)

C60	1911(3)	-819(3)	3580(2)	26(1)
C61	1814(3)	-408(3)	3242(2)	27(1)
C62	1622(3)	191(3)	3300(2)	24(1)
C63	1527(3)	379(3)	3712(2)	25(1)
C64	1634(3)	-46(3)	4054(2)	27(1)
C65	1884(3)	-1145(4)	4336(2)	40(1)
C66	1472(3)	614(3)	2946(2)	31(1)
K1	3079(1)	1980(1)	6056(1)	20(1)
K2	4673(1)	4443(1)	3978(1)	20(1)
O1	3554(2)	3303(2)	3536(1)	32(1)
C67	3489(4)	2606(3)	3339(2)	44(2)
C68	3378(4)	2647(4)	2877(2)	46(2)
O2	2691(2)	2702(2)	2783(1)	36(1)
C69	2753(4)	3393(3)	2988(2)	32(1)
C70	2856(3)	3362(3)	3447(2)	27(1)
O3	3583(2)	3647(2)	4596(1)	32(1)
C71	3964(4)	4010(3)	4976(2)	39(1)
C72	3396(5)	3620(3)	5334(2)	49(2)
O4	3148(2)	2794(2)	5355(1)	39(1)
C73	2744(3)	2416(3)	4976(2)	38(1)
C74	3292(3)	2800(3)	4601(2)	36(1)
O5	3200(2)	3221(2)	6448(1)	33(1)
C75	2548(14)	3280(30)	6645(8)	50(5)
C76	2636(13)	3329(17)	7105(8)	61(6)
O6	3396(13)	4008(18)	7238(7)	45(3)
C77	4051(12)	3960(20)	7038(8)	37(3)
C78	3942(10)	3900(20)	6579(8)	29(3)
C75'	2526(12)	3340(20)	6529(7)	50(5)
C76'	2402(11)	3303(14)	6988(8)	61(6)
O6'	3132(12)	3923(15)	7185(6)	45(3)
C77'	3837(12)	3865(19)	7090(6)	37(3)
C78'	3923(9)	3850(17)	6631(7)	29(3)

Table 10. Crystal data and structure refinement for $(Ind^{3Me-2,4,7})_2Mn$.

Empirical formula	C24 H26 Mn
Formula weight	369.39
Temperature	100.0(1) K
Wavelength	0.71073 Å
Crystal system	Tetragonal
Space group	$I4_1/a$
Unit cell dimensions	$a = 27.094(5)$ Å $\quad\quad \alpha = 90°$
	$b = 27.094(5)$ Å $\quad\quad \beta = 90°$
	$c = 10.212(2)$ Å $\quad\quad \gamma = 90°$
Volume	7496(3) Å^3
Z	16
Density (calculated)	1.309 Mg/m^3
Absorption coefficient	0.707 mm^{-1}
$F(000)$	3120
Crystal color, morphology	orange, needle
Crystal size	0.32 x 0.12 x 0.10 mm^3
Theta range for data collection	1.50 to 27.47°
Index ranges	$-35 \leq h \leq 35, -35 \leq k \leq 35, -13 \leq l \leq 13$
Reflections collected	45500
Independent reflections	4296 [R(int) = 0.1770]
Observed reflections	2891
Completeness to theta = 27.47°	100.0%
Absorption correction	Multi-scan
Max. and min. transmission	0.9327 and 0.8054
Refinement method	Full-matrix least-squares on F^2
Data / restraints / parameters	4296 / 0 / 236
Goodness-of-fit on F^2	1.018
Final R indices [$I>2sigma(I)$]	$R1 = 0.0512, wR2 = 0.1100$
R indices (all data)	$R1 = 0.0899, wR2 = 0.1292$
Largest diff. peak and hole	0.449 and -0.321 e.Å^{-3}

Table 11. Atomic coordinates ($\times 10^4$) and equivalent isotropic displacement parameters ($\mathring{A}^2 \times 10^3$) for $(Ind^{3Me-2,4,7})_2Mn$. U_{eq} is defined as one third of the trace of the orthogonalized U_{ij} tensor.

	x	y	z	U_{eq}
Mn1	1358(1)	4394(1)	4147(1)	20(1)
C1	714(1)	4433(1)	5927(3)	24(1)
C2	632(1)	4786(1)	4941(3)	25(1)
C3	535(1)	4535(1)	3744(3)	26(1)
C4	415(1)	3598(1)	3239(3)	26(1)
C5	428(1)	3141(1)	3826(3)	28(1)
C6	555(1)	3080(1)	5162(3)	26(1)
C7	660(1)	3474(1)	5955(3)	22(1)
C8	637(1)	3952(1)	5389(3)	21(1)
C9	529(1)	4015(1)	4016(3)	23(1)
C10	626(1)	5336(1)	5159(4)	31(1)
C11	262(1)	3662(1)	1838(3)	38(1)
C12	781(1)	3414(1)	7382(3)	27(1)
C13	1906(1)	3886(1)	5195(3)	19(1)
C14	2171(1)	4266(1)	5860(3)	19(1)
C15	2632(1)	4330(1)	5222(3)	20(1)
C16	3032(1)	3892(1)	3210(3)	22(1)
C17	2952(1)	3506(1)	2351(3)	24(1)
C18	2530(1)	3202(1)	2419(3)	25(1)
C19	2160(1)	3290(1)	3326(3)	22(1)
C20	2222(1)	3697(1)	4165(3)	20(1)
C21	2659(1)	3985(1)	4141(3)	19(1)
C22	1994(1)	4542(1)	7038(3)	25(1)
C23	3504(1)	4180(1)	3213(3)	29(1)
C24	1718(1)	2961(1)	3448(3)	28(1)

Table 12. Crystal data and structure refinement for [Ind$^{3Me-2,4,7}$MnCl(thf)]$_2$.

Empirical formula	C32 H42 Cl2 Mn2 O2
Formula weight	639.44
Temperature	173.0(5) K
Wavelength	0.71073 Å
Crystal system	Triclinic
Space group	*P*-1
Unit cell dimensions	*a* = 9.5845(5) Å α = 85.269(1)°
	b = 9.6973(5) Å β = 88.141(1)°
	c = 17.1564(10) Å γ = 83.660(1)°
Volume	1578.99(15) Å^3
Z	2
Density (calculated)	1.345 Mg/m^3
Absorption coefficient	0.995 mm^{-1}
F(000)	668
Crystal color, morphology	yellow, block
Crystal size	0.28 x 0.20 x 0.18 mm^3
Theta range for data collection	1.19 to 35.63°
Index ranges	-15 ≤ *h* ≤ 15, -15 ≤ *k* ≤ 15, -28 ≤ *l* ≤ 28
Reflections collected	35286
Independent reflections	14299 [*R*(int) = 0.0303]
Observed reflections	9523
Completeness to theta = 35.63°	98.2%
Absorption correction	Multi-scan
Max. and min. transmission	0.8412 and 0.7681
Refinement method	Full-matrix least-squares on *F*^{2}
Data / restraints / parameters	14299 / 10 / 356
Goodness-of-fit on *F*^{2}	1.031
Final *R* indices [*I*>2sigma(*I*)]	*R*1 = 0.0470, *wR*2 = 0.1246
R indices (all data)	*R*1 = 0.0762, *wR*2 = 0.1419
Largest diff. peak and hole	1.015 and -0.428 e.Å^{-3}

Table 13. Atomic coordinates (x 10^4) and equivalent isotropic displacement parameters (Å^2 x 10^3) for $[\text{Ind}^{3\text{Me-2,4,7}}\text{MnCl(thf)}]_2$. U_{eq} is defined as one third of the trace of the orthogonalized U_{ij} tensor.

	x	y	z	U_{eq}
Mn1	4312(1)	8590(1)	433(1)	41(1)
Cl1	6286(1)	8858(1)	-466(1)	51(1)
C1	4865(2)	8096(2)	1743(1)	44(1)
C2	5567(2)	6986(2)	1355(1)	46(1)
C3	4577(2)	6165(2)	1109(1)	46(1)
C4	1880(2)	6249(2)	1355(2)	56(1)
C5	784(2)	7034(3)	1692(2)	67(1)
C6	939(2)	8267(3)	2031(2)	60(1)
C7	2221(2)	8748(2)	2074(1)	50(1)
C8	3396(2)	7936(2)	1773(1)	39(1)
C9	3234(2)	6707(2)	1386(1)	42(1)
C10	7135(2)	6713(3)	1245(1)	64(1)
C11	1712(3)	4939(3)	978(2)	87(1)
C12	2391(3)	10079(3)	2437(2)	69(1)
O1	2788(1)	8334(2)	-375(1)	52(1)
C13	2945(3)	7639(3)	-1078(2)	68(1)
C14	1510(3)	7790(4)	-1423(2)	80(1)
C15	518(3)	8173(3)	-779(2)	71(1)
C16	1348(2)	8953(3)	-289(1)	58(1)
Mn2	6246(1)	786(1)	4464(1)	33(1)
Cl2	6324(1)	-1315(1)	5345(1)	41(1)
C17	8505(2)	524(2)	3600(1)	35(1)
C18	7461(2)	-280(1)	3379(1)	35(1)
C19	6279(2)	623(2)	3129(1)	33(1)
C20	5806(2)	3320(2)	2969(1)	35(1)
C21	6464(2)	4498(2)	3041(1)	44(1)
C22	7847(2)	4426(2)	3298(1)	47(1)
C23	8639(2)	3194(2)	3505(1)	41(1)
C24	8002(2)	1953(1)	3447(1)	32(1)

C25	6600(2)	2025(1)	3164(1)	30(1)
C26	7599(2)	-1838(2)	3395(1)	47(1)
C27	4343(2)	3375(2)	2680(1)	45(1)
C28	10143(2)	3120(2)	3742(2)	63(1)
O2	6816(1)	2172(1)	5247(1)	44(1)
C29	6138(11)	3608(8)	5181(5)	48(2)
C30	7125(6)	4453(4)	5559(3)	68(1)
C31	7861(6)	3389(4)	6153(3)	68(1)
C32	8110(20)	2087(16)	5670(20)	71(1)
C29'	6154(15)	3555(12)	5370(8)	48(2)
C30'	7055(8)	4077(7)	5952(4)	68(1)
C31'	8524(8)	3419(6)	5779(4)	68(1)
C32'	8170(30)	1930(20)	5620(30)	71(1)

Table 14. Crystal data and structure refinement for [Ind^{Me-2}MnI(thf)]$_2$.

Empirical formula	C28 H34 I2 Mn2 O2
Formula weight	766.23
Temperature	100.0(1) K
Wavelength	0.71073 Å
Crystal system	Triclinic
Space group	*P*-1
Unit cell dimensions	a = 8.0217(5) Å α = 85.518(1)°
	b = 9.3747(6) Å β = 86.954(1)°
	c = 9.6781(6) Å γ = 80.887(1)°
Volume	715.80(8) Å^3
Z	1
Density (calculated)	1.778 Mg/m^3
Absorption coefficient	3.061 mm^{-1}
F(000)	374
Crystal color, morphology	yellow-green, block
Crystal size	0.20 x 0.18 x 0.12 mm^3
Theta range for data collection	2.11 to 36.32°
Index ranges	-13 ≤ h ≤ 13, -15 ≤ k ≤ 15, -16 ≤ l ≤ 16
Reflections collected	16603
Independent reflections	6805 [*R*(int) = 0.0231]
Observed reflections	5910
Completeness to theta = 36.32°	98.0%
Absorption correction	Multi-scan
Max. and min. transmission	0.6902 and 0.5696
Refinement method	Full-matrix least-squares on *F*^{2}
Data / restraints / parameters	6805 / 0 / 155
Goodness-of-fit on *F*^{2}	1.057
Final *R* indices [*I*>2sigma(*I*)]	R1 = 0.0257, *w*R2 = 0.0608
R indices (all data)	R1 = 0.0318, *w*R2 = 0.0637
Largest diff. peak and hole	1.143 and -0.598 e.Å^{-3}

Table 15. Atomic coordinates (x 10^4) and equivalent isotropic displacement parameters (Å^2x 10^3) for [Ind$^{\text{Me-2}}$MnI(thf)]$_2$. U_{eq} is defined as one third of the trace of the orthogonalized U_{ij} tensor.

	x	y	z	U_{eq}
Mn1	3673(1)	6428(1)	926(1)	17(1)
I1	5205(1)	6522(1)	-1732(1)	21(1)
C1	788(2)	6333(2)	1215(2)	19(1)
C2	873(2)	7515(2)	213(1)	18(1)
C3	1389(2)	8660(2)	862(2)	18(1)
C4	1886(2)	8980(2)	3447(2)	25(1)
C5	1913(3)	8268(2)	4746(2)	31(1)
C6	1636(2)	6820(2)	4953(2)	30(1)
C7	1277(2)	6074(2)	3872(2)	25(1)
C8	1171(2)	6782(2)	2530(2)	18(1)
C9	1520(2)	8247(2)	2307(2)	18(1)
C10	410(2)	7558(2)	-1274(2)	23(1)
O1	5478(2)	7305(1)	1957(1)	23(1)
C11	5842(3)	8756(2)	1512(2)	33(1)
C12	7047(3)	9089(2)	2520(2)	34(1)
C13	6676(3)	8163(2)	3837(2)	34(1)
C14	6237(3)	6807(2)	3271(2)	31(1)

Table 16. Crystal data and structure refinement for $(\text{Ind}^{\text{Me-2}})_2(\mu\text{-Ind}^{\text{Me-2}})\text{Mn}_2(\mu\text{-BHT})$.

_____

Empirical formula	C45 H50 Mn2 O
Formula weight	716.73
Temperature	100.0(1) K
Wavelength	0.71073 Å
Crystal system	Monoclinic
Space group	$P2_1/c$
Unit cell dimensions	$a = 19.8480(19)$ Å $\quad\quad \alpha = 90°$
	$b = 10.3790(10)$ Å $\quad\quad \beta = 110.487(2)°$
	$c = 18.8577(17)$ Å $\quad\quad \gamma = 90°$
Volume	3639.0(6) Å^3
Z	4
Density (calculated)	1.308 Mg/m^3
Absorption coefficient	0.728 mm^{-1}
$F(000)$	1512
Crystal color, morphology	yellow, block
Crystal size	0.32 x 0.24 x 0.20 mm^3
Theta range for data collection	1.10 to 37.78°
Index ranges	$-33 \leq h \leq 34, -17 \leq k \leq 17, -32 \leq l \leq 32$
Reflections collected	87504
Independent reflections	19356 [R(int) = 0.0595]
Observed reflections	12301
Completeness to theta = 37.78°	99.1%
Absorption correction	Multi-scan
Max. and min. transmission	0.8681 and 0.8005
Refinement method	Full-matrix least-squares on F^2
Data / restraints / parameters	19356 / 38 / 484
Goodness-of-fit on F^2	1.008
Final R indices [$I>2\text{sigma}(I)$]	$R1 = 0.0465$, $wR2 = 0.1063$
R indices (all data)	$R1 = 0.0896$, $wR2 = 0.1270$
Largest diff. peak and hole	0.720 and -0.599 e.Å^{-3}

Table 17. Atomic coordinates (x 10^4) and equivalent isotropic displacement parameters (Å^2x 10^3) for $(\text{Ind}^{\text{Me-2}})_2(\mu\text{-Ind}^{\text{Me-2}})\text{Mn}_2(\mu\text{-BHT})$. U_{eq} is defined as one third of the trace of the orthogonalized U_{ij} tensor.

	x	y	z	U_{eq}
Mn1	8517(1)	862(1)	2495(1)	18(1)
Mn2	6816(1)	-521(1)	2276(1)	25(1)
O1	7506(1)	335(1)	1823(1)	16(1)
C1	9077(1)	2845(1)	2372(1)	24(1)
C2	9195(1)	1926(2)	1869(1)	25(1)
C3	9656(1)	956(2)	2303(1)	25(1)
C4	10333(1)	715(2)	3748(1)	27(1)
C5	10428(1)	1282(2)	4435(1)	31(1)
C6	10075(1)	2436(2)	4483(1)	31(1)
C7	9621(1)	3036(2)	3844(1)	26(1)
C8	9515(1)	2487(1)	3129(1)	22(1)
C9	9877(1)	1311(1)	3082(1)	22(1)
C10	5583(3)	203(5)	1754(3)	31(1)
C11	5651(3)	-921(5)	1365(2)	32(1)
C12	5775(5)	-1964(5)	1872(3)	30(1)
C13	5829(7)	-2165(10)	3290(4)	30(1)
C14	5714(10)	-1432(9)	3852(6)	40(2)
C15	5582(7)	-117(9)	3755(5)	38(2)
C16	5530(7)	508(9)	3106(5)	33(1)
C17	5591(9)	-216(7)	2496(6)	23(1)
C18	5747(1)	-1578(1)	2593(1)	23(1)
C29	5526(3)	-1005(7)	527(2)	61(2)
C10'	5633(4)	-212(6)	1647(4)	31(1)
C11'	5726(3)	-1444(6)	1404(3)	32(1)
C12'	5842(6)	-2306(6)	1992(4)	30(1)
C13'	5734(8)	-2008(13)	3297(5)	30(1)
C14'	5685(12)	-1088(12)	3807(8)	40(2)
C15'	5566(9)	202(11)	3609(7)	38(2)
C16'	5547(10)	613(11)	2924(7)	33(1)

C17'	5661(12)	-244(9)	2416(7)	23(1)
C18'	5747(1)	-1578(1)	2593(1)	23(1)
C29'	5637(4)	-1803(8)	604(3)	61(2)
C19	8572(1)	100(1)	3636(1)	20(1)
C20	7920(1)	496(1)	3715(1)	20(1)
C21	7431(1)	-536(1)	3550(1)	20(1)
C22	7607(1)	-2963(1)	3291(1)	24(1)
C23	8100(1)	-3841(2)	3215(1)	29(1)
C24	8784(1)	-3443(2)	3244(1)	29(1)
C25	8991(1)	-2169(2)	3363(1)	25(1)
C26	8507(1)	-1263(1)	3466(1)	19(1)
C27	7805(1)	-1662(1)	3418(1)	20(1)
C28	8907(1)	1994(2)	1017(1)	34(1)
C30	7796(1)	1787(2)	4000(1)	28(1)
C31	7222(1)	514(1)	1047(1)	16(1)
C32	7298(1)	-490(1)	567(1)	16(1)
C33	6986(1)	-313(1)	-211(1)	19(1)
C34	6606(1)	791(1)	-532(1)	19(1)
C35	6555(1)	1755(1)	-49(1)	20(1)
C36	6851(1)	1661(1)	741(1)	18(1)
C37	7726(1)	-1739(1)	866(1)	19(1)
C38	7669(1)	-2691(1)	229(1)	26(1)
C39	7468(1)	-2455(2)	1429(1)	38(1)
C40	8526(1)	-1429(2)	1248(1)	35(1)
C41	6263(1)	923(1)	-1377(1)	25(1)
C42	6766(1)	2887(1)	1171(1)	23(1)
C43	7011(1)	2798(2)	2038(1)	29(1)
C44	7200(1)	3977(2)	984(1)	34(1)
C45	5972(1)	3309(2)	904(1)	33(1)

Table 18. Crystal data and structure refinement for $(BHT)_2(\mu\text{-}BHT)Mn_2(\mu\text{-}Cl)$.

Empirical formula	C58 H97 Cl Mn2 O5
Formula weight	1019.69
Temperature	100.0(1) K
Wavelength	0.71073 Å
Crystal system	Triclinic
Space group	P-1
Unit cell dimensions	$a = 16.190(3)$ Å $\alpha = 113.001(4)°$
	$b = 17.593(3)$ Å $\beta = 91.821(4)°$
	$c = 22.018(4)$ Å $\gamma = 91.897(4)°$
Volume	5763(2) Å^3
Z	4
Density (calculated)	1.175 Mg/m^3
Absorption coefficient	0.528 mm^{-1}
F(000)	2208
Crystal color, morphology	colorless, block
Crystal size	0.30 x 0.25 x 0.25 mm^3
Theta range for data collection	1.01 to 36.32°
Index ranges	$-26 \leq h \leq 26, -29 \leq k \leq 26, 0 \leq l \leq 36$
Reflections collected	282787
Independent reflections	54939 [R(int) = 0.0787]
Observed reflections	33031
Completeness to theta = 36.32°	98.2%
Absorption correction	Multi-scan
Max. and min. transmission	0.8793 and 0.8577
Refinement method	Full-matrix least-squares on F^2
Data / restraints / parameters	54939 / 71 / 1268
Goodness-of-fit on F^2	1.022
Final R indices [I>2sigma(I)]	$R1 = 0.0648$, $wR2 = 0.1218$
R indices (all data)	$R1 = 0.1303$, $wR2 = 0.1450$
Largest diff. peak and hole	0.644 and -0.465 e.Å^{-3}

Table 19. Atomic coordinates (x 10^4) and equivalent isotropic displacement parameters (Å^2x 10^3) for $(BHT)_2(\mu\text{-}BHT)Mn_2(\mu\text{-}Cl)$. U_{eq} is defined as one third of the trace of the orthogonalized U_{ij} tensor.

	x	y	z	U_{eq}
Mn1	1394(1)	9801(1)	2492(1)	19(1)
Mn2	3424(1)	10038(1)	2580(1)	18(1)
Cl1	2413(1)	10294(1)	3428(1)	26(1)
O1	2400(1)	9710(1)	1926(1)	18(1)
O2	383(1)	10263(1)	2372(1)	23(1)
O3	4361(1)	9364(1)	2357(1)	21(1)
C1	2540(1)	9525(1)	1273(1)	18(1)
C2	2568(1)	8682(1)	832(1)	18(1)
C3	2813(1)	8514(1)	194(1)	20(1)
C4	3024(1)	9130(1)	-23(1)	22(1)
C5	2947(1)	9940(1)	407(1)	22(1)
C6	2689(1)	10164(1)	1048(1)	18(1)
C7	2269(1)	7964(1)	1012(1)	25(1)
C8	2697(2)	7957(1)	1645(1)	31(1)
C9	1335(2)	8024(1)	1088(1)	33(1)
C10	2410(2)	7117(1)	465(1)	44(1)
C11	3331(2)	8920(1)	-703(1)	33(1)
C12	2628(1)	11104(1)	1452(1)	21(1)
C13	2164(2)	11485(1)	1026(1)	29(1)
C14	3502(1)	11510(1)	1627(1)	27(1)
C15	2146(1)	11351(1)	2086(1)	26(1)
C16	-385(1)	10526(1)	2416(1)	19(1)
C17	-662(1)	11084(1)	3029(1)	21(1)
C18	-1488(1)	11292(1)	3057(1)	23(1)
C19	-2047(1)	10991(1)	2518(1)	24(1)
C20	-1748(1)	10485(1)	1919(1)	24(1)
C21	-933(1)	10242(1)	1846(1)	21(1)
C22	-86(1)	11461(1)	3650(1)	24(1)
C23	662(2)	11922(1)	3519(1)	32(1)

C24	199(1)	10790(1)	3881(1)	27(1)
C25	-513(2)	12091(2)	4236(1)	33(1)
C26	-2947(1)	11186(1)	2578(1)	31(1)
C27	-673(1)	9638(1)	1170(1)	26(1)
C28	-577(2)	8791(1)	1203(1)	33(1)
C29	-1327(2)	9512(2)	616(1)	40(1)
C30	127(2)	9935(2)	960(1)	31(1)
C31	5148(1)	9218(1)	2450(1)	17(1)
C32	5706(1)	9099(1)	1938(1)	18(1)
C33	6535(1)	8996(1)	2061(1)	20(1)
C34	6839(1)	8999(1)	2658(1)	21(1)
C35	6280(1)	9068(1)	3134(1)	19(1)
C36	5436(1)	9159(1)	3047(1)	18(1)
C37	5408(1)	9051(1)	1253(1)	19(1)
C38	5043(1)	9863(1)	1294(1)	27(1)
C39	4755(1)	8336(1)	940(1)	24(1)
C40	6113(1)	8881(1)	773(1)	24(1)
C41	7753(1)	8933(1)	2775(1)	26(1)
C42	4846(1)	9197(1)	3592(1)	23(1)
C43	5266(1)	8968(2)	4127(1)	30(1)
C44	4556(1)	10077(1)	3943(1)	27(1)
C45	4102(1)	8575(1)	3310(1)	28(1)
O7	926(1)	8794(1)	2724(1)	26(1)
C91	50(1)	8622(1)	2742(1)	30(1)
C92	-22(2)	8433(2)	3349(1)	35(1)
C93	738(2)	7944(1)	3328(1)	32(1)
C94	1378(2)	8336(2)	3043(2)	43(1)
O8	4041(1)	11247(1)	3032(1)	25(1)
C95	3698(2)	11993(2)	3496(1)	39(1)
C96	4335(7)	12664(7)	3625(7)	55(1)
C97	5051(8)	12299(7)	3271(8)	60(2)
C98	4931(1)	11398(2)	3014(1)	32(1)
C95'	3698(2)	11993(2)	3496(1)	39(1)
C96'	4407(2)	12468(3)	3935(2)	55(1)
C97'	5132(3)	12246(3)	3537(3)	60(2)
C98'	4931(1)	11398(2)	3014(1)	32(1)

156

Mn3	6559(1)	5166(1)	2486(1)	19(1)
Mn4	8525(1)	4756(1)	2428(1)	18(1)
Cl2	7465(1)	4581(1)	1562(1)	24(1)
O4	7601(1)	5239(1)	3072(1)	17(1)
O5	5518(1)	4778(1)	2658(1)	24(1)
O6	9594(1)	5300(1)	2628(1)	22(1)
C46	7629(1)	5517(1)	3750(1)	16(1)
C47	7571(1)	4936(1)	4047(1)	17(1)
C48	7597(1)	5243(1)	4735(1)	19(1)
C49	7656(1)	6079(1)	5130(1)	21(1)
C50	7708(1)	6628(1)	4825(1)	21(1)
C51	7708(1)	6376(1)	4139(1)	17(1)
C52	7553(1)	3988(1)	3666(1)	18(1)
C53	8447(1)	3740(1)	3528(1)	25(1)
C54	7021(1)	3653(1)	3013(1)	22(1)
C55	7207(1)	3537(1)	4082(1)	24(1)
C56	7667(2)	6369(1)	5872(1)	31(1)
C57	7743(1)	7072(1)	3874(1)	19(1)
C58	8252(2)	7836(1)	4354(1)	30(1)
C59	8131(1)	6851(1)	3204(1)	22(1)
C60	6860(1)	7330(2)	3824(1)	32(1)
C61	4719(1)	4541(1)	2590(1)	18(1)
C62	4354(1)	3993(1)	1968(1)	19(1)
C63	3512(1)	3792(1)	1927(1)	21(1)
C64	3010(1)	4084(1)	2458(1)	21(1)
C65	3384(1)	4593(1)	3063(1)	19(1)
C66	4223(1)	4827(1)	3152(1)	18(1)
C67	4862(1)	3625(1)	1354(1)	24(1)
C68	5567(2)	3135(1)	1485(1)	31(1)
C69	5194(1)	4299(2)	1138(1)	29(1)
C70	4341(2)	3011(2)	756(1)	33(1)
C71	2095(1)	3867(1)	2381(1)	28(1)
C72	4589(1)	5390(1)	3841(1)	22(1)
C73	3954(1)	5580(1)	4375(1)	28(1)
C74	5296(2)	4977(2)	4056(1)	38(1)
C75	4900(2)	6216(2)	3842(1)	36(1)

C76	10359(1)	5579(1)	2596(1)	18(1)
C77	10926(1)	5791(1)	3152(1)	19(1)
C78	11736(1)	6037(1)	3095(1)	23(1)
C79	12011(1)	6085(1)	2520(1)	25(1)
C80	11439(1)	5918(1)	1996(1)	23(1)
C81	10612(1)	5676(1)	2017(1)	20(1)
C82	10669(1)	5741(1)	3800(1)	23(1)
C83	10459(2)	4843(1)	3695(1)	30(1)
C84	9925(1)	6265(2)	4067(1)	30(1)
C85	11361(1)	6063(2)	4347(1)	31(1)
C86	12909(1)	6299(2)	2472(1)	37(1)
C87	10007(1)	5530(1)	1426(1)	22(1)
C88	10400(2)	5752(2)	888(1)	30(1)
C89	9709(1)	4616(1)	1092(1)	26(1)
C90	9272(1)	6092(1)	1648(1)	27(1)
O9	6172(1)	6176(1)	2245(1)	28(1)
C99	5340(2)	6482(2)	2336(1)	33(1)
C100	5189(2)	6836(2)	1822(2)	49(1)
C101	5938(2)	6687(2)	1432(2)	48(1)
C102	6595(2)	6554(2)	1856(1)	41(1)
O10	8887(1)	3488(1)	2001(1)	25(1)
C103	8393(2)	2772(2)	1554(1)	43(1)
C104	8948(5)	2080(4)	1272(4)	45(2)
C105	9817(4)	2517(4)	1401(4)	50(1)
C106	9729(2)	3244(2)	2052(1)	35(1)
C03'	8393(2)	2772(2)	1554(1)	43(1)
C04'	9012(7)	2230(6)	1142(6)	45(2)
C05'	9732(6)	2320(5)	1625(5)	50(1)
C06'	9729(2)	3244(2)	2052(1)	35(1)
C107	3467(2)	7881(2)	4951(2)	67(1)
C108	3104(2)	8699(2)	5313(2)	71(1)
C109	2389(2)	8875(2)	4956(1)	42(1)
C110	1990(2)	9685(2)	5329(2)	48(1)
C111	1260(2)	9832(2)	4969(1)	45(1)
C112	3690(5)	5340(6)	201(5)	50(1)
C113	3068(3)	5026(3)	551(2)	43(1)

C114	2627(3)	4203(3)	118(2)	43(1)
C115	2052(3)	3857(3)	467(2)	46(1)
C116	1634(9)	3032(7)	71(5)	90(3)
C12'	3469(9)	5154(11)	218(10)	50(1)
C13'	2745(5)	4678(6)	338(4)	43(1)
C14'	2459(5)	3903(5)	-228(4)	43(1)
C15'	1675(5)	3493(5)	-131(4)	46(1)
C16'	1734(18)	3153(14)	386(9)	90(3)

Appendix B

SOLID STATE MAGNETIC DATA

Table 20. SQUID data for $[(Ind^{3Me-2,4,7})MnCl(thf)]_2$.

Temp (K)	χ_m	μ eff	$1/\chi_m$	$\chi_m T$
5.00	0.02599	1.02	38.48	0.13
10.00	0.03975	1.78	25.15	0.40
14.99	0.04473	2.32	22.36	0.67
19.99	0.04698	2.74	21.29	0.94
24.98	0.04833	3.11	20.69	1.21
30.00	0.04934	3.44	20.27	1.48
35.00	0.05010	3.75	19.96	1.75
40.00	0.05074	4.03	19.71	2.03
45.00	0.05123	4.29	19.52	2.31
50.02	0.05181	4.55	19.30	2.59
55.06	0.05207	4.79	19.20	2.87
60.08	0.05138	4.97	19.46	3.09
65.08	0.05119	5.16	19.54	3.33
70.10	0.05086	5.34	19.66	3.57
75.12	0.05044	5.51	19.82	3.79
80.13	0.04994	5.66	20.03	4.00
85.14	0.04936	5.80	20.26	4.20
90.15	0.04873	5.93	20.52	4.39
95.18	0.04805	6.05	20.81	4.57
100.21	0.04734	6.16	21.12	4.74
105.21	0.04661	6.26	21.46	4.90
110.20	0.04586	6.36	21.81	5.05
115.24	0.04510	6.45	22.17	5.20
120.24	0.04435	6.53	22.55	5.33
125.24	0.04359	6.61	22.94	5.46
130.27	0.04284	6.68	23.34	5.58
135.28	0.04209	6.75	23.76	5.69
140.30	0.04136	6.81	24.18	5.80
145.31	0.04065	6.87	24.60	5.91
150.33	0.03995	6.93	25.03	6.00
155.33	0.03926	6.99	25.47	6.10
160.35	0.03860	7.04	25.91	6.19
165.36	0.03796	7.09	26.34	6.28
170.37	0.03734	7.13	26.78	6.36
175.39	0.03674	7.18	27.22	6.44
180.40	0.03615	7.22	27.66	6.52
185.41	0.03558	7.26	28.11	6.60
190.41	0.03501	7.30	28.57	6.67
195.43	0.03445	7.34	29.03	6.73
200.43	0.03390	7.37	29.50	6.79
205.45	0.03339	7.41	29.95	6.86
210.46	0.03285	7.44	30.44	6.91
215.44	0.03235	7.47	30.91	6.97

Temp (K)	χ_m	μ eff	$1/\chi_m$	$\chi_m T$
220.44	0.03186	7.50	31.39	7.02
225.45	0.03138	7.52	31.87	7.07
230.44	0.03091	7.55	32.36	7.12
235.45	0.03045	7.57	32.84	7.17
240.47	0.03001	7.60	33.33	7.22
245.46	0.02957	7.62	33.82	7.26
250.47	0.02915	7.64	34.30	7.30
255.46	0.02874	7.66	34.79	7.34
260.46	0.02834	7.68	35.29	7.38
265.47	0.02794	7.70	35.79	7.42
270.45	0.02756	7.72	36.29	7.45
275.46	0.02718	7.74	36.79	7.49
280.46	0.02682	7.76	37.29	7.52
285.47	0.02646	7.77	37.79	7.55
290.47	0.02612	7.79	38.29	7.59
295.47	0.02578	7.81	38.79	7.62
300.47	0.02545	7.82	39.30	7.65

REFERENCES

(1)   Shatruk, M.; Avendano, C.; Dunbar, K. R. *Prog. Inorg. Chem.* **2009**, *56*, 155.

(2)   *Topics in Current Chemistry, Spin Crossover in Transition Metal Compounds I-III*; Gütlich, P.; Goodwin, H. A., Eds.; Springer: Berlin, 2004; Vol. 233-235.

(3)   Gütlich, P.; Hauser, A.; Spiering, H. *Angew. Chem. Int. Ed. Engl.* **1994**, *33*, 2024.

(4)   Craig, D.; Goodwin, H.; Onggo, D. *Aust. J. Chem.* **1988**, *41*, 1157.

(5)   Berry, J. F.; Bill, E.; GarcIa-Serres, R.; Neese, F.; Weyhermüller, T.; Wieghardt, K. *Inorg. Chem.* **2006**, *45*, 2027.

(6)   König, E.; Madeja, K. *Chem. Commun. (London)* **1966**, 61.

(7)   Onggo, D.; Goodwin, H. *Aust. J. Chem.* **1991**, *44*, 1539.

(8)   Fleisch, J.; Gütlich, P. *Chem. Phys. Lett.* **1976**, *42*, 237.

(9)   Hauser, A.; Adler, J.; Gütlich, P. *Chem. Phys. Lett.* **1988**, *152*, 468.

(10)   Figg, D. C.; Herber, R. H.; Potenza, J. A. *Inorg. Chem.* **1992**, *31*, 2111.

(11)   Constable, E. C.; Baum, G.; Bill, E.; Dyson, R.; van Eldik, R.; Fenske, D.; Kaderli, S.; Morris, D.; Neubrand, A.; Neuburger, M.; Smith, D. R.; Wieghardt, K.; Zehnder, M.; Zuberbühler, A. D. *Chem. Eur. J.* **1999**, *5*, 498.

(12)   Nelson, J.; Nelson, S. M.; Perry, W. D. *J. Chem. Soc., Dalton Trans.* **1976**, 1282.

(13)   Sasaki, Y.; Shigematsu, T. *Bull. Chem. Soc. Jap.* **1973**, *46*, 3438.

(14)   Long, G. J.; Hutchinson, B. B. *Inorg. Chem.* **1987**, *26*, 608.

(15)   Reger, D. L.; Gardinier, J. R.; Elgin, J. D.; Smith, M. D.; Hautot, D.;
         Long, G. J.; Grandjean, F. *Inorg. Chem.* **2006**, *45*, 8862.

(16)   Sohrin, Y.; Kokusen, H.; Matsui, M. *Inorg. Chem.* **1995**, *34*, 3928.

(17)   Christiansen, L.; Hendrickson, D. N.; Toftlund, H.; Wilson, S. R.; Xie, C.
         L. *Inorg. Chem.* **1986**, *25*, 2813.

(18)   Toftlund, H. *Monatsch. Chem.* **2001**, *132*, 1269.

(19)   Geiger, D. K.; Lee, Y. J.; Scheidt, W. R. *J. Am. Chem. Soc.* **1984**, *106*,
         6339.

(20)   Weiss, R.; Gold, A.; Terner, J. *Chem. Rev.* **2006**, *106*, 2550.

(21)   McCusker, J. K.; Rheingold, A. L.; Hendrickson, D. N. *Inorg. Chem.*
         1996, *35*, 2100.

(22)   Wilson, L. J.; Georges, D.; Hoselton, M. A. *Inorg. Chem.* **1975**, *14*, 2968.

(23)   Wei, H.-H.; Kao, S.-P.; Jean, Y.-C. *Transition Metal Chem.* **1986**, *11*, 405.

(24)   Chia, P. S. K.; Livingstone, S. E. *Aust. J. Chem.* **1969**, *22*, 1825.

(25)   Ammeter, J. H.; Bucher, R.; Oswald, N. *J. Am. Chem. Soc.* **1974**, *96*,
         7833.

(26)   Cozak, D.; Gauvin, F. *Organometallics* **1987**, *6*, 1912.

(27)   Freyberg, D. P.; Robbins, J. L.; Raymond, K. N.; Smart, J. C. *J. Am.
         Chem. Soc.* **1979**, *101*, 892.

(28)   Hays, M. L.; Burkey, D. J.; Overby, J. S.; Hanusa, T. P.; Yee, G. T.;
         Sellers, S. P.; Young, V. G., Jr. *Organometallics* **1998**, *17*, 5521.

(29)   Walter, M. D.; Sofield, C. D.; Booth, C. H.; Andersen, R. A.
         Organometallics **2009**, *28*, 2005.

(30)   Sitzmann, H.; Schar, M.; Dormann, E.; Kelemen, M. *Z. Anorg. Allg.
         Chem.* **1997**, *623*, 1850.

(31)   Hernandez-Molina, R.; Mederos, A.; Dominguez, S.; Gili, P.; Ruiz-Perez,
         C.; Castineiras, A.; Solans, X.; Lloret, F.; Real, J. A. *Inorg. Chem.* **1998**,
         37, 5102.

(32)   Green, J. C. *Chem. Soc. Rev.* **1998**, *27*, 263.

(33)   Brady, E. D.; Overby, J. S.; Meredith, M. B.; Mussman, A. B.; Cohn, M.
         A.; Hanusa, T. P.; Yee, G. T.; Pink, M. *J. Am. Chem. Soc.* **2002**, *124*,
         9556.

(34)   Heinemann, O.; Jolly, P. W.; Krüger, C.; Verhovnik, G. P. J.
         Organometallics **1996**, *15*, 5462.

(35)   Meredith, M. B.; Crisp, J. A.; Brady, E. D.; Hanusa, T. P.; Yee, G. T.;
         Brooks, N. R.; Kucera, B. E.; Young, V. G., Jr. *Organometallics* **2006**, *25*,
         4945.

(36)   Meredith, M. B.; Crisp, J. A.; Brady, E. D.; Hanusa, T. P.; Yee, G. T.;
         Pink, M.; Brennessel, W. W.; Young, J., V. G. *Organometallics* **2008**, *27*,
         5464.

(37)   O'Hare, D.; Murphy, V. J.; Kaltsoyannis, N. *J. Chem. Soc., Dalton Trans.*
         1993, 383.

(38)   Overby, J. S.; Hanusa, T. P.; Sellers, S. P.; Yee, G. T. *Organometallics*
         1999, *18*, 3561.

(39)   Mond, L.; Langer, C. *J. Chem. Soc., Trans.* **1891**, *59*, 1090.

(40)   Job, A.; Cassal, A. *Compt. rend.* **1926**, *183*, 392.

(41)   Brimm, E. O.; Lynch, M. A.; Sesny, W. J. *J. Am. Chem. Soc.* **1954**, *76*, 3831.

(42)   Gilman, H.; Bailie, J. C. *J. Org. Chem.* **1937**, *2*, 84.

(43)   Gilman, H.; Kirby, R. H. *J. Am. Chem. Soc.* **1941**, *63*, 2046.

(44)   Hein, F. *Ber. Dtsch. Chem. Ges.* **1919**, *52*, 195.

(45)   Bünder, W.; Weiss, E. *Z. Naturforsch., B* **1978**, *33*, 1235.

(46)   Eiland, P. F.; Pepinsky, R. *J. Am. Chem. Soc.* **1952**, *74*, 4971.

(47)   Beermann, C.; Clauss, K. *Angew. Chem.* **1959**, *71*, 627.

(48)   Fischer, R.; Görls, H.; Friedrich, M.; Westerhausen, M. *J. Organomet. Chem.* **2009**, *694*, 1107.

(49)   Andersen, R. A.; Carmona-Guzman, E.; Gibson, J. F.; Wilkinson, G. *J. Chem. Soc., Dalton Trans.* **1976**, 2204.

(50)   Shannon, R. D. *Acta Crystallogr., Sect A* **1976**, *32*, 751.

(51)   Alberola, A.; Blair, V. L.; Carrella, L. M.; Clegg, W.; Kennedy, A. R.; Klett, J.; Mulvey, R. E.; Newton, S.; Rentschler, E.; Russo, L. *Organometallics* **2009**, *28*, 2112.

(52)   Layfield, R. A. *Chem. Soc. Rev.* **2008**, *37*, 1098.

(53)   Gansow, O. A.; Burke, A. R.; Mar, G. N. L. *J. Chem. Soc., Chem. Commun.* **1972**, 456.

(54)   Kump, R. L.; Todd, L. J. *J. Organomet. Chem.* **1980**, *194*, C43.

(55)   Rentsch, D.; Nill, L.; von Philipsborn, W.; Sidler, D. R.; Rybczynski, P. J.; DeShong, P. *Magn. Reson. Chem.* **1998**, *36*, S54.

(56)   Onaka, S.; Sugawara, T.; Kawada, Y.; Iwamura, H. *J. Chem. Soc., Chem. Commun.* **1982**, 257.

(57)   Onaka, S.; Sugawara, T.; Kawada, Y.; Yokoyama, Y.; Iwamura, H. *Bull. Chem. Soc. Jpn.* **1986**, *59*, 3079.

(58)   Onaka, S.; Kato, Y. *Bull. Chem. Soc. Jpn.* **1988**, *61*, 304.

(59)   Morris, R. J.; Girolami, G. S. *Organometallics* **1991**, *10*, 799.

(60)   Unseld, D.; Krivykh, V. V.; Heinze, K.; Wild, F.; Artus, G.; Schmalle, H.; Berke, H. *Organometallics* **1999**, *18*, 1525.

(61)   Blümel, J.; Hebendanz, N.; Hudeczek, P.; Köhler, F. H.; Strauss, W. *J. Am. Chem. Soc.* **1992**, *114*, 4223.

(62)   Hebendanz, N.; Köhler, F. H.; Müller, G.; Riede, J. *J. Am. Chem. Soc.* **1986**, *108*, 3281.

(63)   Wrackmeyer, B.; Hofmann, T.; Herberhold, M. *J. Organomet. Chem.* **1995**, *486*, 255.

(64)   Pregosin, P. S. *Transition Metal Nuclear Magnetic Resonance*; Elsevier: New York, 1991.

(65)   Kececi, A.; Rehder, D. *Z. Naturforsch., B: Anorg. Chem., Org. Chem.* **1981**, *36B*, 20.

(66)   Torocheshnikov, V.; Rentsch, D.; von Philipsborn, W. *Magn. Reson. Chem.* **1994**, *32*, 348.

(67)   Bühl, M. *Theor. Chem. Acc.* **2002**, *107*, 336.

(68)   Ooms, K. J.; Feindel, K. W.; Terskikh, V. V.; Wasylishen, R. E. *Inorg. Chem.* **2006**, *45*, 8492.

(69)   Feindel, K. W.; Ooms, K. J.; Wasylishen, R. E. *Phys. Chem. Chem. Phys.* **2007**, *9*, 1226.

(70)   Antonova, A. B.; Chudin, O. S.; Kirik, S. D. *Powder Diffr.* **2004**, *19*, 165.

(71)   Dahl, L. F.; Ishishi, E.; Rundle, R. E. *J. Chem. Phys.* **1957**, *26*, 1750.

(72)   Berndt, A. F.; Marsh, R. F. *Acta Crystallogr.* **1963**, *16*, 118.

(73)   Pauling, L. *The Nature of the Chemical Bond*; 3rd. ed.; Cornell University Press: Ithaca, 1960.

(74)   Schubert, U.; Ackermann, K.; Woerle, B. *J. Am. Chem. Soc.* **1982**, *104*, 7378.

(75)   Schubert, U.; Scholz, G.; Müller, J.; Ackermann, K.; Wörle, B.; Stansfield, R. F. D. *J. Organomet. Chem.* **1986**, *306*, 303.

(76)   McGrady, G. S.; Sirsch, P.; Chatterton, N. P.; Ostermann, A.; Gatti, C.; Altmannshofer, S.; Herz, V.; Eickerling, G.; Scherer, W. *Inorg. Chem.* **2009**, *48*, 1588.

(77)   Gupta, H. K.; Lock, P. E.; Reginato, N.; Britten, J. F.; McGlinchey, M. J. *Can. J. Chem.* **2006**, *84*, 277.

(78)   Mawby, A.; Pringle, G. E. *J. Inorg. Nucl. Chem.* **1972**, *34*, 877.

(79)   Begum, N.; Kabir, S. E.; Hossain, G. M. G.; Rahman, A. F. M. M.; Rosenberg, E. *Organometallics* **2004**, *24*, 266.

(80)   Adams, R. D.; Chen, G.; Chi, Y. *Organometallics* **1992**, *11*, 1473.

(81)   Çetin, A.; Durfee, W. S.; Ziegler, C. J. *Inorg. Chem.* **2007**, *46*, 6239.

(82)   Alvarez, C. S.; Boss, S. R.; Burley, J. C.; Humphry, S. M.; Layfield, R. A.; Kowenicki, R. A.; McPartlin, M.; Rawson, J. M.; Wheatley, A. E. H.; Wood, P. T.; Wright, D. S. *Dalton Trans.* **2004**, 3481.

(83)   Masters, A. P.; Richardson, J. F.; Sorensen, T. S. *Can. J. Chem.* **1990**, *68*, 2221.

(84)   DeShong, P.; Sidler, D. R.; Rybczynski, P. J.; Slough, G. A.; Rheingold, A. L. *J. Am. Chem. Soc.* **1988**, *110*, 2575.

(85)   Gibson, D. H.; Mandal, S. K.; Owens, K.; Richardson, J. F. *Organometallics* **1990**, *9*, 1936.

(86)   Venkatesan, K.; Blacque, O.; Fox, T.; Alfonso, M.; Schmalle, H. W.; Berke, H. *Organometallics* **2004**, *23*, 1183.

(87)   Kheradmandan, S.; Venkatesan, K.; Blacque, O.; Schmalle, H. W.; Berke, H. *Chem.—Eur. J.* **2004**, *10*, 4872.

(88)   Rheingold, A. L.; White, C. B.; Haggerty, B. S.; Terry, M. R.; Geoffroy, G. L. *Acta Crystallographica Section C* **1992**, *48*, 1832.

(89)   Bellamy, D.; G. Connelly, N.; M. Hicks, O.; Guy Orpen, A. *Journal of the Chemical Society, Dalton Transactions* **1999**, 3185.

(90)   Brunner, H.; Langer, M. *Journal of Organometallic Chemistry* **1973**, *54*, 221.

(91)   Evrard, G.; Thomas, R.; Davis, B. R.; Bernal, I. *Inorganic Chemistry* **1976**, *15*, 52.

(92)   Kheradmandan, S.; Fox, T.; Schmalle, H. W.; Venkatesan, K.; Berke, H. *Eur. J. Inorg. Chem.* **2004**, 3544.

(93)   Jeffreys, J. A. D.; MacFie, J. *Journal of the Chemical Society, Dalton Transactions* **1978**, 144.

(94)   Herberhold, M.; Hofmann, T.; Milius, W.; Wrackmeyer, B. *Journal of Organometallic Chemistry* **1994**, *472*, 175.

(95)   Schubert, U.; Bahr, K.; Müller, J. *J. Organomet. Chem.* **1987**, *327*, 357.

(96)   Sun, J.; Lu, R. S.; Bau, R.; Yang, G. K. *Organometallics* **1994**, *13*, 1317.

(97)   La Placa, S. J.; Hamilton, W. C.; Ibers, J. A.; Davison, A. *Inorganic Chemistry* **1969**, *8*, 1928.

(98)   Koehler, F. H.; Hebendanz, N.; Mueller, G.; Thewalt, U.; Kanellakopulos, B.; Klenze, R. *Organometallics* **1987**, *6*, 115.

(99)   Robbins, J. L.; Edelstein, N. M.; Cooper, S. R.; Smart, J. C. *J. Am. Chem. Soc.* **1979**, *101*, 3853.

(100)   Wilkinson, G.; Cotton, F. A.; Birmingham, J. M. *J. Inorg. Nucl. Chem.* **1956**, *2*, 95.

(101)   Jonas, K.; Rüsseler, W.; Krüger, C.; Raabe, E. *Angewandte Chemie International Edition in English* **1986**, *25*, 928.

(102)   Almenningen, A.; Samdal, S.; Haaland, A. *J. Chem. Soc., Chem. Commun.* **1977**, 14.

(103)   Smart, J. C.; Robbins, J. L. *J. Am. Chem. Soc.* **1978**, *100*, 3936.

(104)   Bottomley, F.; Keizer, P. N.; White, P. S. *Journal of the American Chemical Society* **1988**, *110*, 137.

(105)   Howard, C. G.; Girolami, G. S.; Wilkinson, G.; Thornton-Pett, M.; Hursthouse, M. B. *J. Am. Chem. Soc.* **1984**, *106*, 2033.

(106)   Heck, J.; Massa, W.; Weinig, P. *Angewandte Chemie* **1984**, *96*, 699.

(107)   Abernethy, C. D.; Cowley, A. H.; Jones, R. A.; Macdonald, C. L. B.;
          Shukla, P.; Thompson, L. K. *Organometallics* **2001**, *20*, 3629.

(108)   Abernethy, C. D.; Clyburne, J. A. C.; Cowley, A. H.; Jones, R. A. *Journal
          of the American Chemical Society* **1999**, *121*, 2329.

(109)   Faulmann, C.; Rivière, E.; Dorbes, S.; Senocq, F.; Coronado, E.; Cassoux,
          P. *European Journal of Inorganic Chemistry* **2003**, *2003*, 2880.

(110)   Faulmann, C.; Dorbes, S.; Rivière, E.; Andase, A.; Cassoux, P.; Valade, L.
          Inorganica Chimica Acta **2006**, *359*, 4317.

(111)   Broderick, W. E.; Thompson, J. A.; Day, E. P.; Hoffman, B. M. *Science
          (Washington, D. C., 1883-)* **1990**, *249*, 401.

(112)   Rabaça, S.; Vieira, B. J. C.; Meira, R.; Santos, I. C.; Pereira, L. C. J.;
          Duarte, M. T.; da Gama, V. *European Journal of Inorganic Chemistry*
          2008, *2008*, 3839.

(113)   Bond, A. D.; Layfield, R. A.; MacAllister, J. A.; McPartlin, M.; Rawson,
          J. M.; Wright, D. S. *Chemical Communications* **2001**, 1956.

(114)   Kheradmandan, S.; Schmalle, H. W.; Jacobsen, H.; Blacque, O.; Fox, T.;
          Berke, H.; Gross, M.; Decurtins, S. *Chem.–Eur. J.* **2002**, *8*, 2526.

(115)   Alvarez, C. S.; Bashall, A.; McInnes, E. J. L.; Layfield, R. A.; Mole, R.
          A.; McPartlin, M.; Rawson, J. M.; Wood, P. T.; Wright, D. S. *Chem–Eur.
          J.* **2006**, *12*, 3053.

(116)   Heinemann, O.; Jolly, P. W.; Kruger, C.; Verhovnik, G. P. J.
          Organometallics **1996**, *15*, 5462.

(117)   Westcott, S. A.; Kakkar, A. K.; Stringer, G.; Taylor, N. J.; Marder, T. B. *Journal of Organometallic Chemistry* **1990**, *394*, 777.

(118)   Crisp, J. A.; Meier, R. M.; Overby, J. S.; Hanusa, T. P.; Rheingold, A. L.; Brennessel, W. W. *Organometallics* **2010**, *29*, 2322.

(119)   Meredith, M. B.; Crisp, J. A.; Brady, E. D.; Hanusa, T. P.; Yee, G. T.; Brooks, N. R.; Kucera, B. E.; Young, V. G. *Organometallics* **2006**, *25*, 4945.

(120)   Meredith, M. B.; Crisp, J. A.; Brady, E. D.; Hanusa, T. P.; Yee, G. T.; Pink, M.; Brennessel, W. W.; Young, V. G. *Organometallics* **2008**, *27*, 5464.

(121)   Bradley, C. A.; Flores-Torres, S.; Lobkovsky, E.; Abruña, H. D.; Chirik, P. J. *Organometallics* **2004**, *23*, 5332.

(122)   Fern, G. M.; Klaib, S.; Curnow, O. J.; Lang, H. *Journal of Organometallic Chemistry* **2004**, *689*, 1139.

(123)   Curnow, O. J.; Fern, G. M.; Klaib, S.; Boehme, U.; Lang, H.; Holze, R. *J. Electroanal. Chem.* **2005**, *585*, 167.

(124)   Cadierno, V.; Díez, J. n.; Pilar Gamasa, M.; Gimeno, J.; Lastra, E. *Coordination Chemistry Reviews* **1999**, *193–195*, 147.

(125)   Chien, J. C. W. In *Proceedings of International Congress on Metallocene Polymers* Duesseldorf, 1996; Vol. 2nd, p 223.

(126)   Green, M. *Polyhedron* **1986**, *5*, 427.

(127)   Leino, R.; Lehmus, P.; Lehtonen, A. *European Journal of Inorganic Chemistry* **2004**, *2004*, 3201.

(128)   O'Connor, J. M.; Casey, C. P. *Chemical Reviews* **1987**, *87*, 307.

(129)   Stradiotto, M.; McGlinchey, M. J. *Coordination Chemistry Reviews* **2001**, *219–221*, 311.

(130)   Sui-Seng, C.; Castonguay, A.; Chen, Y.; Gareau, D.; Groux, L.; Zargarian, D. *Topics in Catalysis* **2006**, *37*, 81.

(131)   Werner, H. *Organometallics* **2005**, *24*, 1036.

(132)   Zargarian, D. *Coordination Chemistry Reviews* **2002**, *233–234*, 157.

(133)   Jonas, K.; Rüsseler, W.; Krüger, C.; Raabe, E. *Angewandte Chemie* **1986**, *98*, 905.

(134)   Heinemann, O.; Jolly, P. W.; Krüger, C.; Verhovnik, G. P. J. *Organometallics* **1996**, *15*, 5462.

(135)   Westcott, S. A.; Kakkar, A. K.; Stringer, G.; Taylor, N. J.; Marder, T. B. *Journal of Organometallic Chemistry* **1990**, *394*, 777.

(136)   Weiss, E.; Fischer, E. O. *Zeitschrift für anorganische und allgemeine Chemie* **1956**, *284*, 69.

(137)   Comment:, A. *Several patents mention the synthesis of bis(indenyl)manganese and a number of ring-substituted derivatives in the context of hydrocarbon fuel additives. Their characterization was limited to elemental analysis, and there has been no subsequent mention of them in either the open or patent literature.*

(138)   Hymin, S., Witt, Earl DE. G., Brown, Jerome E.; ETHYL CORP: United States, 1958.

(139)   Crisp, J. A.; Meier, R. M.; Overby, J. S.; Hanusa, T. P.; Rheingold, A. L.; Brennessel, W. W. *Organometallics* **2010**, *29*, 2322.

(140)   Hays, M. L.; Hanusa, T. P. In *Advances in Organometallic Chemistry*; Stone, F. G. A., Robert, W., Eds.; Academic Press: 1996; Vol. Volume 40, p 117.

(141)   Hays, M. L.; Burkey, D. J.; Overby, J. S.; Hanusa, T. P.; Sellers, S. P.; Yee, G. T.; Young, V. G. *Organometallics* **1998**, *17*, 5521.

(142)   Alvarez, C. S.; Bashall, A.; McInnes, E. J. L.; Layfield, R. A.; Mole, R. A.; McPartlin, M.; Rawson, J. M.; Wood, P. T.; Wright, D. S. *Chemistry – A European Journal* **2006**, *12*, 3053.

(143)   Sitzmann, H.; Schär, M.; Dormann, E.; Kelemen, M. *Zeitschrift für anorganische und allgemeine Chemie* **1997**, *623*, 1609.

(144)   Yee, G. T.; Manriquez, J. M.; Dixon, D. A.; McLean, R. S.; Groski, D. M.; Flippen, R. B.; Narayan, K. S.; Epstein, A. J.; Miller, J. S. *Adv. Mater.* **1991**, *3*, 309.

(145)   Narayan, K. S.; Heres, O.; Epstein, A. J. *J. Magn. Magn. Mater.* **1992**, *110*, L6.

(146)   Faulmann, C.; Rivière, E.; Dorbes, S.; Senocq, F.; Coronado, E.; Cassoux, P. *Eur. J. Inorg. Chem.* **2003**, 2880.

(147)   Crisp, J. A.; Meredith, M. B.; Hanusa, T. P.; Wang, G.; Brennessel, W. W.; Yee, G. T. *Inorg. Chem.* **2005**, *44*, 172.

(148)   Evans, D. F. *Journal of the Chemical Society (Resumed)* **1959**.

(149)   Hays, M. L., Vanderbilt University, 1996.

(150)   SHELXTL; 6.1 ed.; Bruker Analytical X-Ray Systems, Madison, WI.: 2000.

(151)   Cedheim, L.; Eberson, L. *Synthesis* **1973**, 159.

(152)   Ready, T. E.; Chien, J. C. W.; Rausch, M. D. *J. Organomet. Chem.* **1999**, *583*, 11.

(153)   Miyamoto, T. K.; Tsutsui, M.; Chen, L.-B. *Chem. Lett.* **1981**, 729.

(154)   *Crystals of {(Ind2Me-4,7)2Mn}8 are monoclinic, space group C2/c, with a = 41.211(8) Å, b = 10.223(2) Å, c = 40.415(11) Å, β = 119.178(2)°, V = 14,867(6) Å3, Z = 4, and ρcalc = 1.302 g cm-3 for fw = 2914.96. Refinement of 3472 reflections collected at the University of Rochester at 100.0(1) K with I > 2.0σ(I) led to residuals of R(F2) = 0.114 and Rw (F2) = 0.204.*

(155)   Bond, A. D.; Layfield, R. A.; MacAllister, J. A.; McPartlin, M.; Rawson, J. M.; Wright, D. S. *Chem. Commun.* **2001**, 1956.

(156)   Almenningen, A.; Haaland, A.; Samdal, S. *J. Organomet. Chem.* **1978**, *149*, 219.

(157)   Sitzmann, H.; Schär, M.; Dormann, E.; Keleman, M. *Z. Anorg. Allg. Chem.* **1997**, *623*, 1609.

(158)   Overby, J. S.; Schoell, N. S.; Hanusa, T. P. **Unpublished results**.

(159)   Fern, G. M.; Klaib, S.; Curnow, O. J.; Lang, H. *J. Organomet. Chem.* **2004**, *689*, 1139.

(160)   Schlenk, W.; Schlenk, W. *Berichte der deutschen chemischen Gesellschaft (A and B Series)* **1929**, *62*, 920.

(161)   Halliwell, B. G., J. M. C. *Free radicals in biology and medicine*; Oxford

          University Press: New York, 1999.

(162)   Cabelli, D. E. R., D.; Rodriguez, J. A.; Valentine, J. S.; Zhu, H. In

          Biomimetic Oxidations Catalyzed by Transition Metal Complexes;

          Meunier, B., Ed.; Imperial College Press: London, 2000, p 461.

(163)   Rulisek, L.; Jensen, K. P.; Lundgren, K.; Ryde, U. *J. Comput. Chem.*

          2006, *27*, 1398.

(164)   Rivalta, I.; Brudvig, G. W.; Batista, V. S. *Curr. Opin. Chem. Biol.* **2012**,

          16, 11.

(165)   McConnell, I. L.; Grigoryants, V. M.; Scholes, C. P.; Myers, W. K.; Chen,

          P.-Y.; Whittaker, J. W.; Brudvig, G. W. *J. Am. Chem. Soc.* **2012**, *134*,

          1504.

(166)   Lang, K.; Vondrak, J.; Wagnerova, D. M. *Collect. Czech. Chem. Commun.*

          1994, *59*, 1059.

(167)   Urban, M. W.; Nakamoto, K.; Basolo, F. *Inorg. Chem.* **1982**, *21*, 3406.

(168)   Schappacher, M.; Weiss, R. *Inorg. Chem.* **1987**, *26*, 1189.

(169)   Seo, M. S.; Kim, J. Y.; Annaraj, J.; Kim, Y.; Lee, Y.-M.; Kim, S.-J.; Kim,

          J.; Nam, W. *Angewandte Chemie International Edition* **2007**, *46*, 377.

(170)   Singh, U. P.; Sharma, A. K.; Hikichi, S.; Komatsuzaki, H.; Moro-oka, Y.;

          Akita, M. *Inorg. Chim. Acta* **2006**, *359*, 4407.

(171)   Shook, R. L.; Gunderson, W. A.; Greaves, J.; Ziller, J. W.; Hendrich, M.

          P.; Borovik, A. S. *Journal of the American Chemical Society* **2008**, *130*,

          8888.

(172)   McAuliffe, C. A.; Al-Khateeb, H.; Jones, M. H.; Levason, W.; Minten, K.; McCullough, F. P. *Journal of the Chemical Society, Chemical Communications* **1979**.

(173)   Conry, R. R. In *Encyclopedia of Inorganic Chemistry*; John Wiley & Sons, Ltd: 2006.

(174)   Liu, H.-Y.; Yam, F.; Xie, Y.-T.; Li, X.-Y.; Chang, C. K. *Journal of the American Chemical Society* **2009**, *131*, 12890.

(175)   Groni, S.; Blain, G.; Guillot, R.; Policar, C.; Anxolabehere-Mallart, E. *Inorganic Chemistry* **2007**, *46*, 1951.

(176)   Policar, C.; Artaud, I.; Mansuy, D. *Inorganic Chemistry* **1996**, *35*, 210.

(177)   Bleaney, B.; Bowers, K. D. *Philos. Mag. (1798-1977)* **1952**, *43*, 372.

(178)   Xu, Z.; Thompson, L. K.; Miller, D. O. *Inorganic Chemistry* **1997**, *36*, 3985.

(179)   *The Chemistry of Metal Alkoxides*; Nataliya Ya. Turova, E. P. T., Vadim G. Kessler and Maria I. Yanovskaya, Ed.; Springer, 2002.

(180)   Gaus, P. L.; Kao, S. C.; Youngdahl, K.; Darensbourg, M. Y. *J. Am. Chem. Soc.* **1985**, *107*, 2428.

(181)   Tooley, P. A.; Ovalles, C.; Kao, S. C.; Darensbourg, D. J.; Darensbourg, M. Y. *J. Am. Chem. Soc.* **1986**, *108*, 5465.

(182)   Bradley, D. C. *Chem. Rev.* **1989**, *89*, 1317.

(183)   Chandler, C. D.; Roger, C.; Hampden-Smith, M. J. *Chem. Rev.* **1993**, *93*, 1205.

(184)   Hubert-Pfalzgraf, L. G. *Nouv. J. Chem.* **1987**, *11*, 663.

(185)   Meyer, D.; Osborn, J. A.; Wesolek, M. *Polyhedron* **1990**, *9*, 1311.

(186)   Bartlett, R. A.; Ellison, J. J.; Power, P. P.; Shoner, S. C. *Inorg. Chem.*
          1991, *30*, 2888.

(187)   Deacon, Glen B.; Goh, L. Y.; Jackson, W. R.; Skelton, Brian W.; Chen,
          W.; White, Allan H. *Zeitschrift für anorganische und allgemeine Chemie*
          2010, *636*, 1478.

(188)   Mandal, S. K.; Ho, D. M.; Orchin, M. *Inorganic Chemistry* **1991**, *30*,
          2244.

(189)   Sasaki, Y.; Akamatsu, T.; Tsuchiya, K.; Ohba, S.; Sakamoto, M.; Nishida,
          Y. *Polyhedron* **1998**, *17*, 235.

(190)   Coucouvanis, D.; Greiwe, K.; Salifoglou, A.; Challen, P.; Simopoulos, A.;
          Kostikas, A. *Inorganic Chemistry* **1988**, *27*, 593.

(191)   Wesolek, M.; Meyer, D.; Osborn, J. A.; De Cian, A.; Fischer, J.; Derory,
          A.; Legoll, P.; Drillon, M. *Angewandte Chemie International Edition in*
          English **1994**, *33*, 1592.

(192)   *Several patents mention the synthesis of bis(indenyl)manganese and a*
          number of ring-substituted derivatives in the context of hydrocarbon fuel
          additives. Their characterization was limited to elemental analysis, and
          there has been no subsequent mention of them in either the open or patent
          literature.